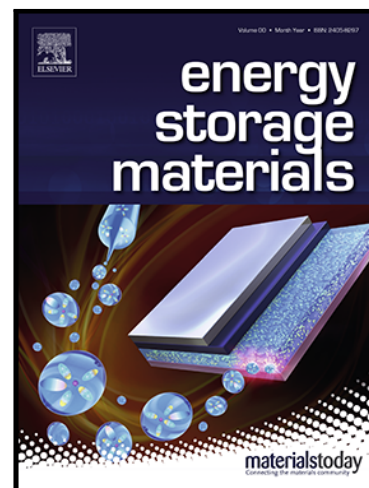


Hydrogen Clathrates: Next Generation Hydrogen Storage Materials

Anshul Gupta , Gino V. Baron , Patrice Perreault , Silvia Lenaerts , Radu-George Ciocarlan , Pegie Cool , Paulo G.M. Mileo , Sven Rogge , Veronique Van Speybroeck , Geert Watson , Pascal Van Der Voort , Maarten Houllberghs , Eric Breynaert , Johan Martens , Joeri F.M. Denayer

PII: S2405-8297(21)00256-7  
DOI: <https://doi.org/10.1016/j.ensm.2021.05.044>  
Reference: ENSM 1682



To appear in: *Energy Storage Materials*

Received date: 18 March 2021  
Revised date: 27 May 2021  
Accepted date: 28 May 2021

Please cite this article as: Anshul Gupta , Gino V. Baron , Patrice Perreault , Silvia Lenaerts , Radu-George Ciocarlan , Pegie Cool , Paulo G.M. Mileo , Sven Rogge , Veronique Van Speybroeck , Geert Watson , Pascal Van Der Voort , Maarten Houllberghs , Eric Breynaert , Johan Martens , Joeri F.M. Denayer , Hydrogen Clathrates: Next Generation Hydrogen Storage Materials, *Energy Storage Materials* (2021), doi: <https://doi.org/10.1016/j.ensm.2021.05.044>

This is a PDF file of an article that has undergone enhancements after acceptance, such as the addition of a cover page and metadata, and formatting for readability, but it is not yet the definitive version of record. This version will undergo additional copyediting, typesetting and review before it is published in its final form, but we are providing this version to give early visibility of the article. Please note that, during the production process, errors may be discovered which could affect the content, and all legal disclaimers that apply to the journal pertain.

## Hydrogen Clathrates: Next Generation Hydrogen Storage Materials

Anshul Gupta<sup>1,2</sup>, Gino V. Baron<sup>1</sup>, Patrice Perreault<sup>3,4</sup>, Silvia Lenaerts<sup>5</sup>, Radu-George Ciocarlan<sup>6</sup>, Pegie Cool<sup>6</sup>, Paulo G.M. Mileo<sup>7</sup>, Sven Rogge<sup>7</sup>, Veronique Van Speybroeck<sup>7</sup>, Geert Watson<sup>8</sup>, Pascal Van Der Voort<sup>8</sup>, Maarten Houllberghs<sup>9</sup>, Eric Breynaert<sup>9</sup>, Johan Martens<sup>9</sup> and Joeri F.M. Denayer\*<sup>1</sup>

1: *Vrije Universiteit Brussel, Department of Chemical Engineering, Pleinlaan 2, B-1050, Brussel, Belgium*

2: *Department of Metallurgical and Materials Engineering, National Institute of Technology, Srinagar, India-190006.*

3: *University of Antwerp, Faculty of Science, Institute for Environment and Sustainable Development (IMDO), Groenenborgerlaan 171, 2020 Antwerpen, Belgium*

4: *University Of Antwerp, Blue App, Middelheimlaan 1, 2020 Antwerpen, Belgium*

5: *University of Antwerp, Department of Bioscience Engineering, Sustainable Energy Air and Water Technology, Groenenborgerlaan 171, 2020 Antwerpen, Belgium*

6: *Laboratory of Adsorption and Catalysis, Department of Chemistry, University of Antwerp, Universiteitsplein 1, 2610 Wilrijk, Belgium*

7: *Center for Molecular Modeling (CMM), Ghent University, Zwijnaarde, Belgium*

8: *Center for Ordered Materials, Organometallics and Catalysis, Department of Chemistry, Ghent University, Krijgslaan 281-S3, 9000 Ghent, Belgium*

9: *Centre for Surface Chemistry and Catalysis, NMRCORE - NMR - XRAY - EM Platform for CONvergence Research, Department of Microbial and Molecular systems (M2S) – KU Leuven, B-3001 Leuven*

\*Author for correspondence: [Joeri.Denayer@vub.be](mailto:Joeri.Denayer@vub.be)

### Abstract

Extensive research has been carried on the molecular adsorption in high surface area materials such as carbonaceous materials and MOFs as well as atomic bonded hydrogen in metals and alloys. Clathrates stand among the ones to be recently suggested for hydrogen storage. Although, the simulations predict lower capacity than the expected by the DOE norms, the additional benefits of clathrates such as low production and operational cost, fully reversible reaction, environmentally benign nature, low risk of flammability make them one of the most promising materials to be explored in the next decade. The inherent ability to tailor the properties of clathrates using techniques such as addition of promoter molecules, use of porous supports and

formation of novel reverse micelles morphology provide immense scope customisation and growth. As rapidly evolving materials, clathrates promise to get as close as possible in the search of “holy grail” of hydrogen storage. This review aims to provide the audience with the background of the current developments in the solid-state hydrogen storage materials, with a special focus on the hydrogen clathrates. The in-depth analysis of the hydrogen clathrates will be provided beginning from their discovery, various additives utilised to enhance their thermodynamic and kinetic properties, challenges in the characterisation of hydrogen in clathrates, theoretical developments to justify the experimental findings and the upscaling opportunities presented by this system. The review will present state of the art in the field and also provide a global picture for the path forward.

## 1. Introduction

Protection of the environment is of paramount importance for sustainable development and growth of a nation. The development of alternate energy sources, which can address serious issues like global warming, have gained grave urgency. Hydrogen, with its high fuel efficiency (141.7 MJ/kg) and environment friendly nature (by product of combustion is water), is the most promising alternative to fossil fuel-based energy sources<sup>1</sup>. However, due to its low density (0.08 g/L) and highly flammable nature (at as low as 4 % concentration in air), safe and efficient storage is a challenge<sup>1</sup>. US Department of Energy has specified storage requirements of ~5.5 % hydrogen by weight for a commercial vehicle on-board storage system, with amicable pressure (5-12 bar) and temperature (<85°C) conditions<sup>2</sup>. In this regard, storage of hydrogen in materials is an attractive alternative to the conventional high-pressure cylinders. Important classes of materials developed for hydrogen storage include: (i) metals and alloys (intermetallics), (ii) carbonaceous materials, (iii) metal organic frameworks (MOFs), (iv) zeolites & (v) clathrates. Multiple studies have been carried out to investigate the hydrogen storage characteristics of these materials. However, none of the materials has been found to be suitable for commercial use in an on-board vehicular application.

Hydrogen storage in clathrates drew attention of the scientist in the beginning of 21<sup>st</sup> century. After their discovery in 1810 by Sir Humphry Davy<sup>3</sup>, clathrates were proposed as hydrogen storage materials in 2002 by Mao *et al.*<sup>4</sup>. They showed successful formation of water-based hydrogen clathrates with classic *sII* structure at 249 K, under a pressure of 250 MPa; it had hydrogen storage capacity of 5.3 wt.%. This was followed by detailed investigations of occupation of hydrogen in hydrate cages, interaction of H<sub>2</sub> with water molecules, electronic environment around water molecules<sup>5</sup>. Advanced characterisation tools have been used to confirm the presence of hydrogen; in-situ Raman spectroscopy to study the modes of vibration of H<sub>2</sub> molecules, synchrotron radiation under high pressure to determine the precise structure and <sup>1</sup>H NMR to determine the cage occupancy<sup>6</sup>. This paper discusses in detail the hydrogen storage characteristics of the clathrates with an in-depth analysis

of their thermodynamic and kinetic properties, challenges in the characterisation of hydrogen in clathrates and the upscaling techniques so as to bring out the key issues limiting the growth of the clathrates as the next revolutionary on-board hydrogen storage material.

## 2. Hydrogen storage materials: A brief overview

Interaction of hydrogen with materials can be divided into two broad categories; physisorption and chemisorption. During physisorption, molecular hydrogen interacts with the host material using weak Vander Waals' forces, apart from electrostatic and orbital interactions<sup>7,8</sup>. The problem arises as these interactions are quite weak and hydrogen molecule possess no dipole moment or charge and is only weakly polarizing<sup>7</sup>. The adsorption is favoured at low temperatures (77 K) and decreases upon increasing temperature. At the same time, pore size forms an important parameter governing the amount of gas adsorbed. It has been found that enthalpy of adsorption increases with decreasing pore size<sup>9</sup>. In narrow pores, the potentials of neighbouring atoms overlap and interaction strength increases<sup>10</sup>. As a result, with decreasing pore size, the amount of adsorption increases and usually Type I isotherm (IUPAC nomenclature) is followed by physisorption based materials at 77 K<sup>11</sup>. The adsorption increases monotonically with pressure and saturates at a certain pressure. Chemisorption, on the other hand takes place by dissociation of molecular hydrogen into atomic form. Activation energy barrier has to be crossed for the chemisorption to take place. Atomic hydrogen can further diffuse to the bulk of the material and form either disordered solid solution or a compound. This is accompanied by a phase transformation resulting in change in crystal structure or lattice parameter. A typical sequence of steps during hydrogen adsorption in magnesium is provided in the Figure 1.

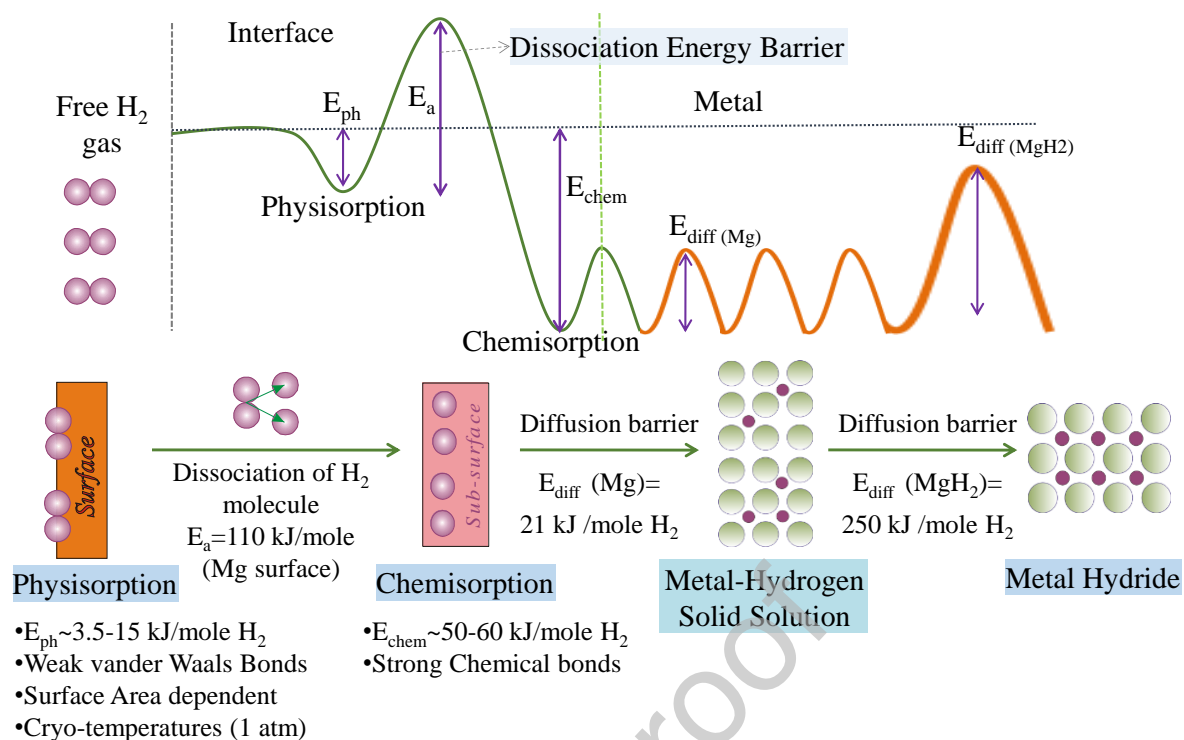


Figure 1. Interaction of hydrogen with material in various steps: (i) physisorption, (ii) chemisorption, (iii) solid solution and (iv) compound formation<sup>12</sup>.

A plethora of materials exist for solid state hydrogen storage<sup>13</sup>. These can be classified based on the form of hydrogen stored: the materials which store hydrogen in molecular form fall under the category of physisorption viz. the molecular hydrogen is physically adsorbed on the surface of the material<sup>14</sup>. Materials such as carbonaceous, MOFs and zeolites fall under this category. On the other hand, the materials which absorb hydrogen in atomic form are classified under chemisorption<sup>15</sup>. Metal hydrides and complex hydrides are examples of few such materials. Metal hydrides usually form interstitial hydrides in which atomic hydrogen occupies interstitial voids in the crystal and complex hydrides form ionic or covalent bond with hydrogen. An important set of criteria which governs the ability of the material to be utilised in on-board application have been formulated by Department of Energy (DOE), United States<sup>16</sup>. These criteria not only focus on the overall hydrogen storage capacity of system (5.5 wt.%), but also take into account the rate of tank filling (1.65 wt.% H<sub>2</sub> per minute), temperature ( $\sim 85^\circ\text{C}$ ) and pressure of storage and release (5-12 bar), the ability of the material to undergo multiple cycles without degradation ( $>1000$  cycles) among other factors. However, no material has been able to meet these targets till now. Recently developed materials closely meeting these targets have been shown in Figure 2.

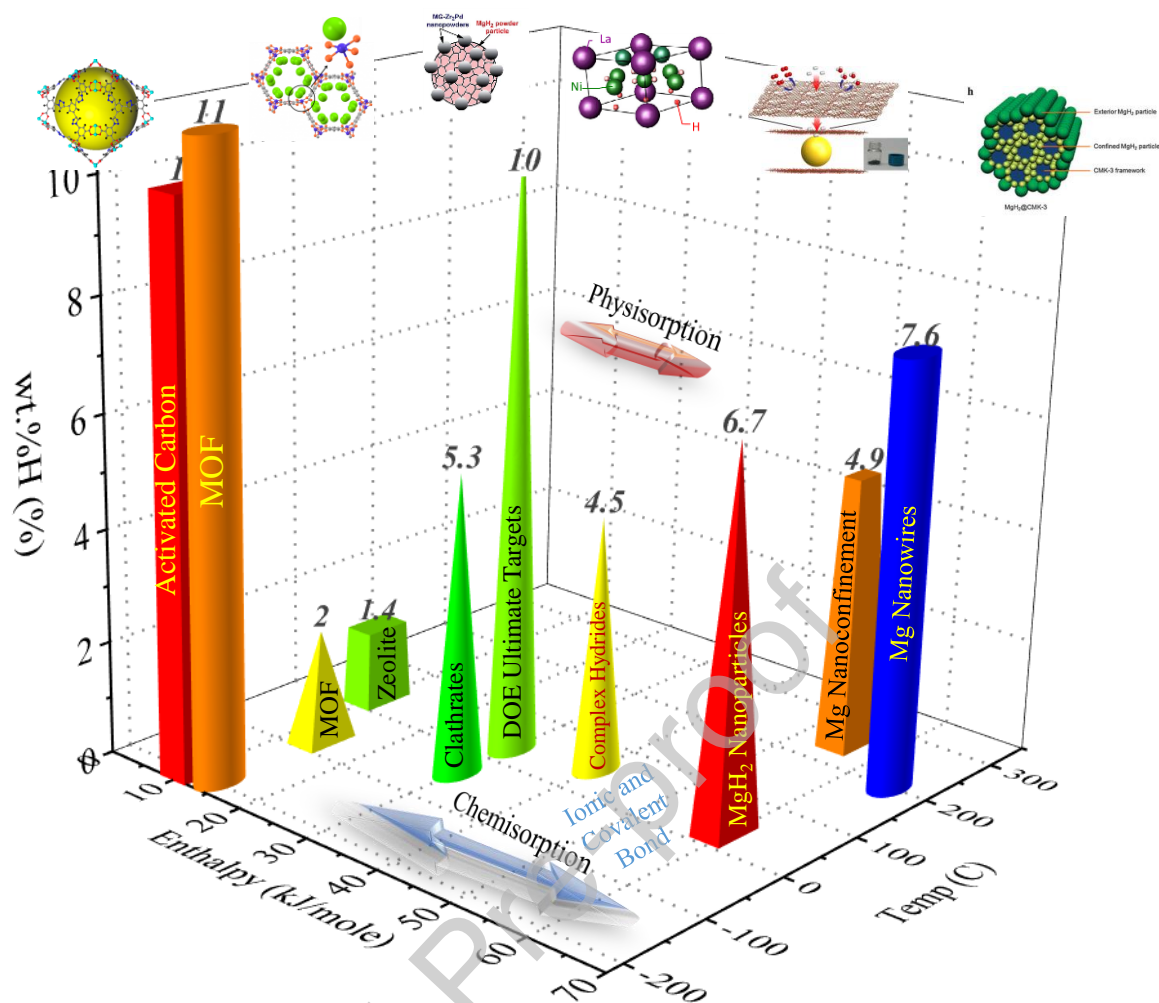


Figure 2. An overview of the hydrogen storage materials, from the perspective of DOE requirements<sup>16</sup>. A representative material of each category has been taken to plot the data. These are: (a) Activated Carbon (Cellulose Derived Activated Carbon)<sup>17</sup>, (b) MOF (MOF-5)<sup>18</sup>, (c) Complex Hydrides (LiBH<sub>4</sub>/MgH<sub>2</sub>)<sup>19</sup>, (d) Nanoconfinement (Mg@CMK)<sup>20</sup>, (e) Complex Hydride (NaAlH<sub>4</sub>@TiO<sub>2</sub> & Carbon)<sup>21</sup>, (f) MgH<sub>2</sub> nanoparticles<sup>22</sup> and (g) Mg nanowires<sup>23</sup>. DOE targets refer to material based targets (an estimate keeping in mind the weight of auxiliaries).

## 2.1. Carbonaceous materials

Among the physisorption based materials, carbon based materials have attracted the largest attention<sup>24,25</sup>. Quite a few types of carbon materials have been extensively studied such as activated carbon, microporous templated carbon, carbon nanotubes and nanofibers and graphene<sup>26-31</sup>. Among these, activated carbons are amorphous in nature and exhibit extremely large surface area (3000 m<sup>2</sup>/g for AX-21) and porosity<sup>32</sup>. This property makes them ideal for absorption of hydrogen with capacity reported upto 5 wt.% at 77 k and 20 bar<sup>32</sup>. Several computational models have been developed to optimise the pore structure and surface properties of activated carbon for enhanced hydrogen storage<sup>33,34</sup>. Zuetel *et al.*<sup>35</sup> have developed a computational model which suggests that density of hydrogen on the surface of carbon material is expected to be 2.28 wt.% m<sup>2</sup>/g. This corroborates well with the model

developed by experimentally comparing the specific surface area (SSA) and the hydrogen storage capacity<sup>36</sup>.

To enhance the ambient temperature hydrogen storage, doping with metal nanoparticle catalysts such as Ni, Pd, Pt, V and Co has been carried out<sup>37</sup>. Pt doped superactivated carbon shows 1.2 wt.% hydrogen absorption at 298 K and 100 bar<sup>38</sup>. The increase has been attributed to 'hydrogen spillover' mechanism<sup>39</sup>. This refers to the dissociation of hydrogen molecules atop the catalyst, diffusion of hydrogen atoms towards the carbonaceous support and adsorption at surface sites, which were inaccessible otherwise<sup>39</sup>. The presence of surface oxygen groups has found to further enhance the effect of metal catalyst<sup>40</sup>. It has been reported that Pd-doped reduced graphene oxide absorbs 3 wt.% hydrogen at 298 K and 40 bar<sup>41</sup>. Surface oxygen functional groups have been found to act secondary surface for the hydrogen spillover<sup>42</sup>. Other elements such as boron and nitrogen have also shown to have beneficial effect on the hydrogen absorption in carbon materials<sup>43-46</sup>. In a recent study, boron doped activated carbon have been irradiated by neutrons to optimise the pore size and structure<sup>47</sup>. They have shown ~9 wt.% hydrogen storage capacity at 80 K and 100 bar. In a recent study, cellulose acetate derived activated carbon (SSA=3800 m<sup>2</sup>/g) have been reported to store ~8.9 wt.% hydrogen at 77 K and 30 bar<sup>17</sup>. However, their hydrogen storage capacity at room temperature (298 K) remains low (~ 1.2 wt.% at 30 bar), with heat of adsorption being 10 kJ/mol<sup>17</sup>. Turning around the dangerous waste to useful materials, microporous porous carbons derived from cigarette butt have been reported to show 11.2 wt.% hydrogen absorption at 77 K and 40 bar<sup>48</sup>. They exhibit ultra-high surface area (4300 m<sup>2</sup>/g) and pore volume of 2.09 cm<sup>3</sup>/g. This is the highest reported capacity till date for the carbonaceous materials at cryogenic temperatures. However, reproducibility and accuracy of results are a cause of concern for the carbon materials and multiple round robin tests have been conducted to verify the same<sup>49-51</sup>.

In contrast to activated carbons, the templated carbons represent materials with narrow range of pore size, giving better control over structure. Zeolite template carbon, with high surface area (3200 m<sup>2</sup>/g) and fine pore size (0.5-0.9 nm), have shown hydrogen storage capacity upto 6.9 wt.% at 77 K and 20 bar with heat of adsorption of 4-8 kJ/mol<sup>52</sup>. Carbon nanotubes, especially single wall carbon nanotubes (SWNTs), show moderate hydrogen absorption capacity of ~2 wt.% at 77 K<sup>53</sup>. Multiple attempts have been made to enhance the hydrogen storage capacity by decorating the surface with elements such as aluminium, lithium, calcium and nickel<sup>54</sup>. Doping with Ni nanoparticles has shown enhancement in the hydrogen storage capacity of multi-walled carbon nanotube (MWNTs), with ~2.27 wt.% hydrogen stored at 298 K and 80 bar<sup>55</sup>. Atomic oxygen irradiated MWCNTs have shown 1.6 wt.% hydrogen storage capacity at 100 kPa and 298 K<sup>56</sup>. Although computational studies have predicted hydrogen storage capacity as high as 19 wt.% in 3-D assemblies of carbon nanotubes, experimental validation of these results have not yet been achieved<sup>57</sup>. While carbon materials have been studied from the early stages

of research, several other materials have gained attention in the recent past for hydrogen storage such as MOFs (Metal Organic Frameworks)<sup>58,59</sup>, COFs (Covalent Organic Frameworks)<sup>60,61</sup>, zeolites<sup>62</sup> and PIMs (Polymers with intrinsic Microporosity)<sup>63</sup>.

## 2.2. Metal Organic Frameworks (MOFs)

MOFs including MOF-5, IRMOF-6 and IRMOF-8 were first reported for hydrogen storage by Rosi et al<sup>64</sup>. They reported 4.5 wt.% at 77 K and 0.07 MPa for MOF-5. Pore size has been one of the important parameters for tuning the hydrogen storage capacity in MOFs. A pore size close to the kinetic diameter of hydrogen molecule (2.89 Å) is suggested; it would enhance the interaction of hydrogen with the framework and strengthen the Vander Walls forces. This phenomenon has been observed at low pressures (1 bar) and cryogenic temperatures (77 K); e.g. MIL-53 (1.66 wt.%, pores size: 6.8Å) and IRMOF-3 (1.42 wt.%, pore size: 9.6 Å).

In a recent study, nearly half a million MOFs were screened using GCMC (Grand Canonical Monte Carlo) calculations and exceptional hydrogen storage capacity was reported for the three MOFs: NU-100, UMCM-9 and SNU-70<sup>65</sup>. Capacity of 13.9 wt.% (NU-100), 11.3 wt.% (UMCM-9) and 10.6 wt.% (SNU-70) was observed at 77 K and 100 bar. This exceeded the capacity for the bench mark MOFs i.e. 7.8 wt.% for MOF-5 and 9.1 wt.% for the IRMOF-20, under similar conditions<sup>18</sup>. Apart from the gravimetric storage capacity, volumetric storage capacity is also vital in MOFs, as their density is lowest among the crystalline materials (0.61 g/cm<sup>3</sup> for MOF-5)<sup>66,67</sup>. Another MOF with composition Ni<sub>2</sub>(m-dobdc) has shown impressive volumetric capacity of 23 g/l (equivalent to 2 wt.%H) for the absorption at -75 °C and desorption at 25°C, the highest reported in this temperature range<sup>68</sup>. They also reported a gravimetric hydrogen storage capacity of 1.2 wt.% at 110 bar and 298 K<sup>68</sup>. In conforming with tank design recommendations of DOE, NU-125 (BET area = 1870 m<sup>2</sup>/cm<sup>3</sup>) was reported to have 49 g/l volumetric capacity and 8.5 wt.% gravimetric capacity, with absorption at 100 bar and 77 K and desorption at 5 bar and 160K<sup>69</sup>. They have also observed an exception to the well know Chahin's rule, which states that for every 500 m<sup>2</sup>/g surface area, an excess adsorption of 1 wt.% is observed<sup>18,69</sup>. The rule is applicable only upto surface area of 3000 m<sup>2</sup>/g, whereas after that approximately 0.5 wt.% excess adsorption is observed for every additional 1000 m<sup>2</sup>/g<sup>69</sup>. Many other strategies such as introduction of metal nanoparticles in the pores<sup>70</sup>, restricting the pore size using catenation<sup>71</sup>, nanoconfinement<sup>72,73</sup> and incorporation of guest metal ions<sup>74,75</sup> have been utilised to enhance the hydrogen storage capacity of MOFs.

## 2.3. Zeolites

Zeolites represent microporous materials with high surface area and porosity, but have been unable to achieve promising results with regard to hydrogen storage<sup>62,76</sup>. For Na-Y zeolite, hydrogen absorption capacity of 1.81 wt.% was observed at 77 K

and 1.5 MPa<sup>77</sup>. Around 2.55 wt.% hydrogen absorption was reported at 77 K and 40 bar Na-X<sup>62</sup>. Computational studies have shown that the upper limit for hydrogen absorption in zeolites lies in the range of 2.65 to 2.68 wt.%<sup>78</sup>. Among the PIMs, triptycene based polymers have shown hydrogen capacity upto 2.7 wt.% at 1 MPa and 77 K<sup>79</sup>. A similar class of materials, Hypercrosslinked Polymers (HCPs), have shown higher capacity of 3.68 wt.% at 15 MPa and 77 K<sup>80</sup>. Among the emerging set of materials, COFs have fared better than HCPs and PIMs in terms of gravimetric hydrogen storage capacities<sup>60</sup>. COF-102 and 103 have shown 7.2 wt.% and 7.3 wt.% hydrogen storage capacity, respectively at 77 K and 9 MPa<sup>61,81</sup>. Tong *et al.*<sup>60</sup> have carried out similar screening exercise as Ahmed *et al.*<sup>65</sup> on COFs and have theoretically calculated volumetric storage capacity of 56.1 g/L and gravimetric capacity of 10.3 wt.% in a hypothetical 3-D bor-GCOF. Although, none of the above materials has been able to meet the criteria for practical hydrogen storage media, important advancements have been made in the context of hydrogen adsorption in microporous materials which bring us one step closer to the DOE targets<sup>82</sup>.

#### 2.4. Metal Hydrides

As stated earlier, metal hydrides distinguish themselves from the above materials with regard to the presence of hydrogen in the atomic form. Typically, metals (such as Mg, Pd) and intermetallic compounds (such as LaNi<sub>5</sub>) constitute the typical examples of such materials. Among metals, Mg is one of the most attractive material due to its easy availability and high hydrogen storage capacity (7.6 wt.%), which exceeds the ultimate DOE targets (6.5 wt.)<sup>83</sup>. However, in its native form it suffers from high temperatures of absorption (>300 °C), sluggish kinetics and sensitivity to oxidation upon exposure to air<sup>84</sup>. Some of the strategies used to improve the hydrogen absorption characteristics of Mg-based materials include alloying (Mg<sub>2</sub>Ni<sup>85</sup>, Mg<sub>2</sub>Fe<sup>86</sup>, Mg<sub>3</sub>Cd<sup>87</sup>, Mg<sub>0.95</sub>In<sub>0.05</sub><sup>88</sup>, Mg<sub>3</sub>Ag<sup>89</sup>, Mg<sub>2</sub>Si<sup>90</sup>, Mg<sub>5</sub>Ga<sub>2</sub><sup>91</sup>, Mg<sub>3</sub>LaNi<sub>0.1</sub><sup>92</sup>), addition of catalysts (such as B<sup>93</sup>, Co<sup>94</sup>, Cu<sup>95</sup>, Fe<sup>96</sup>, Ge<sup>97</sup>, Gd<sup>98</sup>), formation of metastable phases<sup>99</sup>, hybrids<sup>100-103</sup>, nanocomposites<sup>104-108</sup> and nanostructured materials (prepared using ball milling<sup>109</sup>, chemical vapour deposition<sup>23</sup>, hybrid combustion<sup>110</sup>, chemical synthesis<sup>111,112</sup> and melt spinning<sup>113-115</sup>) and nanoconfinement<sup>116-119</sup> (to keep the particles in the nanosized regime by restricting their growth using a scaffold). A brief timeline of the developments is given in Table 1. Some of the most promising results have been seen when the nanocomposites have been prepared by combining the high surface or amorphous materials with nanoscale magnesium. For example, polymer embedded Mg nanocrystals have been synthesised without addition of heavy metal catalysts and show ~6 wt.% hydrogen storage at 200°C and 35 bar within 60 min<sup>104</sup>. Hard carbon sphere wrapped Ni-Mg composite have shown 3.5 wt.% hydrogen absorption at 75°C and 30 bar within 200 min<sup>120</sup>. Magnesium nanocrystals have been also been ball milled with metallic glass and Zr<sub>2</sub>Pd alloy to give ~2 wt.% hydrogen absorption at 50°C and 10 bar within 10 min<sup>121</sup>. MgH<sub>2</sub> nanoparticles have also been investigated for hydrogen storage and have shown promising properties<sup>122</sup>. Of recent interest has been introduction of graphene in the composites. MgH<sub>2</sub>

nanoparticles on graphene were synthesised by Xia and co-workers, in which graphene provided the necessary structural support as well as acted as a barrier to prevent the growth of nanoparticles<sup>123</sup>. Mg nanocrystals encapsulated nanocomposite has been proposed by Cho and co-workers, consisting of atomically thin layer of reduced graphene oxide (rGO)<sup>108</sup>. This composite shows 6.5 wt.% hydrogen absorption at 200°C and 15 bar in 120 min. A recent publication by Zhang et al.<sup>22</sup> has shown 6.7 wt.% hydrogen at 30°C under a pressure of 30 bar in ultrafine MgH<sub>2</sub> nanoparticles (4-5 nm). Although this technique does not ensure industrial scale-up production, there has still been continued interest in the Mg based hydrogen storage materials and recent works have shown some considerable progress in reaching towards DOE goals<sup>83</sup>. For details, the reader is referred to the dedicated review articles on the magnesium-based hydrogen storage materials<sup>83,124-126</sup>.

Journal Pre-proof

Table 1 Brief timeline of the progress in the development of magnesium-based hydrogen storage materials.

| Year | Material  | Wt.%<br>H | T<br>(°C) | Ref            |
|------|---|-----------|-----------|----------------|
| 1968 | $\text{Mg}_2\text{NiH}_4$                       | 3.6       | 325       | <sup>85</sup>  |
| 1996 | $\text{La}_2\text{Mg}_{17}-\text{LaNi}_5$       | 3.5       | 250       | <sup>127</sup> |
| 2000 | $\text{MgH}_2-\text{Ge}$                        | 7.6       | 350       | <sup>128</sup> |
| 2001 | $(\text{Mg}_{0.68}\text{Ca}_{0.32})\text{Ni}_2$ | 1.4       | 40        | <sup>129</sup> |
| 2004 | $\text{MgH}_2-\text{Si}$                        | 5         | 20        | <sup>130</sup> |
| 2007 | Mg nanowires                                    | 3         | 100       | <sup>23</sup>  |
| 2013 | $\text{MgH}_2-\text{C}$                         | 5         | 270       | <sup>131</sup> |
| 2014 | $\gamma\text{-MgH}_2$ (1.99 wt%)                | 5         | 300       | <sup>132</sup> |
| 2018 | Ni-Mg-C   | 6         | 200       | <sup>120</sup> |
| 2019 | Mg-Glass-Zr <sub>2</sub> Pd                     | 2         | 50        | <sup>121</sup> |
| 2020 | $\text{MgH}_2$ nanoparticles                    | 6.7       | 30        | <sup>22</sup>  |

Apart from metals, intermetallic compounds also exhibit good hydrogen absorption characteristics, partly due to the large number of interstitial sites present in their crystal structure<sup>133</sup>. For example,  $\text{LaNi}_5$ , an intermetallic compound between La and Ni, readily reacts with hydrogen under ambient temperature and pressure conditions, with a reasonably quick reaction<sup>134</sup>. Although the amount of hydrogen stored by volume in this material is almost equal to the that of liquid hydrogen (71 g/L), the presence of heavy element such as La makes the gravimetric storage capacity dismal (~1.4 wt.% at 25°C and 2 bar)<sup>135,136</sup>. Another important intermetallic compound which has been of lot of interest is TiFe, with the current focus on improving the activation characteristics and enhancing kinetics<sup>137-139</sup>. Several review articles give detailed insight into the developments in the intermetallics for hydrogen storage storage<sup>140-142</sup>.

## 2.5. Complex Hydrides

Complex hydrides form when the ionic hydrides (alkali metal hydrides such as NaH and LiH) react with covalent hydrides (such as  $\text{BH}_3$  and  $\text{AlH}_3$ ), leading to formation of metal salts (such as  $\text{NaAlH}_4$  and  $\text{NaBH}_4$ ). Hydrogen is covalently bonded to the central atom in the anionic unit<sup>143</sup>, consisting of alanates  $[\text{AlH}_4]^{-1}$ , amides  $[\text{NH}_2]^{-1}$  or borohydrides  $[\text{BH}_4]^{-1}$ . They are easier to handle than covalent or ionic hydrides and offer much more stability<sup>144</sup>. Complex hydrides are relatively new among chemisorption based materials and have attracted much attention in the past

decade<sup>145,146</sup>. This is partly due to their high theoretical hydrogen storage capacity in the range of 7-18 wt.%. However, due to their strong interaction with hydrogen (heat of adsorption in the range 40-100 kJ/mol), issues such as irreversibility, high temperature of desorption (>400°C), sluggish kinetics and difficult synthesis protocols have limited their successful use<sup>147</sup>. Some of the earliest studies which indicated their use as an attractive hydrogen storage material proposed TiCl<sub>3</sub> as a catalyst for NaAlH<sub>4</sub><sup>148</sup>. This was followed by use of various other additives such as Sc and Nb (transition metals), Ce and Sm (rare-earth metals) and carbonaceous materials<sup>149,150</sup>. Few other studies also focussed on the use of nano-catalysts such as nano-TiN (5.4 wt.% H at 130°C)<sup>151</sup> and nano-CeB<sub>6</sub> (4.9 wt.%H within 20 min at 180°C)<sup>152</sup>.

Some progress has also been made in overcoming these bottlenecks by using the previously suggested techniques for metal hydrides. Among these, nanoconfinement of complex hydrides in porous materials, coupled with catalytic additive, has been one of the most rapidly explored methods<sup>153-156</sup>. Earliest developments in this area were reported by Blade *et al.*<sup>156</sup>, in which as small as 2-10 nm NaAlH<sub>4</sub> particles were confined in carbon fibers. This led to a sharp decrease in hydrogen desorption temperature to 70°C. At the same time, another study by Zheng *et al.*<sup>153</sup> reported the space confined NaAlH<sub>4</sub> in ordered mesoporous silica and were able to achieve hydrogenation in the temperature range of 125-150°C. NaAlH<sub>4</sub>, confined in nanocrystalline TiO<sub>2</sub> embedded in carbon matrix, has shown 4.5 wt.% hydrogen absorption at 50°C and 100 bar<sup>157</sup>. The hybrid was able to release complete hydrogen at temperatures as low as 63°C. Under a similar strategy, Ti nanoparticles (3-5 nm) were incorporated in amorphous carbon (nano-Ti@C) to enhance the hydrogen storage in NaAlH<sub>4</sub><sup>21</sup>. The nano-Ti@C-NaAlH<sub>4</sub> hybrid showed 5 wt.% hydrogen absorption in 3 min at 100°C and 120 bar. The hydrogen can be released at 140°C within 60 min. The hybrid stays stable till 100 cycles of hydrogen absorption/desorption. However, multiple lacunae need to be overcome before it can fulfil the requirements of a practical storage material. The reader is referred to the review articles on complex hydrides for details<sup>143-146,158-160</sup>.

## 2.6. Core-shell and hollow structures

Novel structures being explored for hydrogen storage include core-shell structures<sup>161</sup>, hollow nanostructures<sup>162,163</sup> and hierarchical structures<sup>164</sup>. Hollow nanospheres, as compared to nanospheres, have the advantages of high surface area, greater structural stability and better chemical inertness<sup>162</sup>. Nitrogen-doped hollow carbon spheres have shown improved performance at ambient temperature, with 2.25 wt.% hydrogen absorption at 80 bar. Hollow glass microspheres have also been explored for hydrogen storage<sup>165</sup>. Among the metal hollow spheres, multi-mode hydrogen absorption philosophy has been demonstrated by Shervani *et al.*<sup>166</sup>, further carried forward by Gupta *et al.*<sup>167,168</sup> and Amaladasse *et al.*<sup>169</sup>. In their work, existence of hydrogen in multiple forms i.e. free gaseous form, weakly adsorbed form, solid solution form as well as compound form has been demonstrated in palladium and

nickel hollow spheres. Although the maximum hydrogen absorption is well below the DOE norms, it forms promising technique for further development of hydrogen storage materials.

A comparison of hydrogen storage capacity with temperature is shown schematically in Figure 3 for selected set of materials. It is evident from the figure that significant strides have been made in the efforts towards development of hydrogen storage materials. On one hand, materials such as MOFs, activated carbons have shown promising hydrogen storage capacity at low temperatures (77 K), complex hydrides and nano-confined structures have been able to show considerable improvement in performance near room temperature (as shown in Figure 2 and Figure 3). Hybrids seem to be most promising among them with characteristics closest to the DOE requirements. However, for a material to be practically viable, it has to be easily amenable to scale up production and provide low cost. Advanced materials such as the hybrids are nonetheless excellent in terms of laboratory use, but their sensitivity to the atmosphere, difficult synthesis process, harmful effects to the environment and sometimes higher cost act as deterrent to their use in the practical applications. It is therefore imperative that efforts are invested in an alternative set of materials which can overcome these limitations, without compromising the underlying performance characteristics. An emerging and promising class of materials in this regard are hydrogen hydrates. They are not only environment friendly, but also low in cost and easy to synthesise. Clathrate compounds are different from either MOF or Zeolites in terms of their flexibility in tuning the structure. Parameters such as temperature, pressure, concentration of guest molecules, among others, can be modified to achieve the desired properties. A brief introduction to the structure and properties of clathrates is given in next section, followed by their hydrogen storage properties. Due to the rapidly growing interest in the field, scientific literature is being continuously reviewed, with a special focus on the thermodynamic and kinetic aspects of the hydrogen clathrates<sup>3,6,170-174</sup>. However, the current review not only covers the essential scientific aspects of the hydrogen clathrates, but correlates them with the theoretical and techno-economical aspects of the field. Distinctively, this review also takes a sharp look at the accuracy of hydrogen characterisation in clathrates, which is one of the biggest challenge prevailing in the solid-state hydrogen storage.

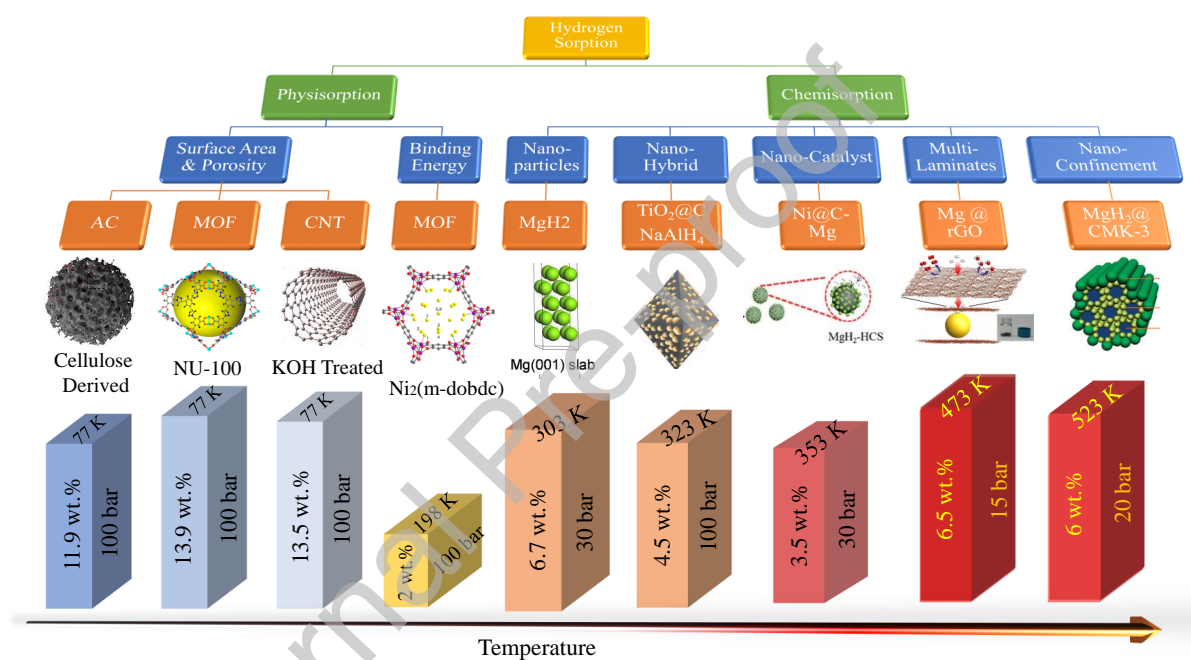


Figure 3. A comparison of hydrogen storage capacity of the various materials with increasing temperature. The materials presented above are (i) AC<sup>17</sup>, (ii) MOF<sup>65</sup>, (iii) CNT<sup>175</sup>, (iv) MOF<sup>68</sup>, (v) MgH<sub>2</sub><sup>22</sup>, (vi) TiO<sub>2</sub>@C,NaAlH<sub>4</sub><sup>21</sup>, (vii) Ni@C-Mg<sup>120</sup>, (viii) Mg@rGO<sup>108</sup> and (viii) MgH<sub>2</sub>@CMK-3<sup>20</sup>.

### 3. Clathrates: Origin and Structure

Clathrates are a class of inclusion compounds, where the guest molecules reside in the cages formed by the host lattice. Clathrates are conventionally classified in two categories based on the interaction of the guest species with the host structure: clathrate hydrates and semi-clathrate hydrates. Clathrate hydrates exhibit weak van der Waal's forces of attraction between the guest molecules and the host. Semi-clathrate hydrates, in addition to van der Waal's interaction, show partial hydrogen bonding between the guest species and the host framework.

A brief outline of the structures formed by hydrogen clathrates is given in Table 2<sup>3</sup>. Pure hydrogen hydrates form sII structure, with a small dodecahedron cage ( $5^{12}$ ) and large hexakaidecahedron cage ( $5^{12}6^4$ ). Other structures of hydrates include sI having similar small cage and large tetrakaidecahedron cage ( $5^{12}6^2$ ) and sH with same smaller cage and irregular dodecahedron ( $4^35^66^3$ ) along with icosahedron ( $5^{12}6^8$ ) as large cages. As per the earlier studies and theoretical estimates<sup>4,176</sup>, it has been observed that the number of hydrogen molecules that can be accommodated in a hydrate depends on the type of cage present;  $5^{12}$  cages can accommodate up to 2 molecules,  $5^{12}6^4$  can accommodate up to 4 molecules,  $4^35^66^3$  cage up to 1,  $5^{12}6^2$  up to 2 and  $5^{12}6^8$  can accommodate up to 5 molecules. Considering the above estimates, hydrogen storage capacities of sI, sII and sH hydrates can reach up to 6.33 wt.%, 4 wt.% and 4.67 wt.%, respectively. One of the important roles played by promoters or secondary guest molecules in the hydrates is the stabilisation of the sI or sH structure with a scope of increasing the hydrogen storage capacity.

In determining which structure is thermodynamically stable, it is important to take into account the molecular diameter of the guest molecule. For example, small molecules such as methane and propane form sI structure (Figure 4), whereas the larger molecules such as THF stabilize the sII structure. The large cages of sII structure act as preferred enclosures for incorporation of these molecules. Further, very small molecules such as  $H_2$  also form sII structure as they have been proposed to occupy small cages (16 such cages), which exceed the total number large cages (8 such cages) in sII structure.

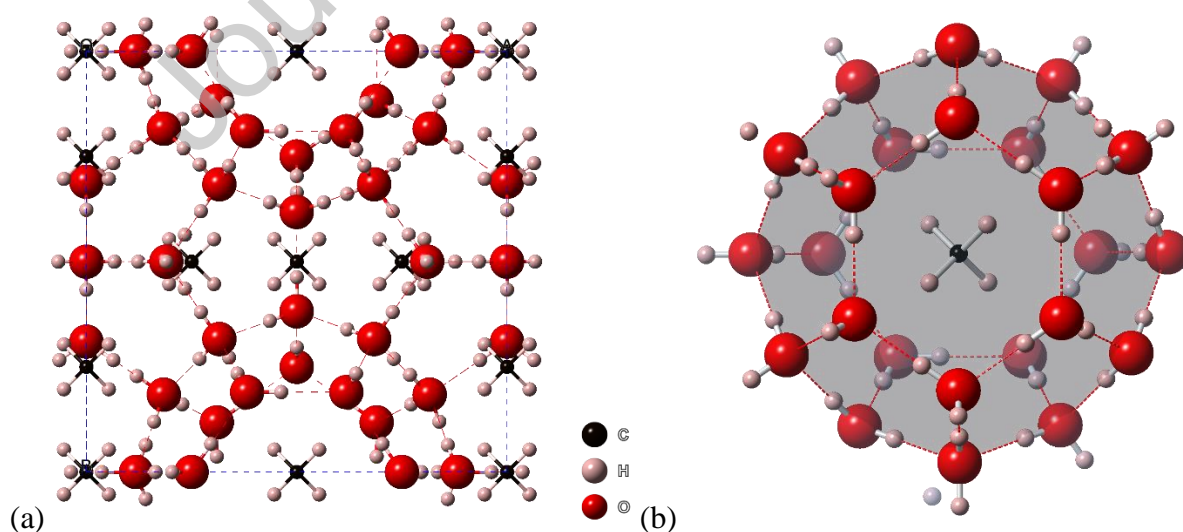
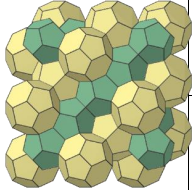
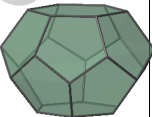
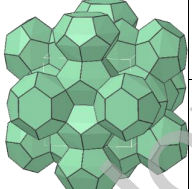
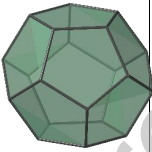
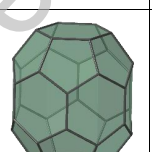


Figure 4. (a) Methane hydrate unit cell forming sI structure and (b) methane molecule enclosed in a large tetrakaidecahedron cage (drawn using Crystal Maker<sup>177</sup>).

Journal Pre-proof

Table 2. Structural properties and hydrogen storage characteristics of clathrate hydrates (structures have been drawn using Crystal Maker<sup>177</sup>).

| Structure Notation | Crystal Structure (space group)   | Cages Present                                       | Cage Characteristics                          | Pictorial Representation  | Cage Type | Number of Cages per unit cell | Max H <sub>2</sub> | Hydrogen Storage Capacity (Wt.%H) | Other Examples of Hosts for the hydrates   |
|--------------------|---|---|---|---|-----------|-------------------------------|--------------------|-----------------------------------|--|
| Type I             |   | Dodecahedron (5 <sup>12</sup> )                     | Twelve 5-vertex faces                         |   | Small     | 2                             | 2                  | 6.33 %                            | Diameter (~5 Å)<br>Methane<br>Ethane<br>Cyclopropane<br>Carbon dioxide<br>Ethylene oxide<br>Hydrogen<br>Sulphide<br>Xenon  |
|                    |   | Tetraicahedron (5 <sup>12</sup> 6 <sup>2</sup> )    | Twelve 5-vertex faces and two 6-vertex faces  |  | Large     | 6                             | 2                  |                                   |  |
| Type II            |  | Dodecahedron (5 <sup>12</sup> )                     | Twelve 5-vertex faces                         |  | Small     | 16                            | 2                  | 4 %                               | Diameter (~4 Å)<br>Argon<br>Helium<br>Nitrogen<br>Oxygen<br>Krypton<br>Neon<br><br>Diameter (~6 Å)<br>Propane<br>Isobutane |
|                    |   | Hexakaidecahedron (5 <sup>12</sup> 6 <sup>4</sup> ) | Twelve 5-vertex faces and four 6-vertex faces |  | Large     | 8                             | 4                  |                                   |  |

|        |   |  |   |   |        |   |   |        |   |
|--------|---|--|---|---|--------|---|---|--------|---|
|        |   |  |   |   |        |   |   |        | Cyclopentane<br>Tetrahydrofuran   |
| Type H |  <p>Hexagonal<br/>(p6mmm)</p> | Dodecahedron<br>(5 <sup>12</sup> )   | Twelve 5-vertex faces   |    | Small  | 3 | 2 | 4.67 % | Diameter (~7 Å)<br><br>2,2<br>Dimethylbutane<br>Methylcyclohexane<br>and<br>Ethylcyclohexane<br>Cycloheptane<br>Cyclooctane<br>Adamantane |
|        |   | Irregular<br>Dodecahedron<br>(4 <sup>3</sup> 5 <sup>6</sup> 6 <sup>3</sup> ) | Three 4-vertex faces, six 5-vertex faces and three 6-vertex faces |   | Medium | 2 | 1 |        |   |
|        |   | Icosahedron<br>(5 <sup>12</sup> 6 <sup>8</sup> )                             | Twelve 5-vertex faces and eight 6-vertex faces                    |  | Large  | 1 | 5 |        |   |

#### 4. Discovery of hydrogen in clathrates: The saga of Tetrahydrofuran (THF)

In a pathbreaking study by Mao *et al.*<sup>4</sup> in 2002, it was proclaimed that pure hydrogen hydrates could store upto 5 wt.% hydrogen under pressure of 200 MPa at 243 K. In spite of the high-pressure conditions reported in this study, it opened up the new vista for search for the holy grail of hydrogen storage. Soon after, Florusse *et al.*<sup>178</sup> used a water soluble reagent (THF) as an additive to bring down the clathrate formation pressure by two orders of magnitude to 5 MPa at 279.6 K. However, this led to a significant drop in the hydrogen storage capacity to 1 wt.%, with single H<sub>2</sub> molecule occupancy in small cages and complete absence in large cages. Florusse *et al.*<sup>178</sup> suggested that THF molecules occupy the large cages, which constraints the presence of hydrogen in these cages and limits the extent of increment possible. However, in an another remarkable study, Lee *et al.*<sup>179</sup> reiterated the use of THF as an additive and showed significantly high hydrogen storage capacity of upto 4 wt.% at 12 MPa and 270 K. This was attributed by Lee *et al.*<sup>179</sup> to the ‘tuning effect’, which allowed hydrogen storage capacity to be increased by controlling the amount of THF in the hydrate. They observed that upon decreasing the amount of THF to 0.15 mol%, the hydrogen occupancy can be increased in the large cages, with co-existence THF and H<sub>2</sub>. They based their postulate on high pressure Raman spectra at different THF concentrations, and additionally confirmed by NMR (under high pressure). Also, in contrast to Mao *et al.*<sup>4</sup>, they confirmed the presence of two H<sub>2</sub> molecules in the small cages. A schematic showing timeline of major events associated with the THF based hydrogen clathrates is shown Figure 5.

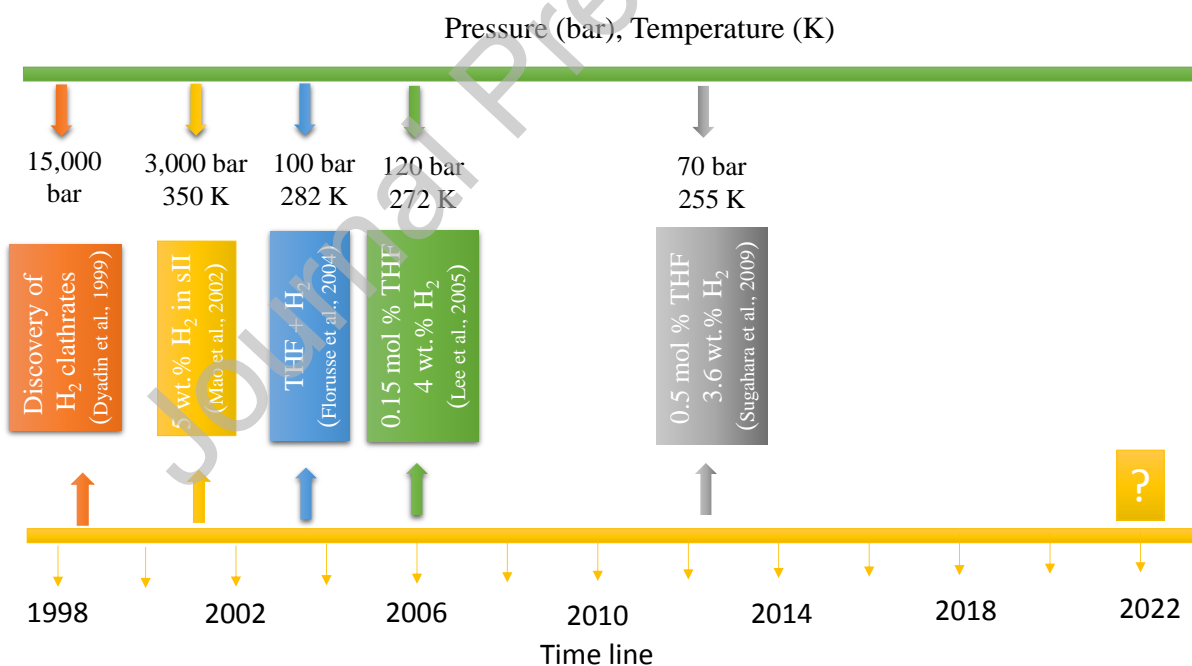


Figure 5. Important milestones in the research path of THF promoted hydrogen clathrates.

With a spike in interest in the field, multiple attempts were made to repeat the promising results of Lee *et al.*<sup>179</sup>. However, only few reported the feasibility of the tuning effect, with most suggesting it to be plainly untenable<sup>180-184</sup>. Strobel *et al.*<sup>180</sup> attributed this aspect to the complete reliance on Raman spectra to quantify the hydrogen storage capacity. To circumvent this issue, they used volumetric gas uptake measurement and observed

maximum 1 wt.% hydrogen uptake, irrespective of the concentration of THF. Raman spectra were in accordance with that of Florusse *et al.*<sup>178</sup>, with maximum one H<sub>2</sub> molecule in small cages. To confirm the observations, Strobel *et al.*<sup>185</sup> used an alternate approach in which concentration of THF was fixed at 5.6 mol%, whereas the pressure of hydrogen was increased to 150 MPa. This would indirectly be similar to the approach of Lee *et al.*<sup>179</sup>, where in lieu of reducing the concentration of THF, the fugacity of hydrogen was increased. They found that at 150 MPa and 250 K, pure hydrogen hydrates showed presence of hydrogen in both small and large cages, whereas the same was not true for the THF based hydrates, as shown in Figure 6 (i). In the latter case, hydrogen only occupied small cages and the larger ones seemed to be fully occupied by THF. Also, Strobel *et al.*<sup>185</sup> found discrepancy in the approach of using the integrated area of the Raman peaks to quantify hydrogen molecules present in each cage. They observed that peak area differed when the spectra was collected at 77 K (0.1 MPa) and 90 K (150 MPa). They ascribed this anomaly to the change in polarization of the hydrogen molecules within the cages, as the internuclear distances even go below the values observed for the solid hydrogen<sup>185</sup>. They concluded that there is need for a more sophisticated technique to accurately characterise the amount of hydrogen present in the cages. In light of these findings, Nishikawa *et al.*<sup>186</sup> performed in-situ Raman spectroscopy measurements on THF promoted (less than stoichiometric concentration) hydrogen hydrates at 74.3 MPa and 265 K. They have reported that hydrogen molecules (with upto double occupancy) are present in large cages along with THF. The occupancy in small cages could not be distinguished in this study due to overlap with fluid phase hydrogen. This led to further support for the 'tuning effect'. However, the measurement system proposed by Nishikawa *et al.*<sup>186</sup> could not accurately quantify the amount of THF added and thus provided only qualitative comparison across earlier works.

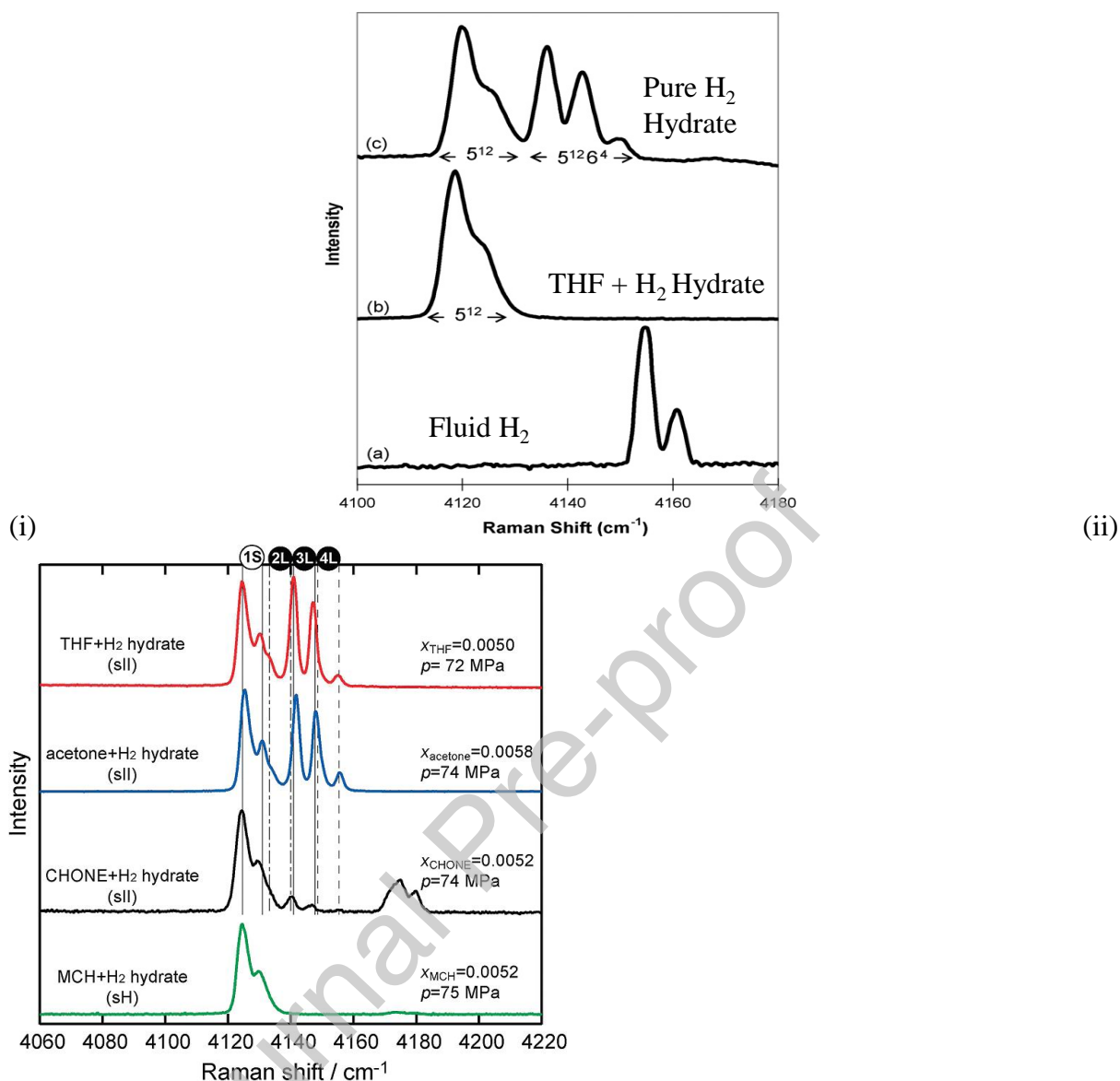


Figure 6. (i) Raman spectra of (a) fluid hydrogen, (b) THF (5.6 mol%) + H<sub>2</sub> hydrate (adapted with permission from Strobel *et al.*<sup>185</sup>, Copyright 2007 Elsevier Ltd). (ii) Raman spectra of non-stoichiometric concentration of guest molecules (THF, acetone, CHONE, MCH) measured ex-situ at 77 K and 0.1 MPa (reprinted with permission from Sugahara *et al.*<sup>187</sup>, Copyright 2010 American Chemical Society).

To investigate the effect of THF on the hydrogen storage capacity of the clathrates, Liu *et al.*<sup>188</sup> carried out *ab initio* molecular dynamic simulations. They showed that small cages are occupied by a single hydrogen molecule while in the large cages one THF molecule is likely to coexist with one hydrogen molecule. It was also observed that the interaction of a THF molecule with the host water framework leads to a slight distortion of the clathrate network, where large cages shrink and small cages expand. However, this effect is diminished as the hydrogen occupancy in the cages increases. They have predicted a hydrogen storage capacity on THF promoted clathrates in the range of 1.6 to 3.8 wt.%, depending on the concentration of the THF promotor<sup>188</sup>. This is in accordance with the experimental studies of Lee *et al.*<sup>179</sup> and Sugahara *et al.*<sup>187</sup>. In another study, Papadimitriou *et al.*<sup>189</sup> carried out Monte Carlo simulations on binary THF+H<sub>2</sub> hydrates assuming that the concentration of THF would not

influence the hydrate's hydrogen storage capacity, in accordance with experimental observations of Strobel *et al.*<sup>180</sup>. Their calculated uptakes were very similar to experimental results, especially from NMR spectroscopy. These results agreed with the previous observation by Strobel *et al.*<sup>180</sup> showing single occupancy of hydrogen molecules in small cages and showed uptakes very close to the maximum assumption of single H<sub>2</sub> occupancies in the large (THF-occupied) and small clathrate cages.

The assignment of peaks in Raman spectra for the hydrogen molecules in large cages has been subjected to debate in literature. To study this aspect in detail, Strobel *et al.*<sup>190</sup> have prepared simple hydrogen hydrates under a pressure of 200 MPa at 250 K and carried out ex-situ Raman spectra measurement at 77 K (after quenching in liquid nitrogen). All the peaks were observed to be red-shifted with respect to the free hydrogen. Highest frequency Raman peaks were assigned to the quadruple occupied hydrogen, middle range frequency to triply occupied hydrogen, lower range frequency to the doubly occupied hydrogen. This is in line with the argument that as density of molecules in a cage increases, greater repulsion between potential surfaces takes place, thus increasing the vibrational frequency of hydrogen molecules. This assignment of peaks is also in accordance with the observation by Lokshin *et al.*<sup>191</sup> carried out using high pressure Neutron diffraction. However, Gianassi *et al.*<sup>192</sup> have proposed a different peak assignment under similar conditions. They have assigned the peaks to triple, double and single occupation in the order of decreasing frequency. Their assignment was based on the integrated intensities of Raman peaks arising due to presence of hydrogen molecules in small and large cage. A possible reason for the discrepancy in assignment of peaks in literature can be due to change in Raman scattering cross-section of the hydrogen molecules with local environment. It is evident from the frequency shift, observed for molecules packed in a cage, that the polarizability of hydrogen molecules is also subject to change<sup>190</sup>. At the same time, at high hydrogen concentration, the interaction of the molecules with the electromagnetic radiation increases, as is evident from the larger breadth of the high frequency bands. To unequivocally explain the phenomenon, detailed quantification using other techniques such as NMR cross calibration is needed<sup>193</sup>. On the whole, there still seems to agreement to the qualitative assignment of Raman bands, with increasing intensity of Raman peaks demonstrating higher occupancy of the cages.

The subject of Raman band assignment has also been computationally dealt by Plattner & Meuwly<sup>194</sup>. They have used atomistic MD simulations to calculate the frequency shifts for hydrogen clathrate hydrates and study the effect of temperature and pressure on the spectra. It has been observed that optimising the structures before frequency calculations leads to overestimation of frequency shifts. Their observed frequency shifts lie within the range of experimental peak maxima observed at 4120 cm<sup>-1</sup> (-35) and 4148 cm<sup>-1</sup> (-7) under pressure of 2000 bar at 99 K. Consideration of quantum dynamical effects leads to shift in frequency for two H<sub>2</sub> in 5<sup>12</sup> cages by 47 cm<sup>-1</sup> (MP2 calculations) at 50 K. The shift in frequency for large cages is small and is less affected by increase in the H<sub>2</sub> molecules, which is also in agreement with the experimental results. The reason for this has been attributed to the distance between the hydrogen atom in a molecule and neighbouring oxygen atom in water molecule. In smaller cages these distances decrease with increase in density of H<sub>2</sub>, whereas these are least affected in the larger cages. The overall differences are less pronounced at higher temperature than at lower temperatures. Computations performed on periodic systems help to capture the effect of lattice vibrations of clathrate molecules. In other words, periodic

system are able to quantify the effect of molecules at large distances. Frequency for two H<sub>2</sub> molecules in small cage 5<sup>12</sup> reduces by 17 cm<sup>-1</sup> at 150 K and increases by the same amount at 50 K due to 1000 bar pressure. This confirms that frequency not only dependent on the number of molecules occupying a cage, but also on pressure (more sensitive at higher pressures).

In majority of the above measurements, the hydrates were prepared separately in high pressure cells and quenched in liquid nitrogen after release of pressure, for subsequent ex-situ characterisation using Raman spectroscopy or X-ray diffraction. It has been suspected that the peaks observed in Raman spectroscopy during ex-situ measurements are due to the formation of hydrates upon quenching and not as per the formation conditions proposed<sup>195</sup>. To bring light to this anomaly, Grim *et al.*<sup>195</sup> have proposed a method of 'hydrate seeding' in which a preformed hydrate is mixed with the powdered ice, before beginning the process of hydrate formation. The hydrate had a lower concentration of promoter (0.55 mol % THF) and was kept under hydrogen pressure a shorter time (~4 hours), as compared to a reference hydrate with 5.6 mol % THF and hydrate formation time of 3-4 days. Both samples were quenched in liquid nitrogen for 20 min upon release of pressure for ex-situ characterisation. It was observed that the 'hydrate seeded' sample shows formation of hydrates at par with the non-hydrate seeded sample, despite having lower concentration of THF (0.5 mol%). This led Grim *et al.*<sup>195</sup> to conclude that liquid nitrogen quenching might lead to unintended growth of hydrate, especially in the non-stoichiometric samples where a some part of the ice was always left without conversion to hydrate. Hence, the 'tuning effect' proposed earlier might be due to pure hydrogen hydrate formation during liquid nitrogen quenching seeded by the surrounding hydrates, instead of THF promoted hydrates. This was unlike the proposed mechanism by Lee *et al.*<sup>179</sup> and Sugahara *et al.*<sup>196</sup>.

An important difference in all the above studies was the method of preparation of hydrates, which might have resulted in discrepancy in the observed results, as observed by Sugahara *et al.*<sup>196</sup>. According to the authors, the rate of hydrate formation was one of the key factors hampering the realisation of 'tuning effect'. To demonstrate this, Sugahara *et al.*<sup>196</sup> used ice and solid THF under pressurised hydrogen gas environment at 77 K and slowly heated the mixture. They observed 3.6 wt.% H<sub>2</sub> storage capacity upon decreasing the THF concentration to 0.5 mol% at 70 MPa and 255 K. Solid THF starts melting at 164.7 K and its high mobility provides rapid rate of hydrate formation. This was in line with the 'tuning effect' and confirmed the observations of Lee *et al.*<sup>179</sup>. This theory was also supported by Lokshin *et al.*<sup>191</sup>, where the rate of hydrate formation upon direct reaction with ice was 100 times faster than that with water, in the temperature range of 77-273 K. On the basis of this evidence, Sugahara *et al.*<sup>196</sup> proposed that during hydrate formation, an intermediate metastable structure is formed which favours encapsulation of hydrogen molecules in the large cages. However, this 'tuning effect' is not observed when the pressurised hydrogen is in contact with the aqueous solution of THF, as was the case in the experiments carried out by Hashimoto *et al.*<sup>182</sup>. A recent study by Zhong *et al.*<sup>197</sup> has shown that it may be possible to trap two hydrogen molecules in the small cages of THF promoted hydrates, leading to hydrogen storage capacity of 3.08 wt.% under moderate conditions of 3.8 MPa and 273 K. However, the hydrate formation was limited to the surface layer of less than 0.5 mm in thickness, beyond which the hydrogen occupancy decreased to single molecule in a time frame of 24 hours. Controversy surrounding the hydrogen storage capacity of THF promoted hydrogen

hydrates has refused to die down, with few recent studies still not fully convinced of the high capacity achieved using the ‘tuning effect’<sup>198–200</sup>.

## 5. Secondary Guest Molecules Promoted Hydrogen Clathrates

As seen in the previous section, binary hydrates consist of a secondary guest molecule along with hydrogen which stabilises the structure due to its higher affinity for the host water molecules. Detailed study carried out by Belosludov *et al.*<sup>176</sup> suggested a set of criteria for selection of ‘ideal’ promoter molecule for formation of binary hydrate with low pressure and high hydrogen storage capacity. The requisite criteria state that: (a) the size of the promoter should be similar to the cavity size of the smaller ( $5^{12}$ ) cage, (b) it should be able to form both s-I and s-II hydrates in pure form and (c) among the above two structures, s-I should be more stable<sup>176</sup>. Many other promoters have been exploited for the advantage of hydrogen storage properties in clathrates and form an important foundation for the future developments in the field.

### 5.1. Hydrocarbons

Among the gaseous additives or co-guests, hydrocarbons have recently been explored as secondary guests in hydrogen clathrates. Hydrocarbons, at the same time, also provide an additional energy medium, as opposed to hydrophobic promoters such as THF which provide no additional advantage. Pure hydrocarbons such as methane form gas hydrates under far milder conditions than pure hydrogen hydrates. For example, propane forms hydrates under mild pressure (0.2 to 0.5 MPa) in the temperature range of 274.15 to 278.15 K<sup>201</sup>. Methane has been the most sought after hydrocarbon with the lowest weight penalty on the hydrogen storage capacity<sup>202</sup>. Moreover, it has been postulated that since methane has a smaller size than THF, hydrogen may be accommodated in the large cages along with methane and thus enhancing the hydrogen storage capacity. Early investigation into the  $H_2-CH_4-H_2O$  system were carried out by Skiba *et al.*<sup>203</sup>, using a gas mixture of 40 %  $H_2$  and 60 %  $CH_4$  in direct contact with ice to form hydrates at 20 MPa and 259 K. However, they failed to observe any evidence of hydrogen in the formed hydrates; methane occupied both small and large cages forming pure methane hydrates. Following this, Skiba *et al.*<sup>204</sup> reported formation of propane promoted hydrogen hydrates at 24 bar and 259 K, with single occupancy of hydrogen molecule in sII structure. This led to many theoretical and experimental studies to investigate the addition of hydrocarbon as promoter in hydrogen hydrates<sup>205,206</sup>.

#### 5.1.1. Methane

Matsumoto *et al.*<sup>202</sup> have shown that when added in concentration of 5 mol% (gas phase), methane reduces the pressure of hydrogen clathrate formation to 50 MPa at 263 K. However, under these conditions, sI structure is formed with single hydrogen molecule occupying the small cage and two hydrogen molecules occupying large cage. The hydrate undergoes phase transformation upon further increase in pressure to 70 MPa. The new phase with sII structure nucleates at the end of 5 h, taking as long as 24 hours for the transformation to complete<sup>202</sup>. The plot showing change in structure with pressure and composition of methane in the gas mixture is shown in Figure 7 (i). It has been proposed that formation of metastable sI structure acts as seed for the nucleation of the sII. The structure sII shows single occupancy of small cages and quartet occupancy for large cages at 263 K and 70 MPa, as confirmed by in-situ Raman spectroscopy<sup>202</sup>. Since, it was not possible to estimate the

hydrogen storage capacity from the experimental data, thermodynamic modelling using der Waals and Platteuw (vdWP) theory was used. It was found that structure sI stores 0.02 wt.%  $H_2$ , whereas the structure sII stores 0.31 wt.%  $H_2$ <sup>202</sup>. The hydrogen storage capacity of these hydrates remained far below the practical requirements.

To explore the additional possibility of increasing the capacity and theoretically estimate the amount of hydrogen that can be entrapped in these hydrates, computational model were developed by Belosludov *et al.*<sup>176</sup>. They studied thermodynamic stability and cage occupancy of the binary  $CH_4+H_2$  hydrates with both s-I and s-II structure using van der Waals and Platteuw (vdW-P) theory under various temperatures and pressures. It has been observed that ~6 % gas phase concentration of methane can stabilise s-I structure at 250 K with hydrogen storage capacity of 1.75 wt.%, but under extreme pressure conditions of 200 MPa. However, structure s-II is stable at 250 K and 70 MPa, with a higher hydrogen storage capacity of 2.6 wt.%. While the hydrogen storage capacity obtained by experimentation were smaller, this fuelled further interest in the investigation of hydrocarbon-based hydrate promoters. The stability of  $CH_4+H_2$  hydrates has been evaluated by Zhang *et al.*<sup>207</sup> using molecular dynamics simulations. They have reported co-occupancy of hydrogen and methane in the large cages, with upto three hydrogen molecules present.

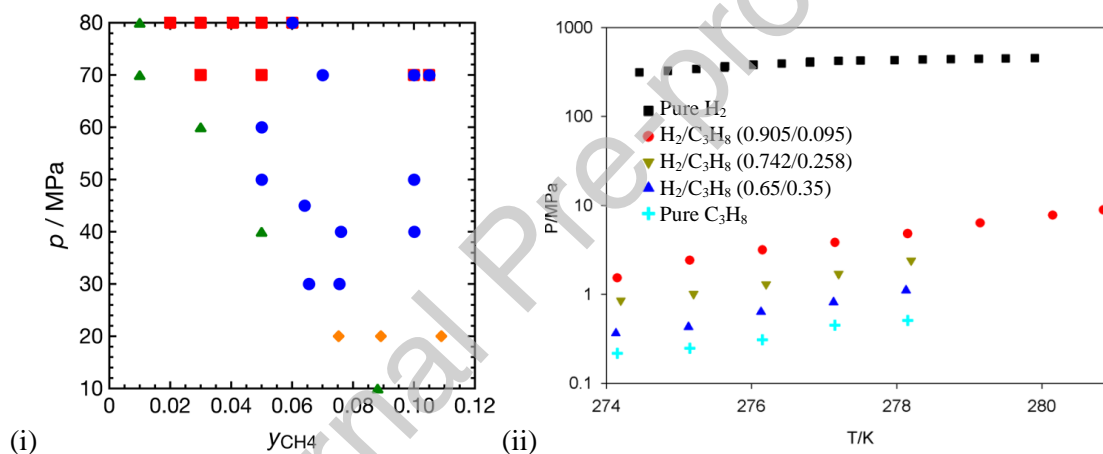


Figure 7. (i) Hydrate structures at different pressure and composition of methane (in  $H_2+CH_4$  gas mixture) at 263 K and  $t = 72$  h (circles represent sI hydrate, squares sII hydrate, diamonds simple methane sI hydrate and triangles no hydrate formation, reprinted with permission from Matsumoto *et al.*<sup>202</sup>, Copyright 2014 American Chemical Society) (ii) Phase equilibrium plots of propane promoted hydrogen gas hydrates. Similar plots for pure propane and pure hydrogen hydrates have been overlaid for clarity (adapted with permission from Veluswamy *et al.*<sup>208</sup>, Copyright 2015 American Chemical Society).

### 5.1.2. Propane and Butane

Propelled by interest in computational and experimental studies in methane promoted hydrogen hydrates, higher hydrocarbons such as propane and butane were examined as promoter molecules. Veluswamy *et al.*<sup>208</sup> have reported that addition of 9.5 mol% propane to hydrogen brings down the equilibrium pressure to 1.53 MPa at 274.2 K (Figure 7 (ii)). However, sluggish kinetics remains a drawback with approximately 16 hours required at 8.5 MPa for clathrate formation. This can be drastically reduced to 30 min by addition of small amounts (500 ppm) of SDS to the propane and hydrogen mixture<sup>209</sup>. In spite of the benefit, their hydrogen storage capacity of still remains low at 0.032 wt.%<sup>208</sup>. Koh *et al.*<sup>210</sup> have shown promising results by experimentally investigating propane and isobutane as guest

molecules. As the structure s-II consist of 16 small cages vis a vis 8 large cages, a small change in the hydrogen occupancy in small cage from single to double, leads to significant increase (~1-2 wt.%) in overall hydrogen storage capacity of hydrate. Keeping this in view, sII hydrate structure with stoichiometric (5.56 mol%) and non-stoichiometric (1 mol%) amounts of propane were compared in terms of their hydrogen occupancy. They have reported that above 30 MPa at 243 K, stoichiometric amount of propane helps to expand the lattice by ~1 % (3 % by volume), as confirmed by synchrotron high resolution XRD. This leads to hydrogen storage capacity of 2.29 wt.% for sII hydrate<sup>210</sup>. This assumption has been verified by GCMC simulations using different promoters such as THF or iso-butane, and the results remain consistent as long as the lattice expansion of similar magnitude is observed<sup>210</sup>.

This study highlights the importance of cage dimensions in tuning the hydrogen storage capacity of the clathrate hydrates. Raman spectroscopy further confirms that propane molecules occupy large cages, thus leaving the small cages to be filled with two hydrogen molecules. However, when the concentration of propane was diluted to 0.5 or 1 mol%, it was found that up to four hydrogen molecules could be accommodated in the larger cages, with single occupancy in small cage. This increases the hydrogen storage capacity to 3.84 wt.%<sup>210</sup>. However, in both the cases, the occupancy of hydrogen in small cages is dependent on temperature of measurement, since Raman and HRXRD measurements were carried out ex-situ at 77 K. Koh *et al.*<sup>210</sup> have observed that upon gradual increase in temperature, double occupancy in small cage starts to diminish at 90 K, with single hydrogen molecule frequency disappearing at 160 K. Similar trend has been observed for the deuterium in the large cages (simple hydrogen hydrates), from four H<sub>2</sub> molecules at 80 K to lowering down to two at 160 K.<sup>211</sup>

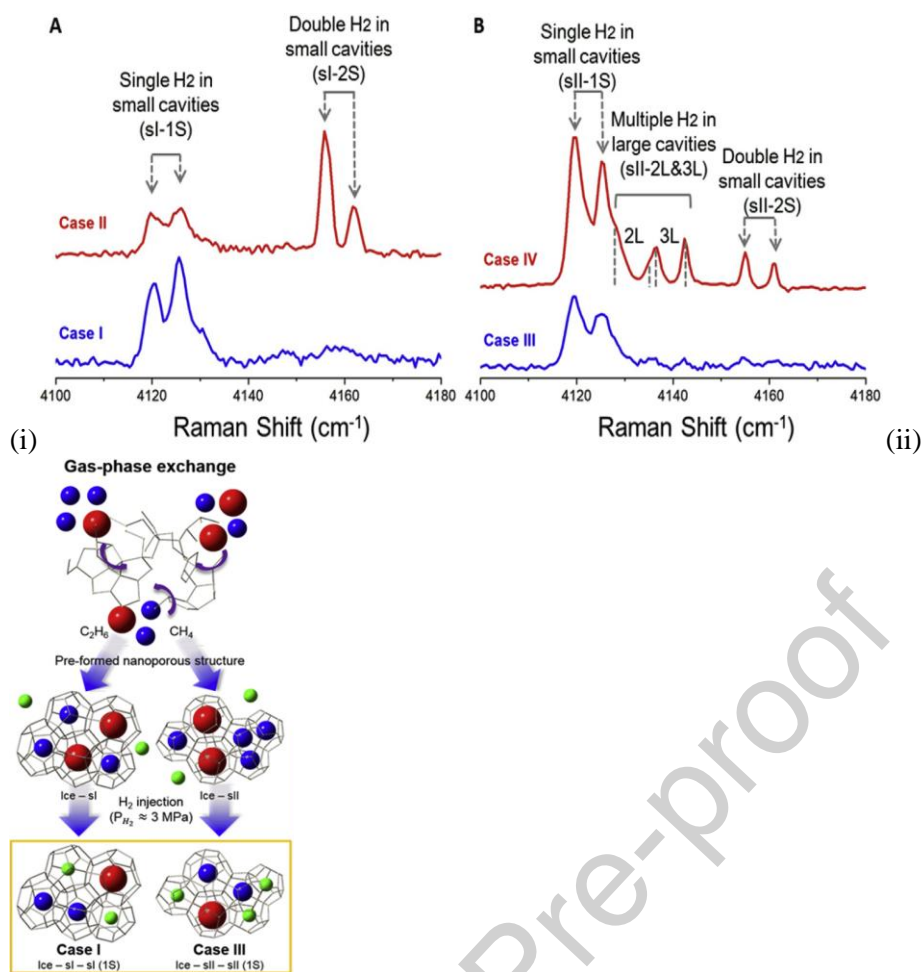


Figure 8. (i) H–H vibron region in Raman spectra of the (A) sI hydrates (Cases I and II) and (B) sII hydrates (Cases III and IV) showing the direct evidence of multiple H<sub>2</sub> occupancies. (ii) A schematic showing the transformation of ice phase to the hydrate structure in case of direct reaction of ice with the gas mixture. (Reprinted with permission from Ahn *et al.*<sup>212</sup>, Copyright 2020 Elsevier Ltd).

In line with the experimental studies highlighting the importance of dimension of the cage on the clathrate formation, Li *et al.*<sup>213</sup> have used high level quantum chemical methods for investigating the same. They have found that the bond energy between hydrogen molecules in a cluster is a sensitive function of the side length of hydrate cages. The bond energy decreases sharply with increase in the cage dimension to 2.84 or 2.86 Å for small cage (2.82 Å without hydrogen), suggesting a possibility of incorporation of upto 4 or more hydrogen molecules. This leads to a hypothesis for stability of hydrogen molecules upon incorporation of promoter molecules. Promoter molecules (such as THF or TBAB) occupy the large cages and in turn help in increasing the edge length of the neighbouring small cages. One of the important requirements of estimation of hydrogen storage in clathrates by simulations is the accurate determination of the interaction energies. This aspect becomes even more significant for weak interactions such as those between the hydrogen molecules in a cluster. For accurate results, Li *et al.*<sup>213</sup> have used CCSD(T) level to calculate these interactions. At the same time, to accurately carry out QM calculations, large basis set have been used by Li *et al.*<sup>213</sup> which include polarization, diffusion and floating functions. An important work highlighting the importance of lattice parameter on the hydrogen storage capacity of sII structure has been done by Papadimitriou *et al.*<sup>214</sup>. Using GCMC simulations, they have found that increase in lattice parameter of 3 % could lead to increase in the

hydrogen storage capacity by 13 %, for the measurements in the pressure range of 100-300 MPa. However, this effect is seen pronounced only in the large cages, with the smaller cages remain unaffected by the changes in lattice parameter. At the same, the number of small cages (singly occupied hydrogen) and large cages (with 2-4 hydrogen) decreased with increase in lattice parameter<sup>214</sup>. Both these studies further support the experimental observations reported by Koh *et al.*<sup>210</sup>.

### 5.1.3. Mixed Hydrocarbons

To explore further scope of addition of hydrocarbon to the hydrogen clathrate, methane and propane mixture has been used as a promoter by Ahn *et al.*<sup>212</sup>. They observed hydrogen storage capacity of 1.78 wt.% under moderate conditions (9 MPa and 250 K). An important aspect of this work has been the direct reaction of powdered ice with mixture of hydrogen, methane and propane gas. Whereas, the reaction of the hydrogen with pre-formed hydrates (of methane and propane) under similar conditions, failed to produce the desired results. The composition of the gas mixture also had a direct impact on the type of structure and subsequently the hydrogen storage capacity of the hydrates. Higher concentration of methane (90%) in the feed gas produced sII structure with higher capacity (1.7 wt.% H<sub>2</sub>), whereas lower concentration (70%) leads to the formation of sI structure (0.67 wt.% H<sub>2</sub>)<sup>212</sup>. Ex-situ Raman spectroscopy carried out at 77 K has revealed a double occupancy of small cages as well as possibility of double to triple occupancy for large cages. This is the first direct evidence of double hydrogen occupancy in small cages found using Raman spectroscopy, although NMR spectroscopy has provided such evidence in the past<sup>179</sup>. The blue shift observed for the double occupancy in the small cages has also been confirmed by computational techniques<sup>194</sup>. It has been suggested that due to the small size of methane as compared to other hydrocarbons, it occupies small cages of hydrate structures and is further substituted by hydrogen in a so called 'replacement reaction'<sup>212</sup>. Ahn *et al.*<sup>212</sup> also observed that directly formed clathrates had ~0.5% larger edge length as compared to indirectly formed ones, thus confirming the previously stipulated role of the cage dimension upon the hydrogen occupancy by Koh *et al.*<sup>210</sup> and Li *et al.*<sup>213</sup>.

## 5.2. Alkyl Amines

Alkyl amines come under a rare class of additives which typically form semi clathrates, with directional hydrogen bonding in stoichiometric hydrates. However, it has been observed that they may undergo structural transformation upon the incorporation as secondary guest molecules such as methane<sup>215,216</sup>. To investigate this in detail, Park *et al.*<sup>217</sup> have employed iso-propylamine (i-PA) and n-propylamine (n-PA) as guest in hydrogen clathrates and examined their behaviour at concentration ranging from 1 to 13.3 mol%. It has been observed that i-PA clathrates with concentration below 5.6 mol% displayed sII structure, with possible 'tuning effect' observed in these hydrates. It was seen that 1 mol% i-PA showed double occupancy of small cages and triple occupancy of large cages (confirmed using ex-situ Raman spectra), unlike the higher concentration (i-PA = 5.6 mol%) hydrates. This amounts to hydrogen storage capacity of 3.08 wt.% at 40 MPa and 243 K. However, similar phenomenon was not observed in another isomer of propyl amine (n-PA), with single occupancy of hydrogen molecules reported irrespective of concentration of n-PA molecules. Crystal structure of n-PA clathrates was indexed to be monoclinic, with no transformation observed with changes in the additional parameters (such as concentration, temperature and

pressure). Park *et al.*<sup>217</sup> have ascribed this to the presence of hydrophilic group in the middle of the ring as in i-PA, unlike at the end of the ring present in n-PA. The same is also applicable to additives such as THF and acetone, which have shown favourable hydrogen absorption. This is shown in Figure 9, highlighting the hydrophilic group. This was significant as few studies have been reported which examine the structural transformation in these systems and this opens new vistas for exploration of suitable hydrogen storage material<sup>218</sup>.

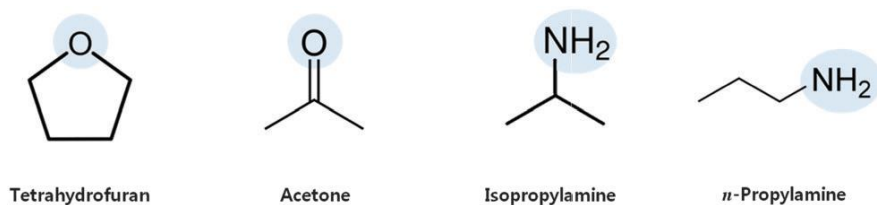


Figure 9. Molecular structures of THF, acetone, i-PA and n-PA (blue circle represents the hydrophilic group in the organic compound). Reprinted from Park *et al.*<sup>217</sup> with permission from the PCCP Owner Societies.

### 5.3. Inert Gases (Ar and N<sub>2</sub>)

Diatomic gases have also been utilised as promoters for the hydrogen clathrates. Amano *et al.*<sup>219</sup> have investigated hydrogen hydrates promoted by Ar gas using in-situ as well as ex-situ Raman spectroscopy measurements. They have observed hydrogen occupancy in large cages as well as small cages at 27 MPa and 276.1 K, with 37 mole % H<sub>2</sub> present in the Ar-H<sub>2</sub> gas mixture. The same results were obtained by ex-situ Raman spectroscopy measurements with upto four H<sub>2</sub> molecules observed in large cages and one molecule in small cages. Another idea of using N<sub>2</sub> as a guest in the clathrate was first floated by Lu *et al.*<sup>220</sup> in 2012. They reported formation of clathrates under mild conditions of 243 K and 15 MPa, with hydrogen reported to be present in both small and large cages. Although they could not produce homogenous and uniform samples in their experiments, hydrogen occupancy results were close to the earlier reports on pure hydrogen hydrates, with two hydrogen molecules present in small cage and four hydrogen molecules in the large cage<sup>220</sup>.

To study the potential of nitrogen as a guest in hydrogen clathrate hydrates, Liu *et al.*<sup>221</sup> have used *ab initio* and standard molecular dynamics calculations in their work. They observed that replacing N<sub>2</sub> with H<sub>2</sub> is thermodynamically favourable in small cages, whereas the large cages favour coexistence of the both molecules. This reflects the close similarity with the experimental observations of Park *et al.*<sup>222</sup>. Liu *et al.*<sup>221</sup> observed presence of 2L-1S as stable configuration from thermodynamics calculations, whereas 3L-2S configuration was favoured under dynamic conditions, at 243 K and 15 MPa. This leads to theoretical hydrogen storage capacity of 2.5 wt.% for the first case (thermodynamically favourable) and 4.4 wt.% for the second case (dynamically favourable)<sup>221</sup>.

### 5.4. Mixed Promoters (Inert Gas and Solid/Liquid)

Park *et al.*<sup>222</sup> proposed addition of solid additives (hydrate forming THF & non-hydrate forming PRD) to the existing N<sub>2</sub> as a guest molecule at 35 MPa and 243 K. The addition of 1 mol% THF with N<sub>2</sub> showed improved hydrogen storage capacity of 2.24 wt.%, with double and quartet occupancy in small and large cages. This was attributed to the 'exchange mechanism' between nitrogen and hydrogen, in which hydrogen replaces the larger diameter nitrogen molecule, thus allowing for reduction in the cage dimensions.

Synchrotron XRD data showed the lattice parameter decreased upon increasing the amount of hydrogen in the cages, confirming the stipulated ‘exchange mechanism’. Also, it was observed that ‘exchange mechanism’ was dominant in small cages, with large cages preferring co-existence of N<sub>2</sub> and H<sub>2</sub> molecules for stability<sup>222</sup>. This was evident from higher hydrogen occupancy seen in the large cages for the PRD+N<sub>2</sub> samples when the partial pressure of hydrogen was reduced to 15 MPa, with remaining gas being N<sub>2</sub> (total pressure of 35 MPa)<sup>222</sup>.

### 5.5. Greenhouse Gases (SF<sub>6</sub> and CO<sub>2</sub>)

Considering the fact that almost all the studies done previously had formation >10 MPa, Lee *et al.*<sup>223</sup> suggested the use of SF<sub>6</sub> as a promoter molecule, which forms hydrates even under atmosphere pressure below 273 K. This was significant as it posed a double advantage: bringing down the hydrogen hydrate formation pressure as well as capturing an extremely potent greenhouse gas, SF<sub>6</sub>, with impact on the atmosphere greater than 23900 times than CO<sub>2</sub>. Molecular size of SF<sub>6</sub> is big enough (~6 Å) to occupy the large cages of the sII structure, leaving the small cages empty for hydrogen. Their study reveals formation of metastable structure, under the formation conditions of 0.5 MPa and 263 K, with single hydrogen molecule present in the small and large cages<sup>223</sup>. However, the presence in large cage is lost with the passage of time, coupled with reduction in the number of small cages occupied. The intensity of Raman bands has been observed over a period of 6 days with significant drop seen in the initial 2-3 days. It is expected that hydrogen molecules diffuse through the large cages until they find an empty small cage. Although it does not represent a significant development with respect to the hydrogen storage capacity (0.014 wt.%), it reflects important development in exploration of new promoter molecules with an ability to co-host the hydrogen in the large cages near ambient temperature and pressure<sup>223</sup>.

In order to study the occupation of hydrogen in sI clathrates, Grim *et al.*<sup>224</sup> used sI hydrate formers (CO<sub>2</sub> and CH<sub>4</sub>) as secondary guests to hydrogen hydrates with sI structure (258 K and 70 MPa). This has been possible by carefully controlling the conditions to be present in the sI phase region of the phase diagram. They have observed, in accordance with the sII structures, hydrogen starts filling with small cages. However, presence of upto two hydrogen molecules in large cages has been observed using Raman spectroscopy along with CH<sub>4</sub>/CO<sub>2</sub> at 70 MPa, as shown in Figure 10 (ii). Upon increase of pressure to 130 MPa, no extra peaks appear in the spectrum. This is unlike the behaviour observed in the sII structure, where the occupancy of four hydrogen is observed at 140 MPa. Monte Carlo simulation studies on the hydrogen occupancy in sI structures have reported that 5<sup>12</sup>6<sup>2</sup> large cages can store upto three molecules, which is in close agreement to the experimental observations<sup>225</sup>. Theoretical estimates show that hydrogen storage capacity of these structures is close to 3.2 wt.%, which is comparable to the THF promoted hydrogen clathrates.

### 5.6. Tertiary alcohol

To throw more light on the phenomenon observed by Prasad *et al.*<sup>226</sup>, Tanabe *et al.*<sup>227</sup> studied phase equilibrium for the (t-BA)-H<sub>2</sub>O-H<sub>2</sub> system. They have observed that in the absence of hydrogen, t-BA occupies large cages of the sVI hydrate structure and no structural phase changes are observed upto 112 MPa at a fixed concentration of 9.3 mol% t-BA. However, when hydrogen is added to the system at 25.3 MPa and 274 K, it transforms to sII structure. The transformation pressure reduces to 2.35 MPa and 267 K if the concentration of

t-BA is reduced to 5.6 mol%, as shown in Figure 10<sup>227</sup>. Notably, the stoichiometric concentration has a lower transformation pressure than non-stoichiometric one. As seen from the Raman Spectra, no hydrogen occupancy is observed below the transformation pressure in the small 4<sup>454</sup> cages of sVI hydrate. In the sII structure, hydrogen was seen to occupy small cages. This shows that the smaller cages of sVI structure are not favourable for the occupation of hydrogen. This led Tanabe *et al.*<sup>227</sup> to propose that pressure alone cannot be a driving force for the structural transformation and presence of smaller guest molecules such as methane or hydrogen was essential for it.

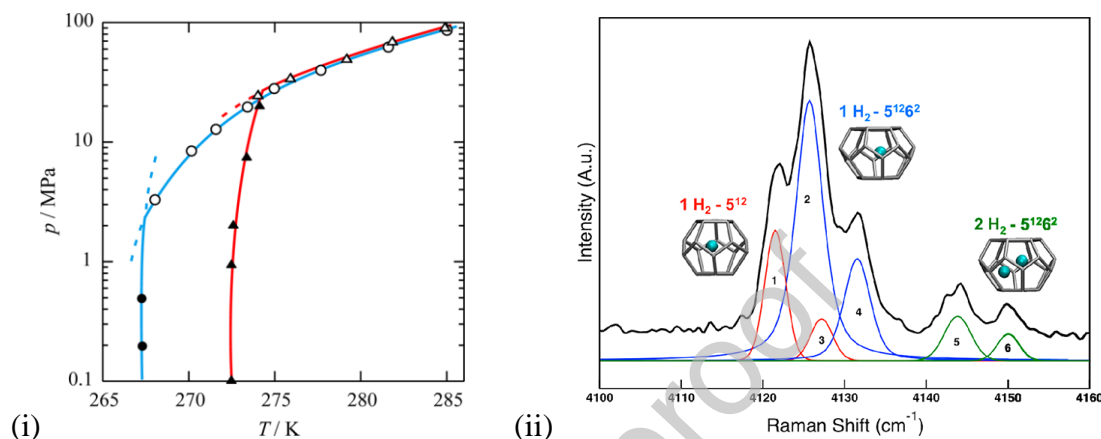


Figure 10. (i) Phase equilibria for the H<sub>2</sub>+t-BA+H<sub>2</sub>O system (blue colour) and t-BA+H<sub>2</sub>O system (red colour) with 5.6 mol% t-BA. The closed symbols represent sVI structure and open symbols represent sII structure (reprinted with permission from Tanabe *et al.*<sup>227</sup>, Copyright 2015 American Chemical Society). (ii) H-H vibron region in the Raman spectrum acquired at 77 K and 1 bar, showing the presence of hydrogen in multiple cages of sI structure in H<sub>2</sub>+CO<sub>2</sub>/CH<sub>4</sub>+H<sub>2</sub>O system (reprinted with permission from Grim *et al.*<sup>224</sup>, Copyright 2012 American Chemical Society).

## 5.7. Organic compounds

In examining the stability of sVI structure for the hydrogen encapsulation, Prasad *et al.*<sup>226</sup> studied the hydrogen occupancy in the H<sub>2</sub>-H<sub>2</sub>O-(t-BuNH<sub>2</sub>) system. It has been observed that pure t-BuNH<sub>2</sub> hydrate (5.86 mol %) forms a sVI structure at 250 K, with lattice parameter of 18.81 Å<sup>228</sup>. However, a transformation to sII is seen under a hydrogen pressure of 13.8 MPa at 250 K. Prasad *et al.*<sup>226</sup> claimed that considering the size of hydrogen molecule (2.72 Å) with the size of the smaller 4<sup>454</sup> cage (5.8 Å), it was expected that hydrogen molecules would be small enough to fit into these cages. This justification is based on the previous study of CH<sub>4</sub>+ (t-BuNH<sub>2</sub>) hydrates, where methane (4.36 Å) was close in size to the smaller cavity of 4<sup>454</sup> cage, but did not stabilize sVI structure. This led to phase transformation from sVI to sII where the small 5<sup>12</sup> cages were occupied by methane molecules<sup>229</sup>. However, the similar phenomenon was observed in the case of H<sub>2</sub>+(t-BuNH<sub>2</sub>) hydrates, where evidence supported the transformation to sII structure and occupancy of hydrogen in smaller cages. Prasad *et al.*<sup>226</sup> perceived this to be pressure induced structural transformation, in spite of the availability of the appropriate cage sizes. Prasad *et al.*<sup>226</sup> further measured the hydrogen storage capacity of the hydrate using volumetric gas release measurements, and they found 0.7 wt.% H<sub>2</sub> present in the hydrate. This was too low to be practically utilised.

Considering the theoretical hydrogen storage potential of sH structures of clathrates to be higher than 5.6 wt.%, Strobel *et al.*<sup>230</sup> have used the well-known sH hydrate formers like

methyl tert-butyl ether (MTBE), methylcyclohexane (MCH), 2,2,3-trimethylbutane (2,2,3-TMB), and 1,1-dimethylcyclohexane (1,1-DMCH) as co-guests to form hydrogen hydrates at 150 MPa and 275 K. The formation of sH structure was confirmed by XRD measurements with peaks indexed to space group hexagonal crystal system (p6/mmm) having lattice parameter  $a = 12.203 \text{ \AA}$  and  $c = 9.894 \text{ \AA}$ . Among the co-guests used, MTBE showed highest rate of hydrate formation due to its enhanced ice-wetting properties and large surface area. It was proposed that any promoter molecule with size large enough to stabilise the icosahedral  $5^{12}6^8$  large cages could lead to the formation of the sH structure under suitable thermodynamic conditions. Due to the similar size of  $5^{12}$  and  $4^35^66^3$  cages in the sH structure, the Raman bands of the hydrogen in the two cages overlapped with each other, thus creating difficulty in identification in each cage. By comparing with the earlier studies of THF/H<sub>2</sub> hydrates, it was concluded that H<sub>2</sub> is present in both the smaller cages of the sH hydrates<sup>180</sup>. Various other liquid hydrocarbon promoters were used for the formation of sH structure in the subsequent studies by Durate *et al.*<sup>231,232</sup>, with predicted hydrogen storage capacities reaching upto 1.4 wt.%.

In a bid to enhance the hydrogen storage properties of sH hydrates, Koh *et al.*<sup>233</sup> applied a strategy to encapsulate hydrogen in large cages along with a water soluble co-former. At the same time, they also investigated the ‘tuning effect’ proposed by Lee *et al.*<sup>179</sup> to increase the occupancy of hydrogen in these cages. For this purpose, they used a water soluble sH co-former (1-methylpiperidine), which had shown superior performance earlier in the case of methane hydrates<sup>234</sup>. They observed that upto a concentration of 2 mol% 1-methylpiperidine, sH hydrates are formed with single occupancy of hydrogen both small and middle cages, under pressure of 58 MPa at 240 K. However, upon decrease in the concentration of co-former below 1%, sH hydrates transform to sII hydrates with multiple hydrogen occupancy (upto four) in large cages and single occupancy in small cages. Koh *et al.*<sup>233</sup> concluded that it was not possible to push hydrogen through the large cages of sH structures, which resulted in transformation to sII structure with favourable  $5^{12}6^4$  cages. Moreover, the formation of sII structure was also favoured by the kinetics of reaction. This is shown schematically in Figure 11.

In the previous studies, the transformation from sH to sII was found to be metastable, with a lifetime of a few hours. However, Koh *et al.*<sup>233</sup> measured the Raman spectra for a period of 48 hours to confirm the stability of sII structure. They observed that peaks for the sII structure start appearing within three hours, and the intensity of peaks increases till the solution is saturated with hydrogen over the complete observation period. In an extension of work carried out by Strobel *et al.*<sup>230</sup>, effect of quaternary phase equilibria (H<sub>2</sub>-H<sub>2</sub>O-CH<sub>4</sub>-MCH) on the formation of sH structure was investigated by Khan *et al.*<sup>235</sup>. They observed equilibrium pressure of 10 MPa at 273 K, when the ratio of hydrogen to methane in the gas mixture was 7:1. The equilibrium pressure decreased with drop in the hydrogen content at a given temperature, as hydrogen hydrates are expected to be stable at higher pressures as compared to methane hydrates. The occupancy of hydrogen found to increase with pressure, in medium and small cages, till 50 MPa. Khan *et al.*<sup>235</sup> ascribed this to the replacement of methane with hydrogen, although the mechanism for the same is not fully understood yet.

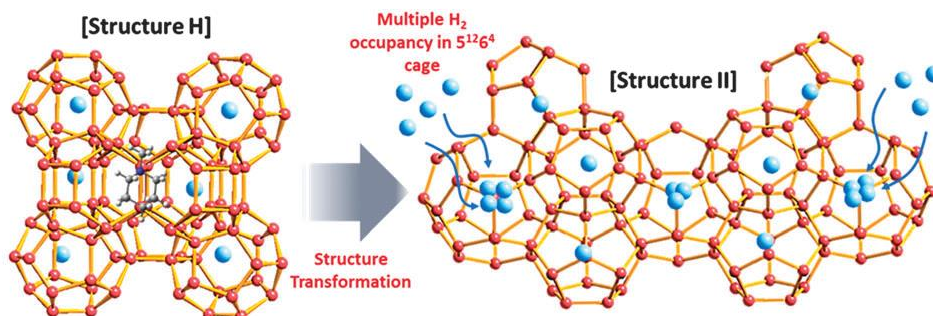


Figure 11. A schematic showing structural transformation from sH to sII upon incorporation of hydrogen in the MCH-promoted clathrates. Reproduced from Koh *et al.*<sup>233</sup> with permission from The Royal Society of Chemistry.

Atamas *et al.*<sup>236</sup> have predicted that an ability of guest molecule to form a given crystal structure is determined by its van der Waals volume, and pressure alone cannot be responsible for it. They have calculated Gibbs free energy using Monte Carlo calculations at finite temperature and pressure to arrive at their conclusion. Liu *et al.*<sup>237</sup> have investigated the parameters required for the efficient sH hydrate former using *ab initio* molecular dynamics simulations. They have observed that the promoter with higher electronegativity, chemical potential or the electrophilicity index can be more efficient, provided the molecular weight is kept constant. Among the alkane molecules, those with number of heavy atoms less than seven have better chances of forming a stable sH hydrate<sup>237</sup>. Above this, cycloalkanes work better. With regard to the cage occupancy, interaction energy results have proven that one hydrogen molecule is stable in the small ( $5^{12}$ ) and medium ( $4^3 5^6 6^3$ ) cages, with  $5^{12}$  cages preferred over the other<sup>237</sup>. This is similar to the experimental results obtained by Khan *et al.*<sup>235</sup> and Koh *et al.*<sup>233</sup>, where Raman spectroscopy along with thermodynamic modelling proved the presence of single hydrogen occupancy in small as well as medium cages. Other studies have been performed to predict the stability of sH hydrates, which signify that the thermodynamic properties are dependent of the multiple parameters including molecular size, molar volume, molar mass of the promoters<sup>238</sup>. Attempts to have sound theoretical understanding of the thermodynamics of sH hydrates have been made consistently and considerable progress has been made to match the experimental and computational results<sup>239</sup>.

## 6. Organic and Inorganic Clathrates

A different approach for enhancing the hydrogen storage capacity of clathrates was proposed by Daschback *et al.*<sup>240</sup> in which hydrogen was encapsulated in the non-aqueous solid crystal to produce an organic clathrate. It was shown by Daschback *et al.*<sup>240</sup> that hydrogen could be stored in Hydroquinone (HQ) clathrate structure using MD simulations. This concept was later improvised by Strobel *et al.*<sup>241</sup> to form a chemical-clathrate hybrid which combined the chemically bound hydrogen with that present in molecular form. The HQ clathrate phase consists of six HQ molecules bound at the top and bottom ends by six hydroxy groups. The cavity radius of these structure is  $4.5 \text{ \AA}$ . These structures retained hydrogen ever after exposure to ambient conditions for at least 10 min, unlike the hydrogen hydrates which quickly dissociate upon exposure to ambient conditions. Due to their large cavity size (close to the cavity size of sII hydrate at  $4.5 \text{ \AA}$ ), they show immense potential as hydrogen storage media, with storage capacity reaching upto 2.4 wt.% if quadruple hydrogen occupancy is assumed (similar to sII hydrates). Strobel *et al.*<sup>230</sup> extended this idea to

chemically dissociate hydrogen from the HQ + clathrate structures, which they estimated could lead to storage capacity as high as 4.2 wt.%.

Undertaking a novel approach, Han *et al.*<sup>242</sup> synthesized guest free HQ clathrates and reported fast hydrogen uptake of 0.35 wt.% at 298 K and 35 MPa. From the previous studies and theoretical arguments, they concluded that 62% of the cages of the structure are occupied by the hydrogen molecules. The entire hydrogen adsorption process was concluded in a fraction of a minute (2 s) and did not show degradation after ten cycles of operation. The structure was maintained throughout these cyclic operations, as confirmed by the synchrotron XRD measurements<sup>242</sup>. These structures fall under the category of novel HOFs (Host Organic Frameworks), where it is expected that the channel cages of the clathrates allow rapid inter cage diffusion and enhance the hydrogen storage capacity. However, structural stability of organic clathrates at high temperatures is poor and they tend to release gas at high pressures due to structural transformation. To address these concerns, Woo *et al.*<sup>243</sup> have proposed a HQ framework with fullerene (C<sub>60</sub>) as a guest molecule. These clathrates demonstrate high volumetric hydrogen storage capacity of 49.5 g/L at 77 K and 8 MPa, which is far higher than similar structures proposed earlier (Figure 12 (i))<sup>180,230,241,242,244-246</sup>. The C<sub>60</sub> stabilised HQ framework structure remains stable upto pressures of 10 GPa and 438 K. However, the gravimetric hydrogen storage capacity remains low (2.9 wt.%) due to absence of porosity in the structure and high crystal density, equivalent to that of C<sub>60</sub> (1.678 g/cc)<sup>247</sup>. A comparison of gravimetric vs. volumetric hydrogen storage of different clathrate structures for hydrogen storage has been shown in Figure 12(ii). It is seen that although C<sub>60</sub> HQ clathrate have highest volumetric storage capacity among the clathrate structures, sII structures still remain superior in terms of gravimetric storage capacity.

To explore further likelihood of improvement in hydrogen storage capacity, GCMC simulations were carried out on the Li doped HQ framework with C<sub>60</sub> guest molecules<sup>243</sup>. They observed that more than 16 H<sub>2</sub> molecules are present in the cages of HQ along with C<sub>60</sub> forming distorted cuboctahedra arrangement. The total hydrogen storage capacity was higher than non-doped frameworks at 6.59 wt.% (81.1 g/L) at 77 K and 8 MPa<sup>243</sup>. It is important to note that volumetric density exceeded that of liquid hydrogen (70.8 g/L), with intermolecular distance between the hydrogen molecules decreasing to 2.0 Å, much below the value in liquid hydrogen (3.4 Å). Woo *et al.*<sup>243</sup> proposed that the doping with light elements poses an attractive alternate to enhance the hydrogen storage capacity of clathrates.

Other clathrates considered for hydrogen storage include Type I inorganic silicon clathrates consisting of open structure with crystalline framework<sup>248,249</sup>. However, a pertinent drawback in each of these structures was high desorption temperature of the order of 673 K, thus making them unsuitable for use in practical applications. Chan *et al.*<sup>250</sup> have tried to address this issue using DFT simulations by substituting the Si framework atoms by other atoms such as Cu, C and Al and guest atoms with elements such as Ba, Na and Li. This was done in order to create optimum void space for the hydrogen atom and modifying the binding energy of the hydrogen with the host framework. The results have shown that the hydrogen storage capacity equivalent to 10 wt.% can be achieved with the binding energy within the desired range (0.1-0.6 eV/H<sub>2</sub>). This could allow the operating temperature to be brought close to the ambient. These studies reflect ample scope for the modification of the silicon clathrates and synthesis of new clathrate materials for hydrogen storage applications.

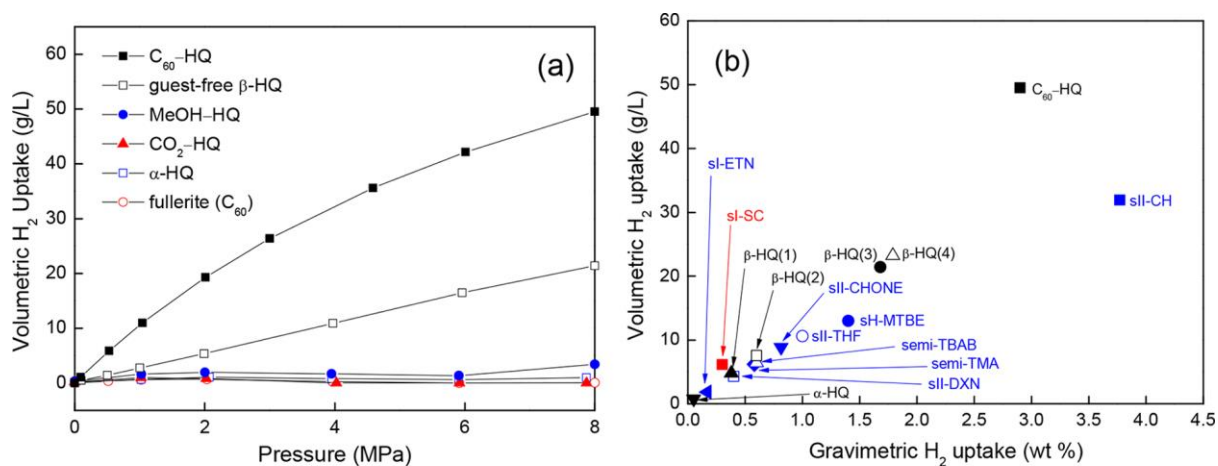


Figure 12. (i) Hydrogen storage characteristics of Organic clathrates showing volumetric uptake with pressure. (ii) A comparison of the volumetric hydrogen storage capacity with gravimetric storage capacity for clathrates. (reprinted with permission from Woo *et al.*<sup>243</sup>, Copyright 2018 American Chemical Society).

## 7. Semi-clathrates

In a recent study, Luo *et al.*<sup>251</sup> used CH<sub>4</sub> in addition to the TBAB compound for the formation of hydrogen semi clathrates. This can lower the formation pressure to as low as 0.46 MPa at 282.55 K, when the mass fraction of TBAB was 0.2 and concentration of methane in the H<sub>2</sub>+CH<sub>4</sub> gas mixture was close to 70%. It was seen that for the similar fraction of THF (0.2), the equilibrium pressure at 288 K is close to 8 MPa<sup>252</sup>, much higher than that observed in the current system (~2 MPa) by Luo *et al.*<sup>251</sup>. In the search for new promoters with better performance, Yu *et al.*<sup>253</sup> have studied 5.6 mol% HCFC-141 b and water mixture at 273 K under different pressures. They observed that system shows 0.24 wt.% hydrogen storage capacity under 6 MPa and 0.40 wt.% under 12 MPa, with the time required to achieve 90% of the total capacity being close to 10.2 h in both cases. They have reported milder equilibrium conditions for HCFC-141 b (6.5 MPa at 284 K) as compared to either methane (20 MPa at 280 K) or t-BA (8 MPa at 278 K)<sup>253</sup>. This can be attributed to two factors: large size of the HCFC-141 b molecule and presence of highly electronegative groups (-F & -Cl) in HCFC-141 b, changing the H-bonding between the water molecules and reinforcing the Vander Waals forces of attraction between guest and water molecules. Detailed investigation with the respect to cage occupancy and structure identification is needed to establish the efficacy of HCFC-141 b as a promoter for hydrogen clathrates.

Strobel *et al.*<sup>185</sup> have demonstrated 0.214 wt.% hydrogen adsorption in 2.71 mol% TBAB solution at 13.8 MPa and 279.5 K. They have observed that, in line with the hydrogen occupancy in THF promoted hydrates, the filling of hydrogen molecules starts with small cages and large cages are occupied later. The behaviour of hydrogen was found to be similar in the small cages, irrespective of the structure of the hydrates. They observed hydrogen occupancy of 0.355 (7) for TBAB promoted hydrates, at par with that observed for THF based at 0.47 (5). In order to explore other alternative guest molecules forming semi clathrates, Deschamps and Dalmazzone<sup>254</sup> have studied the phase equilibria in H<sub>2</sub>+TBACL and H<sub>2</sub>+TBPB hydrates. It has been found that these systems show dissociation temperatures close to ambient (288.9 K for H<sub>2</sub>+TBACL and 286.5 K for H<sub>2</sub>+TBPB) at low pressures in the range of 15-18 MPa. This was a clear improvement as compared to the TBAB promoted

hydrogen hydrates, with their hydrogen storage capacity close to 0.12 wt. % ( $H_2+TBACL$ ) and 0.14 wt.% ( $H_2+TBPB$ )<sup>254</sup>.

## 8. Hydrogen clathrates without promoters

Del Rosso and co-workers<sup>255</sup> experimentally investigated the stability of pure hydrogen hydrates using in-situ Raman spectroscopy at a pressure of 2000 bar at 263 K. The conditions were chosen keeping in view the phase stability region of sII structure in water-hydrogen phase diagram (denoted by red line in Figure 13). They used supercooled water hydrogen solution at 2000 bar to carry out the experiments. With the help of Raman spectra, they identified single occupation of small cages and triple occupation of large cages after an incubation time of 10 h. This is in contrast to the simple hydrates examined by Mao *et al.*<sup>256</sup>, who claimed double hydrogen occupancy in small cages and quadruple occupancy in large cages.

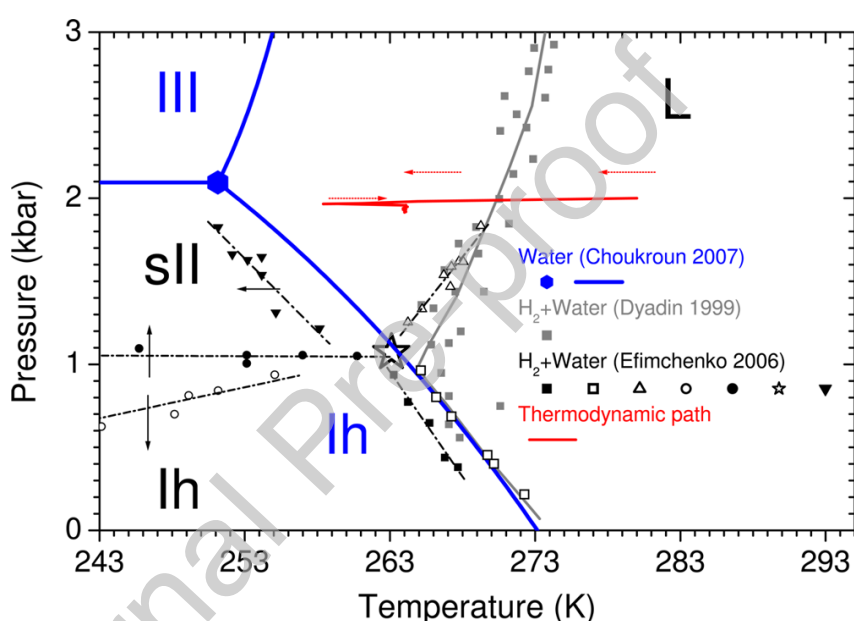


Figure 13. Phase Diagram of water-hydrogen system overlapped with the that of pure water (reprinted with permission from del Rosso *et al.*<sup>255</sup>, Copyright 2015 American Chemical Society).

Del Rosso and co-workers<sup>255</sup> put forth the argument that the rate of hydrate formation is expected to be limited by the diffusion of the hydrogen through the liquid phase. As soon as the transformation to solid is complete (at the end of 18 h), the rate of reaction increases rapidly. It is proposed that large cages are filled first, thus allowing the hydrogen to quickly diffuse through the hexagonal faces (lower energy barrier than pentagonal faces) and complete hydrate formation. Cage occupancy has been determined by Lokshin *et al.*<sup>191</sup> on simple deuterium hydrates using in-situ Neutron diffraction. They found that hydrates formed under pressure of 2000 bar showed quadruple deuterium occupancy in large cages, in the temperature range of 40 K to 180 K. The deuterium molecules were expected to be located at the corners of a tetrahedra, with  $D_2-D_2$  distance close to 2.93 Å. This was similar to the intermolecular distance of 3.78 Å found in solid hydrogen, at atmospheric pressure and 4.2 K<sup>257</sup>. However, at atmospheric pressure, the quadruple occupancy is only stable upto 80 K with progressive decrease to double occupancy at 160 K. This remains in contrary to the works of Strobel *et al.*<sup>190</sup> (ex-situ measurements at 77 K) and Del Rosso *et al.*<sup>255</sup> (in-situ measurements at 200 bar and 263 K), who never observed double occupancy of large cages,

with small amount of triple occupancy reportedly necessary for the hydrate stability. Belosludov *et al.*<sup>176</sup> have reported that for the case of pure hydrogen hydrates, the existence of higher capacity sI structure is not thermodynamically favourable; it requires  $T=200\text{K}$  under very high pressures to be realised. At higher temperatures of 250 K, they have reported that the maximum hydrogen that can be stored in sI, sII and sH is 4 wt.%, 3.8 wt.% and 2.7 wt.%, respectively. Using a thermodynamic computational model, it has been predicted that the pressure for stabilisation of sI structure is higher than 100 MPa at 250 K, whereas it is 84 MPa for the s-II structure<sup>176</sup>.

Liu *et al.*<sup>188</sup> investigated the cage occupancy in pure  $\text{H}_2$  hydrates using *ab initio* molecular dynamic simulations. Their study shows that double hydrogen occupancy is dynamically feasible in the small cages, whereas up to three molecules can populate the large cages. This leads to a maximum hydrogen storage capacity of 4.4 wt.%, lower than the estimates of Mao *et al.*<sup>4</sup>. Liu *et al.*<sup>188</sup> suggested that hydrogen molecules tend to adsorb on different faces of the host framework, rather than forming a cluster. To examine the effect of pressure on the cage occupancy, Brumby *et al.*<sup>258</sup> carried out Gibbs ensemble Monte Carlo simulations. They observed that the cage occupancy decreases with decreasing pressure, going from single occupancy at 400 MPa to half occupancy at 30 MPa at 275 K. However, this effect is not observed at low temperatures of 150 K, with constant single occupancy until 30 MPa. Similar effect is observed for large cages, with quartet occupancy (at 1000 MPa) diminishing to single occupancy at 30 MPa at 250 K. On the other hand, the drop in large occupancy is still evident at low temperatures of 150 K, unlike the small cages. Overall, the hydrogen storage capacity varies linearly with pressure, with 1.5 wt.% at 30 MPa to 4 wt.% at 1000 MPa at 250 K. This is in accordance with the previous simulations of Papadimitriou *et al.*<sup>189,225</sup>. Despite a single occupancy of the small cages was observed at all studied conditions, a small percentage ( $< 1\%$ ) of cages have been found to show double occupancy at pressures higher than 100 MPa. This shows that although the coverage of hydrogen in the small cages is not high, double occupancy does occur for pressures below 400 MPa<sup>258</sup>. Using *ab initio* calculations, Lu *et al.*<sup>259</sup> predicted sII hydrate's stable configurations with two  $\text{H}_2$  in large  $5^{12}6^4$  and  $5^{12}6^2$  cages, and one  $\text{H}_2$  in  $5^{12}$  cages. However, the effects of temperature during structural relaxations were not taken into account in this study, which might affect the final results. Kaur & Ramachandran<sup>260</sup> used DFT studies to predict the hydrogen occupancy in small and large cages. They reported that up to two and seven molecules could be respectively accommodated in the small and large cages of sII hydrates.

One of the reasons for the discrepancy in the experimental and computational results have been accounted to the release of the hydrogen molecules in the vapor form from the hexagonal faces of the larger cages<sup>259</sup>. It has been predicted that presence of larger molecules such as methane or THF, may block the release of such vapors and lead to enhancement in the hydrogen storage capacity of the hydrates. Burnham *et al.*<sup>261</sup> have used *ab initio* molecular dynamic simulations to show the presence of four hydrogen molecules in the large cages. They accounted this to the perfect packing of four molecules in tetrahedral vacancies inside the large cages, which can be violated if the numbers increase to five or decrease to three. This correlates well with the experimental observation of the Mao *et al.*<sup>4</sup> (using Raman spectroscopy) and Lokshin *et al.*<sup>191</sup> (using Neutron Diffraction).

## 9. A Comparison of hydrogen storage capacity of different hydrate structures

Based on the theoretical calculations, depending upon the size of the cavity (cage opening) and occupancy in each cage, Strobel *et al.*<sup>185</sup> have predicted the maximum hydrogen storage capacity possible in each type of structure formed by clathrate hydrates, as shown in Figure 14 (i). They have chosen methylcyclohexane (MCH) to represent sH, ethylene oxide (EO) to represent sI, THF to represent sII, Br<sub>2</sub> to represent sIII, tertbutylamine (t-BA) to represent sVI, hexafluorophosphoric acid (HPF<sub>6</sub>) to represent sVII, and TBAB to represent the semi-clathrate. Their estimates are based on an empirical correlation: #H<sub>2</sub> = (4.0385 x cavity radius (Å) – 15.096), with the values rounded off to the nearest integer. These values are calculated assuming that all the small cages are available for hydrogen occupation, whereas large cages are occupied by the promoters or secondary hydrate forming molecules. It is seen that sVI hydrates have been poised to store more than 7 wt.% hydrogen at 100 % occupancy, followed by sVII structures at more than 5 wt.%. The rest lie in the range of 3-4 wt.%.<sup>185</sup> Although the predicted hydrogen storage capacities have been calculated under various assumptions, it represents the broad spectrum of clathrates with flexibility to modify the structure.

In an yet another attempt to compare the hydrogen storage capacity of various hydrate structures, Tsimpanogiannis *et al.*<sup>262</sup> have proposed a practical methodology to categorise the hydrogen hydrates based on Monte Carlo Simulations. They have divided the hydrogen hydrates with regard to the pressure, molecular weight of the promoters, temperature to assist in their selection for the desired application. As shown in Figure 14 (ii), decreasing the temperature increases the hydrogen storage capacity, with the maximum obtained for the sH hydrates. Similarly, they have also shown that the promoters with least molecular weight will enable to have largest hydrogen storage capacity, keeping other factors constant. Also, the presence of promoters in large or small cages can affect the overall capacity of the hydrates, with highest capacity achievable ~ 3 wt.% when a promoter with molecular weight of 16 g occupies the medium cage in the sH structure<sup>262</sup>.

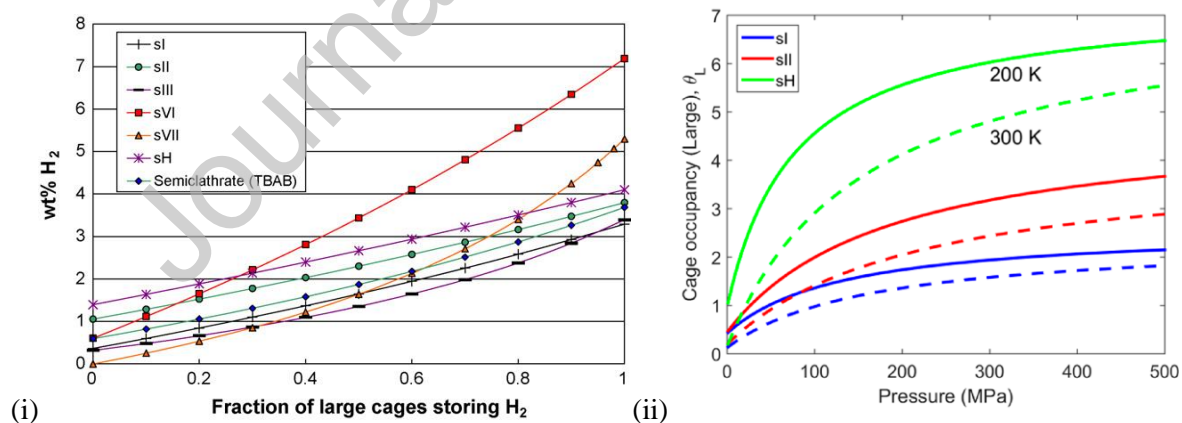


Figure 14. (i) Theoretical hydrogen storage capacity of clathrate structures. (reprinted with permission from Strobel *et al.*<sup>185</sup>, Copyright 2007 Elsevier Ltd). (ii) Cage occupancy for the large cages as a function of pressure for three hydrate structures at 200 K (solid lines) and 300 K (dashed lines). Reprinted with permission from Tsimpanogiannis *et al.*<sup>262</sup>, Copyright 2020 American Chemical Society.

A summary of the important promoter molecules used in the past couple of decades has been given in Table 3, along with their hydrogen storage properties. Although, the comparisons provide here form a crude analysis of the properties of the clathrates, it represents rapid progress in the hydrogen storage characteristics of the clathrates and prove

ample opportunities for the future scope of development. A summary of the promoters and their brief characteristics have been summarised in Figure 15.

Journal Pre-proof

Table 3. Important hydrogen clathrates synthesised along with their hydrogen storage characteristics.

| Promoter                           | Conc. (mol %)       | Synthesis route** | P (MPa) | T (K)   | Synth Time | Structure | L.P. (Å) | Volume Increase ## | Technique for structure determination <sup>s</sup> | Max H <sub>2</sub> Occupancy (Raman spectroscopy/NMR) |                                |                                | H <sub>2</sub> wt.% <sup>€</sup> | H <sub>2</sub> Vol (g/L) <sub>f</sub> | Technique used (to calc wt.% H <sub>2</sub> ) | Year | Ref |
|------------------------------------|---------------------|-------------------|---------|---------|------------|-----------|----------|--------------------|--|---|--------------------------------|--------------------------------|----------------------------------|---------------------------------------|---|------|-----|
|                                    |                     |                   |         |         |            |           |          |                    |  | 5 <sup>12</sup>                                       | 5 <sup>12</sup> 6 <sup>4</sup> | 5 <sup>12</sup> 6 <sub>2</sub> |                                  |                                       |   |      |     |
| <b>Pure H<sub>2</sub> Hydrates</b> |                     |                   |         |         |            |           |          |                    |  |   |                                |                                |                                  |                                       |   |      |     |
| -                                  | Pure H <sub>2</sub> | Direct            | 220     | 234     | -          | sII       | 17.047   | -                  | In-situ EDXRD                                      | 2   | 4                              | -                              | 5.25                             | 43                                    | Ex-situ Raman Spectroscopy <sup>@</sup>       | 2002 | 4   |
| -                                  | Pure H <sub>2</sub> | Direct            | 200     | 263     | 60 h       | sII       | -        | -                  | -  | 1   | 3                              | -                              | 3.2                              | 27                                    | In-situ Raman Spectroscopy <sup>@</sup>       | 2015 | 255 |
| <b>Solid/Liquid Promoters</b>      |                     |                   |         |         |            |           |          |                    |  |   |                                |                                |                                  |                                       |   |      |     |
| THF                                | 5.6 %               | Indirect          | 5       | 279.6   | -          | sII       | 17.236   | 3.3 %              | Ex-situ XRD  | 1   | -                              | -                              | 1.06                             | 10                                    | Volumetric gas Release                        | 2004 | 178 |
| THF                                | 5.6 %               | Indirect          | 5.6     | 270     | -          | sII       | 17.179   | 2.3 %              | Ex-situ XRD (1 bar, 123 K)                         | 2   | -                              | -                              | 2.09                             | 20                                    | In-situ Raman Spectroscopy                    | 2005 | 179 |
|                                    | 0.15 %              | Indirect          | 12      | 270     | -          | sII       | -        | -                  | -  | 2   | 4x H <sub>2</sub> , (1-x)THF   | -                              | 4.03                             | -                                     | In-situ Raman Spectroscopy                    | 2005 | 179 |
|                                    | 0.2 %               | Indirect          | 12      | 270     | -          | sII       | -        | -                  | -  | 2   | 4x H <sub>2</sub> , (1-x)THF   | -                              | 3.81                             | -                                     | Volumetric gas Release                        | 2005 | 179 |
| THF                                | 5.6 %               | Indirect          | 12.6    | 270-278 | 7 days     | sII       | -        | -                  | In-situ Neutron Diffraction <sup>21</sup>          | 1   | -                              | -                              | 1.05                             | 10                                    | Volumetric gas release                        | 2006 | 180 |

|                                |            |                  |       |         |          |     |        |       |                           |   |                               |   |       |    |   |      |     |
|--------------------------------|------------|------------------|-------|---------|----------|-----|--------|-------|---------------------------|---|-------------------------------|---|-------|----|---|------|-----|
|                                | 0.5 %      | Indirect         | 13.8  | 270-278 | 7 days   | sII | -      | -     | -                         | 1 | -                             | - | 1.05  | 10 | Volumetric gas release                  | 2006 | 180 |
| t-BuNH <sub>2</sub>            | 5.86 %     | Indirect         | 13.2  | 250     | 2 days   | sII | 17.44  | 7.1 % | Ex-situ XRD               | 1 | -                             | - | 0.7   | 10 | Volumetric gas release                  | 2009 | 229 |
| THF                            | 0.5 %      | Direct-Indirect  | 74    | 255     | 3-4 days | sII | 17.15  | 1.8 % | Ex-situ XRD               | 1 | 4x H <sub>2</sub> , (1-x)/THF | - | 3.4   | -  | Volumetric gas release                  | 2010 | 187 |
| Acetone                        | 0.5 %      | Direct-Indirect  | 74    | 255     | 3-4 days | sII | 17.17  | 2.2 % | Ex-situ XRD (1 bar, 90 K) | 1 | 4x H <sub>2</sub> , (1-x)     | - | 3.6   | -  | Volumetric gas release                  | 2010 | 187 |
| TBAF                           | 3.6 %      | Indirect         | 13    | 294     | -        | sI  | -      | -     | -                         | 1 | -                             | - | 0.024 | -  | Volumetric gas release                  | 2013 | 263 |
| Ar                             | 1 %        | Indirect         | 40    | 243     | 5 days   | sII | 17.164 | 2.1 % | Ex-situ XRD               | 1 | 3                             | - | 3.08  | 27 | Ex-situ Raman Spectroscopy <sup>®</sup> | 2015 | 217 |
| i-PA                           | 5.6 %      | Indirect         | 40    | 243     | 5 days   | sII | 17.253 | 3.7 % | Ex-situ XRD               | 1 | -                             | - | 1.09  | 10 | Ex-situ Raman Spectroscopy <sup>®</sup> | 2015 | 217 |
| t-BA                           | 5.6 %      | Indirect         | 2.53  | 267     | -        | sII | 17.51  | 8.3 % | Ex-situ XRD               | 1 | -                             | - | 1.02  | 10 | Ex-situ Raman Spectroscopy <sup>®</sup> | 2015 | 227 |
| THF                            | 5.6 %      | Indirect         | 3.8   | 271.1   | 1 day    | sII | -      | -     | -                         | 2 | -                             | - | 2.08  | 32 | Ex-situ Raman Spectroscopy <sup>®</sup> | 2017 | 197 |
| THF                            | 5.6 %      | Reverse Micelles | 10    | 276.2   | 19 min   | sII | -      | -     | -                         | - | -                             | - | 0.12  | -  | Volumetric gas release                  | 2018 | 198 |
| THF                            | 3 %        | Indirect         | 14.53 | 273     | 8 days   | sII | -      | -     | -                         | - | -                             | - | 0.18  | -  | Volumetric gas release                  | 2019 | 264 |
| HCFC-141 b                     | 5.6 %      | Indirect         | 6.5   | 284     | -        | -   | -      | -     | -                         | - | -                             | - | 0.5   | -  | Volumetric gas release                  | 2020 | 253 |
| <b>Gaseous/Mixed Promoters</b> |            |                  |       |         |          |     |        |       |                           |   |                               |   |       |    |   |      |     |
| Ar                             | 25 % (gas) | Direct           | 52    | 276     | -        | sII | -      | -     | -                         | 1 | 4                             | - | 3.1   | 48 | In-situ Raman Spectroscopy <sup>®</sup> | 2010 | 219 |

|                               |                                |          |                          |     |        |     |         |       |               |   |  |   |      |    |  |      |     |
|-------------------------------|--------------------------------|----------|--------------------------|-----|--------|-----|---------|-------|---------------|---|--|---|------|----|--|------|-----|
| CO <sub>2</sub>               | phase)<br>1.7 MPa              | Indirect | 70                       | 258 | 1 day  | sI  | 11.83   | -     | Ex-situ XRD   | 1 | -  | 2 | 3.2  | -  | Ex-situ Raman Spectroscopy <sup>®</sup> <sub>c</sub> | 2012 | 224 |
| CH <sub>4</sub>               | 11 MPa                         | Indirect | 70                       | 258 | 1 day  | sI  | 11.83   | -     | Ex-situ XRD   | 1 | -  | 2 | 3.2  | -  | Ex-situ Raman Spectroscopy <sup>®</sup> <sub>c</sub> | 2012 | 224 |
| N <sub>2</sub>                | -                              | Indirect | 15                       | 243 | 4 days | sII | -       | -     | Ex-situ XRD   | 2 | 4  | - | 5.01 | 43 | Ex-situ Raman Spectroscopy <sup>®</sup> <sub>y</sub> | 2012 | 220 |
| N <sub>2</sub> & THF          | 1 % THF, 20 MPa N <sub>2</sub> | Indirect | 35                       | 243 | 8 days | sII | 17.162  | 2.0 % | Ex-situ EDXRD | 2 | 4x H <sub>2</sub> , (1-x)THF             | - | 2.24 | -  | Ex-situ Raman Spectroscopy                           | 2014 | 222 |
| N <sub>2</sub> & PRD          | -                              | Indirect | 35, p <sub>H2</sub> =1/5 | 243 | 8 days | sII | 17.285  | 4.2 % | Ex-situ EDXRD | 2 | 4x H <sub>2</sub> , (1-x)PRD             | - | -    | -  | Ex-situ Raman Spectroscopy                           | 2014 | 222 |
| CH <sub>4</sub>               | 7 % (gas phase)                | Direct   | 30                       | 263 | -      | sI  | 11.87   |       | Ex-situ XRD   | 1 | -  | 2 | 0.02 | 28 | Thermodynamic modelling                              | 2014 | 202 |
|                               | 5 % (gas phase)                | Direct   | 70                       | 263 | -      | sII | 17.15   | 1.8 % | Ex-situ XRD   | 1 | 4x H <sub>2</sub> , (1-x)CH <sub>4</sub> | - | 0.31 | 32 | Thermodynamic modelling                              | 2014 | 202 |
| C <sub>3</sub> H <sub>8</sub> | 5.6 %                          | Indirect | 30                       | 243 | 3 days | sII | 17.2103 | 2.9 % | Ex-situ EDXRD | 2 | -  | - | 2.29 | 20 | Ex-situ Raman Spectroscopy <sup>®</sup>              | 2014 | 210 |
|                               | 1 %                            | Indirect | 30                       | 243 | 3 days | sII | -       | -     | -             | 1 | 4x H <sub>2</sub> , (1-                  | - | 3.84 | 32 | Ex-situ Raman Spectroscopy <sup>®</sup>              | 2014 | 210 |

|   |   |                           |                       |       |        |     |        |       |                            |                |  |                |       |    |                                 |      |     |
|---|---|---------------------------|-----------------------|-------|--------|-----|--------|-------|----------------------------|----------------|--|----------------|-------|----|---------------------------------|------|-----|
| CH <sub>4</sub> & CO <sub>2</sub>               | 15 % CH <sub>4</sub> , 17 % CO <sub>2</sub> | Direct                    | 6.68                  | 274.9 | 4-6 h  | sI  | -      | -     | -                          | P <sup>x</sup> | x)C <sub>3</sub> H <sub>8</sub>          | P <sup>x</sup> | -     | -  | Thermodynamic Model             | 2015 | 265 |
| CO <sub>2</sub> & THF                           | 5.56 % THF                                  | Direct (CO <sub>2</sub> ) | 6                     | 284.8 | ½ day  | sII | 17.15  | 1.8 % | Ex-situ XRD (1 bar, 185 K) | -              | x H <sub>2</sub> , (1-x) CO <sub>2</sub> | -              | -     | -  | -                               | 2019 | 266 |
| SF <sub>6</sub>                                 | 89.2 % (gas phase)                          | Direct                    | 0.5                   | 263.1 | 6 days | sII | -      | -     | -                          | 1              | 1  | -              | 0.014 | -  | GC                              | 2019 | 223 |
| CH <sub>4</sub> & C <sub>2</sub> H <sub>6</sub> | 46.7 % & 20 % (gas phase)                   | Direct                    | 9, p <sub>H2</sub> =3 | 250   | 7 days | sI  | 11.935 | -     | Ex-situ EDXRD              | 2              | -  | -              | 0.67  | 8  | Gas Chromatography <sup>®</sup> | 2020 | 212 |
|   | 60 % & 6.7 % (gas phase)                    | Direct                    | 9, p <sub>H2</sub> =3 | 250   | 7 days | sII | 17.156 | 1.9 % | Ex-situ EDXRD              | 2              | 3  | -              | 1.78  | 37 | Gas Chromatography <sup>®</sup> | 2020 | 212 |

\*\*Direct Reaction: Ice powder is directly brought in contact with the promoter and hydrogen.

\*\* Indirect Reaction: Hydrogen gas reacts with preformed promoter hydrates.

## Expansion with respect to pure hydrogen hydrates,  $a=17.047 \pm 0.010 \text{ \AA}$  (two molecules in small cage and 4 molecules in large cage).

\$ All ex-situ measurements are carried at 77 K and 1 bar, unless otherwise mentioned.

@ The capacity was calculated keeping in view the number of hydrogen present in each cage in a given structure and the concentration of promoter in the hydrate.

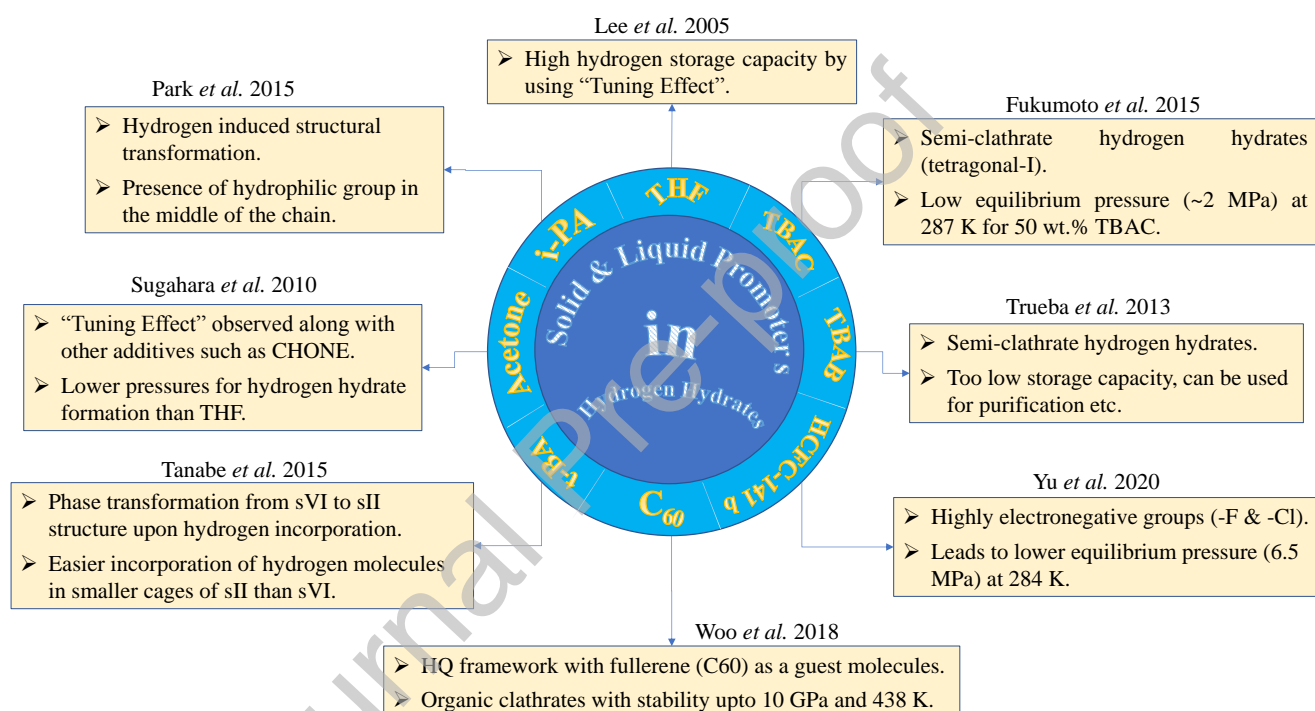
¥ Assuming 100 % replacement of N<sub>2</sub> with H<sub>2</sub>.

€ The wt.% H<sub>2</sub> is the weight of hydrogen present with respect to the total weight (hydrate + hydrogen + promoter). Details of the calculation are given in supplementary information.

£ Calculated using the cage occupancy of H<sub>2</sub> molecules per unit cell. The lattice parameter has assumed to be 17.047 Å (pure hydrogen hydrate), in case data not available.

℄ Concentration of promoter has not been considered in these calculations.

₹ Present. No quantification has been given by the authors.



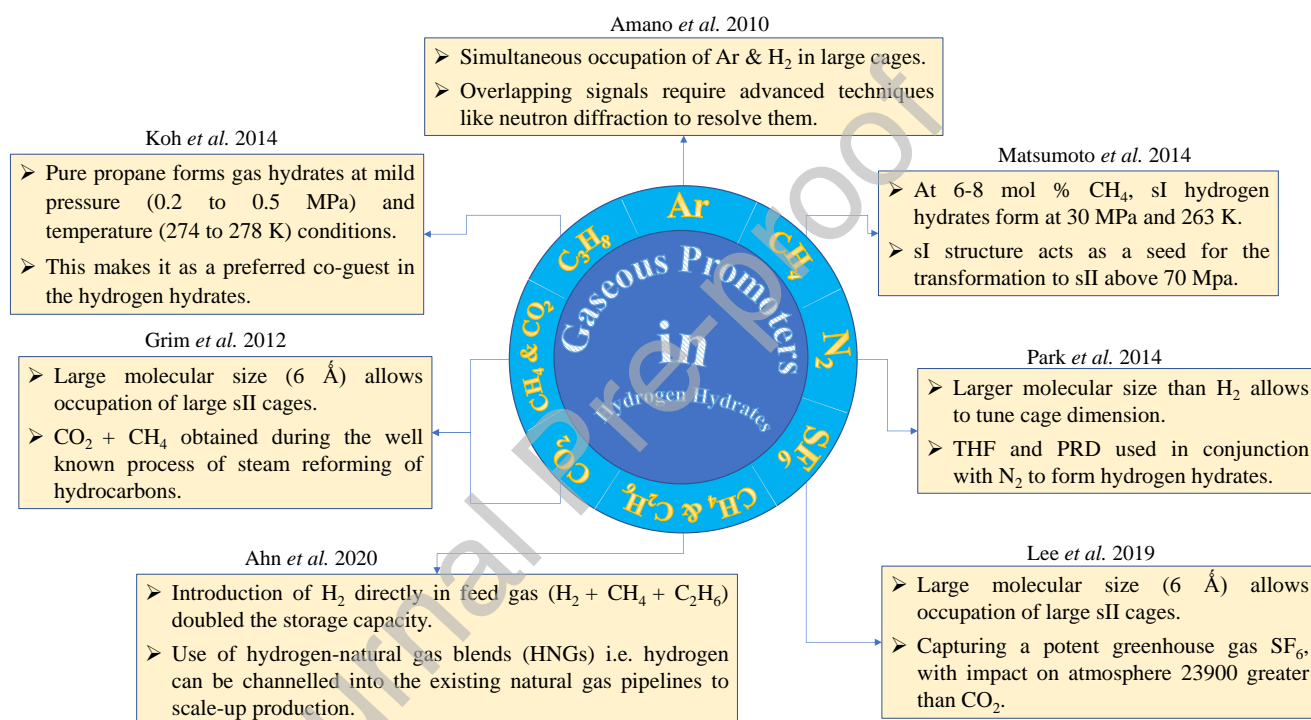


Figure 15. A summary of the critical role played by the promoters/additives in the hydrogen clathrate formation.

## 10. Kinetic Aspects

Although the recent developments have shown promising results with regard to the thermodynamic properties of the clathrates, improvement in their kinetics remains an utmost challenge. As seen in the Table 3, the large time taken for the hydrogen clathrate formation (ranging from days to weeks) is not viable in practical applications. As it has been discussed in the previous sections, the hydrate formation occurs via two routes i.e. by direct reaction of gaseous hydrogen with the aqueous solution or through adsorption into hydrogen free hydrate crystals. In the first case, the hydrate crystals nucleate at the interface of the gas and the liquid; the rate of reaction is governed by the growth of crystals. However, in the second case, the rate determine step is the diffusion of the hydrogen into the cages of the hydrate.

To enhance the rate of reaction via first route, one of the techniques has been dispersion of the aqueous solution using a porous substrate, which leads to enhanced surface area thus increasing the formation rate<sup>179</sup>. This was successfully demonstrated by Lee *et al.*<sup>179</sup>, with the hydrate formation time reduced by more than factor of ten. However, this technique led to additional weight of the substrate, which can be penalty on the overall gravimetric capacity of the hydrate. In continuation of the efforts of Lee *et al.*<sup>179</sup>, Saha *et al.*<sup>267</sup> used mesoporous materials with pore size in range of 49 to 226 Å to enhance the rate of clathrate formation. An additional advantage offered by the porous substrate is to keep the ice particles intact in the pores even after melting, thus allowing rapid reaction upon multiple cycling. Saha *et al.*<sup>267</sup> observed ~1 wt.% hydrogen absorption at 270 K and 65 bar within 27 min, using the media with pore size of 49 Å.

To understand the role of interface in the nucleation and growth of hydrate, Lokshin *et al.*<sup>268</sup> have used an in-situ high pressure neutron diffraction apparatus to study pure hydrogen hydrate formation. They have observed sluggish kinetics upon reaction of water with hydrogen under 1.5 kbar at 260 K, with only 30% conversion of water to clathrate in 3 hours. On the other hand, when ice was used as starting material, 100% conversion to clathrate was completed in less than 10 min. This difference was attributed to the presence of small cavities in the ice-Ih structure, where the hydrogen molecules can penetrate and support the transformation to hydrate structure. The difficulty in the nucleation of hydrate at the gaseous hydrogen-liquid water interface is evident from the work of Rosso *et al.*<sup>255</sup> The time taken for the hydrate crystals to appear under 200 MPa and 263 K was close to 10 hours. A detailed insight into the role played by the secondary guest molecules in the nucleation of hydrate at in the liquid-gas interface was given by Song *et al.*<sup>269</sup>. Using molecular dynamic simulations, they have observed that the hydrates formation is primarily dependent on the arrangement of the secondary guest molecules and smaller hydrogen molecules at the liquid-gas interface. Since the secondary guests such as THF can only occupy large cages, smaller molecules such as hydrogen hinder their movement owing to the entropy effects. To add to this, extremely low solubility of hydrogen in water makes it difficult for the hydrogen molecules to access the growing crystal interface<sup>269</sup>. It has also been an important study to identify the effects of supercooling the solution to form hydrates. It is shown that using intensive thermodynamic forces leads to excess occupancy of hydrogen in the large cages, unlike small cages where it remains unchanged. However, these effects are metastable in nature and may hinder the occupancy of the large cages by secondary molecules<sup>269</sup>.

### 10.1. Macroscopic Reaction Kinetics

Recent studies by Veluswamy *et al.*<sup>200</sup> have focused on the macroscopic kinetics of hydrate formation and dissociation. Veluswamy *et al.*<sup>200</sup> have observed that stoichiometric THF solution stored 0.186 wt.% H<sub>2</sub> at a formation rate of 18.07 mol/min/m<sup>3</sup>, whereas similar amount of TBAB showed 0.035 wt.% H<sub>2</sub> uptake with a slower formation rate of 3.44 mol/min/m<sup>3</sup>. Both measurements were carried out at constant driving force, to keep out the inaccuracies due to measurement parameters. This is one of the important consideration for kinetic studies, as the Veluswamy *et al.*<sup>200</sup> found reversed trend when measurements were taken without keeping this in view (under constant temperature and pressure conditions). Surfactants have traditionally been used to prevent the agglomeration of clathrates in the oil and gas pipelines, where they form spontaneously. Veluswamy *et al.*<sup>270</sup> have also evaluated the effect of ionic (DTAC) and non-ionic (Tween-20) surfactant on the kinetics of the THF promoted hydrogen hydrates. Both these surfactants have shown an increase in the rate of reaction by 20% when added in concentration of 0.5 wt% DTAC and 0.1 wt% Tween-20. However, the decomposition kinetics remained unaffected by the use of surfactants. In a bid to search a better surfactant to enhance the kinetics of hydrate formation, Veluswamy *et al.*<sup>209,271</sup> analysed the effect of sodium dodecyl sulfate (SDS) on the THF/H<sub>2</sub> and CH<sub>4</sub>/H<sub>2</sub> hydrates. While SDS had no effect on the former, it drastically enhanced the rate of hydrate formation in the latter system. The timer required for 90% completion of the reaction was reduced by 10 times to 30 min, from the previous 334 min. This represents the effect of surfactant is dependent upon the secondary guest molecule added and detailed study is required to find the best suitable additive.

In a bid to enhance the rate of reaction, Di Profio *et al.*<sup>198</sup> have used a synthesis method based on reverse micelles formation, which helps to reduce the interface area between the gas and the hydrate to the order of nanometers. This has led to a significantly reduced time of the hydrate formation (in the range of 20-30 min) with a range of promoters including THF, THT, CP and DXL. This was specially relevant for water insoluble promoters such as CP and THT, which had shown difficulty in direct formation with water<sup>198</sup>. The reactor design was also proposed in this study which allowed the hydrate particles to settle at the bottom of the reactor in the form of free flowing slurry. This prevented the hydrate particles from aggregating at the bottom of the reactor and favoured scaling up the technique to the industrial level. However, they had limited success in terms of hydrogen storage capacity, with the highest being reported for THT based hydrates at 0.5 wt.% under 10 MPa and 274.5 K. Based on their study Di Profio *et al.*<sup>198</sup> have concluded that presence of polar surface plays a major role in determining suitability of co-former. This has been one of the reason for better performance of THT (sulphur as polarizable element) than CP.

Cai *et al.*<sup>264</sup> have studied the macroscopic kinetics of 3 mol% THF solution at 273.15 K and 14.53 MPa. They have also captured the images during the course of the experiment using a camera, as shown in Figure 16 (i) & (ii). Upto 48 h, no hydrate formation was seen in the camera captured images. From the standpoint of the rate of hydrate formation, this process was divided into three parts; A, B and C. In the A part, the rate of hydrate formation was low (0.19 mmol/h), and this part lasted till about 128 h. This was followed by B part, in which there is sudden increase in the hydrate formation rate (1.25 mmol/h) and hydrate crystals could be observed in the photographs. The rate of

hydrate formation again decreases in the third part (part C), possibly due to the mass transfer resistance of hydrate crystals growing into bulk solution. Cai *et al.*<sup>264</sup> have carried out time based Raman spectroscopy to study the effect of promoters on the hydrate formation. It has been seen that hydrogen stabilises the metastable THF hydrates formed during the process. The liquid/gas interface provides a nucleation site for the formation of the hydrates.

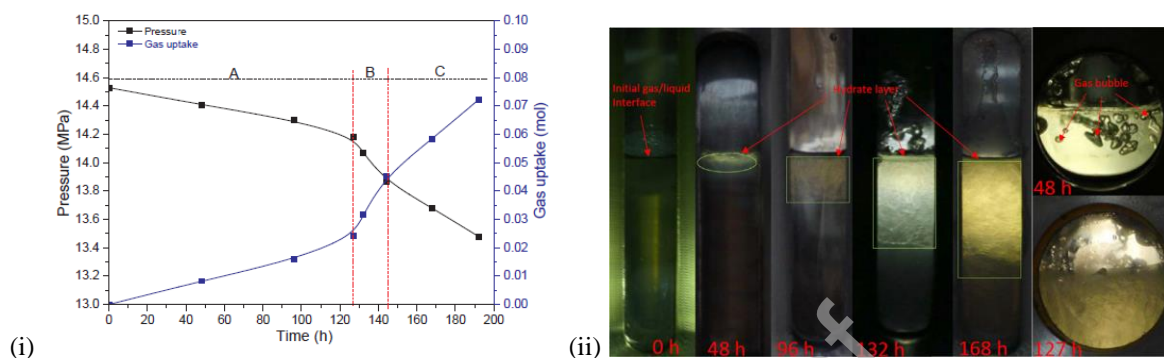


Figure 16. (i) Gas Uptake during hydrate formation with time. (ii) Representative images during the transformation (reprinted with permission from Cai *et al.*<sup>264</sup>, Copyright 2019 Elsevier Ltd).

Matsumoto *et al.*<sup>202</sup> have studied time based structural changes in the methane promoted (3 mol% in gas phase) hydrogen hydrates at 70 MPa and 263 K. Although the thermodynamically stable phase is sII, formation of sI phase was observed during the initial 5 hours. They have explained this with the formation of methane hydrates initially in contact with the ice, further leading to the formation of hydrogen hydrates with time. The structure stabilises at the end of 24 hours. Using molecular dynamics simulations, Zhang *et al.*<sup>207</sup> have shown that although methane thermodynamically stabilises the hydrogen hydrates, the hydrogen acts as a kinetic promoter in this case. They observed a six-fold increase in the growth rate of hydrates when the small cages were doubly occupied by hydrogen, as opposed to almost negligible change in case of pure methane hydrates upon increase of pressure from 20 to 100 MPa. They have concurred that the growth rate is controlled by the mass transfer of the guest molecules, i.e. solubility and diffusivity of methane play a crucial role in the growth of the hydrate. It is self-evident from the increase in the growth rate with pressure, as the diffusivity follows the similar trend.

Belosudov *et al.*<sup>272</sup> have highlighted a kinetic anomaly or ‘self-preservation’ effect in the hydrogen hydrates. In other words, due to extremely small dissociation rate of hydrates in the temperature range of 240-273 K under atmospheric pressure, the hydrate will continue to withhold almost constant amount of hydrogen even if these conditions are thermodynamically unfavourable. This effect can be explained in the following steps: initial liberation of hydrogen gas leads to the decrease in the temperature of the hydrate. This generates thermal gradient across the sample, with the inside of the sample being colder than the outside. A layer of ice is formed surrounding the hydrate. Due to the difference in the thermal expansion coefficients of the ice and the hydrate, the inner hydrate experiences higher pressure than the outside pressure upon increase in temperature<sup>272</sup>. This returns the hydrate to the equilibrium conditions in the hydrogen-water phase diagram. Additionally, to protect distortion of the structure during the heating, it has been found using molecular dynamics simulation that a network of hydrogen bonds forms between the ice and the hydrate. This effect has been proposed to be beneficial for the storage and transport of the

hydrogen hydrates without the need for high pressures or low temperatures, thus saving energy and cost<sup>272</sup>.

## 10.2. Microscopic Reaction Kinetics

To throw light on the microscopic behaviour of the hydrate transformation, Okuchi *et al.*<sup>273</sup> have utilised in-situ high pressure NMR spectroscopy. The stoichiometric sample of THF hydrate was prepared using heavy water and observed under NMR spectrometer at temperature range of 250-256 K and upto 20 MPa. The activation energy for diffusion of hydrogen in the hydrate was found to be  $3 \pm 1$  kJ/mol, much lower than the values obtained using MD and PIMD simulations or mathematical models. A reason for this was attributed to reorientation and diffusion of water molecules in the structure, thus creating favourable conditions for the diffusion to occur. Also, the authors speculate the diffusion of hydrogen through the pentagonal faces of the smaller cages, as the large cages are occupied by the THF molecules. However, as determined later by MD simulations, this process requires large activation energy ( $>50$  kJ/mol) and is not feasible under given conditions. To confirm this, Zhong *et al.*<sup>197</sup> have experimentally measured the diffusion coefficient of H<sub>2</sub> in THF promoted (stoichiometric) hydrates using time-resolved Raman spectra. They used change in the area under the Raman peaks to arrive at a value of  $6.6 \times 10^{-12}$  m<sup>2</sup>/s, which is close to the previous results in the range of  $10^{-11}$  to  $10^{-12}$  m<sup>2</sup>/s. The values observed by NMR are significantly lower ( $\sim 10^{-15}$  m<sup>2</sup>/s), as the measurements are made under equilibrium conditions.

With a view of understanding the factors effecting the microscopic reaction kinetics, Nagai *et al.*<sup>274</sup> have provided a mathematical model governing the rate of hydrate formation. They have proposed a hybrid kinetic model consisting of a hydrogen delocalization and diffusion, in which hydrogen is first adsorbed on the particle surface and subsequently diffuses into the cavities of the structure to form hydrate. It based on presumption that single hydrogen molecule occupied small cages and THF molecule occupied the large cages of sII structure. This model successfully described the experimental results with regard to variations in temperature, pressure or particle size, except during initial period of rapid reaction rate. The activation energies for the diffusion and adsorption were determined to be 78.7 kJ/mol and  $-5.9$  kJ/mol, respectively. In a further study by Yoshioka *et al.*<sup>275</sup>, the model proposed by Nagai *et al.*<sup>274</sup> was extended to study the desorption kinetics and compare it with the absorption. It was found that during the first part of the process i.e. adsorption was two to three times faster than the desorption, whereas the rate of diffusion was almost similar to the desorption process. They also observed a stable occupancy of hydrogen over multiple absorption/desorption cycles. It was a significant development over the previous model<sup>274</sup>, as it took into account the particle size dependence of the kinetics i.e. the distance over which hydrogen diffuses in the clathrate. This led to better agreement with the experimental data, although the activation energy for the adsorption was higher ( $-28$  kJ/mol). This value corresponds to the values comparable to the chemical bonding (e.g. hydrogen bonding), along with a possible rearrangement of water molecules. However, both models calculated the diffusion coefficient of hydrogen to be of the order of  $10^{-12}$  m<sup>2</sup>/s, which agrees well with the previous experimental results<sup>273</sup>.

Improving upon the previous mathematical models, Komatsu *et al.*<sup>276</sup> developed a Multiple Adsorption Resistance (MAR) Model which took into account the hydrogen

occupancy in the cages with the change in pressure during the absorption process. It was due to the fact that an increase in absorbed amount led to decrease in the pressure of the hydrogen and correspondingly the vacancy in the cages, resulting greater resistance for further absorption. The activation energy was calculated to be 30.65 kJ/mol for the stoichiometric THF hydrate, which was closer to the results of Frankcombe and Kroes (32.3 kJ/mol) using MD simulation<sup>277</sup>. Komatsu *et al.*<sup>276</sup> concluded that for this case, diffusion of hydrogen occurred through both small and large cages with transport of water molecules as well in the THF promoted hydrates. For non-stoichiometric THF hydrates (6.2 mol% THF), THF molecules promote formation of grain boundary and Quasi Liquid Layer, thus reducing the activation energy. A summary of the kinetic models has been given in Table 4.

### 10.3. Diffusion Energy Barrier

To gain insight into the phenomenon of diffusion of hydrogen in clathrates, Alavi and Ripmeester<sup>278</sup> determined the activation energy for the diffusion through the hexagonal face of large cage (23 kJ/mol) and pentagonal face of the small cage (121.4 kJ/mol) using DFT calculations. The values observed lied considerably above the experimentally observed results of Okuchi *et al.*<sup>273</sup>. It is important to note that Okuchi *et al.*<sup>273</sup> used NMR pulsed field measurements to arrive at their results, which concur with the macroscopic motion of hydrogen molecules through the hydrates. As compared to cage to cage migration process calculated using simulations, these processes are usually faster<sup>279</sup>. This may help in explaining the discrepancy in the experimental and computational results.

In a series of studies, Burnham *et al.*<sup>261,280</sup> have compared the effect of quantum and classical nature of hydrogen on the diffusion energy barrier in clathrate structure using Path Integral Molecular Dynamics. They have observed that entropy plays a critical role in deciding the effect of temperature on the energy barrier, which in general increases with increase in temperature. It has been found that entropy is lower in the transition state i.e. during inter-cage movement, than within the body of the cage. In the transition state, the H<sub>2</sub> molecule is squeezed in the gap between the hexamer (in case of large cage), forming a bridge around the H<sub>2</sub> molecule. However, the trend is reversed in case four H<sub>2</sub> molecules are present in the cage, as they sit in perfect tetrahedron inside the cage and have lower entropy than the transition state<sup>280</sup>.

In other words, for the case of four H<sub>2</sub> molecules present in a cage, the energy barrier decreases with increase in temperature. The energy barrier also increases for the case of quantisation of the nuclei, due to increase in the size of nuclei, making it difficult for it squeeze through the hexamer connecting adjacent cages. In order to bring theory closer to the real hydrate formation process, Lu *et al.*<sup>259</sup> have considered the hydrogen occupancy effect as well as condensed phase environment during simulations. Lu *et al.*<sup>259</sup> used MP2 simulations to determine the energy barrier for the diffusion of hydrogen molecule through the sI and sII structures. The simulations show that energy barrier depends on two factors: number of molecules crossing the barrier (decreases with increasing number of molecules) and the type of face (hexagonal or pentagonal) through which H<sub>2</sub> molecule is hopping to another cage. They have observed that energy barrier is lower for the hexagonal face as compared to pentagonal face. The values obtained are in close agreement with the experimental results obtained by NMR<sup>273</sup>. The values obtained for the diffusion energy barrier have been summarized in Table 4.

To further delve into the detailed mechanism of diffusion of hydrogen in clathrates, Cendagorta *et al.*<sup>281</sup> have examined the effect of temperature on the diffusion energy barrier. The values reported by them are at the middle of the path travelled from centre of one cage to another. They have noted that the decrease of classical energy barrier on reducing temperature is due to the fact that thermal fluctuations are reduced at low temperatures, thus increasing the cavity size for the H<sub>2</sub> to pass through the hexagonal face. Below 25 K, energy barrier is governed by quantum tunnelling effects. Competing effects of Zero Point Energy (which leads to swelling of the ring polymer shaped H<sub>2</sub> molecule, thus restricting its movement across the hexagonal face) with the tunnelling effect (which causes the ring polymer to be highly delocalised, being either present in one cage or another at any point of time and reducing the free energy barrier) have been observed<sup>281</sup>. At T<25K, tunnelling effect takes precedence and leads to reduction in the free energy barrier. At T<25 K, the quantum rates become much larger than the classical rates due to the tunnelling effect. To have a comparison with the experimental data, multiple iterations would be required with different occupancy of H<sub>2</sub> in neighbouring cages and averaging of these rates<sup>281</sup>. They reported activation barrier for the transition between large cages to be 15.9 kJ mol (classical) and 2.1 kJ/mol (quantum) at 8K. However, these values were identical at 25 K (15.9 kJ/mol) and above for both cases.

In a recent study, Hasegawa *et al.*<sup>282</sup> have considered the effect of the sII structure binary hydrates (e.g. SF<sub>6</sub>+H<sub>2</sub> or t-BuNH<sub>2</sub>+H<sub>2</sub>) on the diffusion of the hydrogen using molecular simulations. It has been observed that the diffusion of hydrogen is unhindered when moving from a one large cage to another through the hexagonal ring. However, in case of movement from large cage to small cage, the pentagonal ring has to partially break up and allow the movement of hydrogen across. The latter case was more frequent, since the large cages were occupied by the secondary molecules (SF<sub>6</sub> or t-BuNH<sub>2</sub>) and no-occupancy of hydrogen was observed in the large cages.

Table 4. Diffusion energy barrier of hydrogen through the sII hydrate calculated using experimental and computational techniques.

| Technique                                     | Hydrate Structure  | Cage                                    | Face Type              | Diffusion barrier (kJ/mol) @ No. of molecules crossing the barrier                         | T (K)   | Comments   | Year | Ref |
|---|--------------------|---|------------------------|--|---------|--|------|-----|
| DFT (B3LYP and MP2 levels)                    | sII                | $5^{12}6^4$                             | Hexagonal              | 23   | 250     | <ul style="list-style-type: none"> <li>• Constraint movement of H<sub>2</sub> along 1-D reaction coordinate</li> <li>• Rigid cages model with full occupancy of hydrogen</li> </ul>  | 2007 | 278 |
|   |                    | $5^{12}$                                | Pentagonal             | 121.4  |         |  |      |     |
| In-situ NMR spectroscopy                      | sII (5.6 mol% THF) | $5^{12}$                                | Pentagonal             | 3 ± 1 (activation energy)<br>$2 \times 10^{-14}$ m <sup>2</sup> /s (diffusion coefficient) | 250     | <ul style="list-style-type: none"> <li>• Lower diffusion rates in cage to cage measurement (by NMR) as compared to other macroscopic techniques due to absence of defects and vacancies.</li> <li>• Considerably lower activation energy as compared to computational (DFT) values.</li> </ul>   | 2007 | 273 |
| Hydrogen Hydrate Phase Diffusion (HHPD) Model | sII (5.6 mol% THF) | $5^{12}$                                | Pentagonal             | 78.7 (E <sub>a</sub> for diffusion)<br>-5.9 (E <sub>a</sub> for adsorption)                | 266-275 | <ul style="list-style-type: none"> <li>• Consideration of the split model with two step process: adsorption on the surface, followed by diffusion into cages.</li> <li>• Cage and face type values arrived at comparison with literature data.</li> </ul>  | 2008 | 274 |
| Multiple Adsorption Resistance (MAR) Model    | sII (5.6 mol% THF) | $5^{12}$ & $5^{12}6^4$                  | Pentagonal & Hexagonal | 30.65 (E <sub>a</sub> for diffusion)<br>-22.59 (E <sub>a</sub> for adsorption)             | 265-269 | <ul style="list-style-type: none"> <li>• Diffusion of hydrogen through both small and large cages with transport of water molecules as well in the THF promoted hydrates.</li> <li>• Non-stoichiometric THF hydrates (6.2 mol% THF), THF molecules promote formation of grain boundary and Quasi Liquid Layer, thus reducing the activation energy.</li> </ul> | 2014 | 276 |
|   | sII (6.2 mol% THF) | (Grain boundary and Quasi Liquid Layer) |                        | 17.97 (E <sub>a</sub> for diffusion)<br>-24.87 (E <sub>a</sub> for adsorption)             | 265-272 |  |      |     |

|   |       |             |            |  |     |   |  |      |
|---|-------|-------------|------------|--|-----|---|--|------|
|   | Furan | $5^{12}6^4$ | Hexagonal  | 28.79 ( $E_a$ for diffusion)<br>-16.84 ( $E_a$ for adsorption) |     | <ul style="list-style-type: none"> <li>• Change in cage occupancy with pressure taken into account.</li> <li>• Lowest activation energy found for secondary guest molecule, Furan.</li> <li>• Diffusion coefficient calculated in the range of values observed in literature.</li> </ul>  |  |      |
|   | CP    | $5^{12}$    | Pentagonal | 100.1 ( $E_a$ for diffusion)<br>-24.15 ( $E_a$ for adsorption) |     |   |  |      |
| Path Integral Molecular Dynamics (PIMD) | sII   | $5^{12}6^4$ | Hexagonal  | $31.3 \pm 0.1$ @ $1H_2$<br>$14.0 \pm 0.4$ @ $5H_2$             | 200 | <ul style="list-style-type: none"> <li>• Effect of hydrogen occupancy in the surrounding cages considered in the simulation.</li> <li>• The activation barriers found to increase with temperature.</li> <li>• Quantisation of nuclear degree of freedom, increases the activation barrier by 2 kJ/mol.</li> </ul>  | 2016   | 280  |
| Ab initio MD simulations                | sII   | $5^{12}6^4$ | Hexagonal  | 20 @ $4H_2$  | 260 |   | <ul style="list-style-type: none"> <li>• Vander Waals interaction between the hydrogen molecules and the host water structure taken into account.</li> </ul> | 2017 |
| EE-GMF (ab initio method)               | sI    | $5^{12}6^2$ | Hexagonal  | $13.5$ @ $1H_2$<br>$3.9$ @ $3H_2$                              | 250 | <ul style="list-style-type: none"> <li>• Effect of condensed phase environment taken into account</li> <li>• Cage flexibility and cage occupancy considered during simulations.</li> <li>• Quantum mechanical zero-point energy effects of confinement of <math>H_2</math> in cages included.</li> <li>• Closely match with the experimental results</li> </ul> | 2019   | 259  |
|   |       | $5^{12}$    | Pentagonal | $57.9$ @ $1H_2$<br>$53.1$ @ $3H_2$                             |     |   |  |      |
|   | sII   | $5^{12}6^4$ | Hexagonal  | $14.5$ @ $1H_2$<br>$2.9$ @ $7H_2$                              |     |   |  |      |
|   |       | $5^{12}$    | Pentagonal | $48.2$ @ $7H_2$  |     |   |  |      |

## 11. Computational Aspects

From previous sections it has already become clear that computational contributions in the field of hydrogen clathrates are of utmost importance to understand and guide experimental findings, as they provide fundamental insights in the atomic-level structure of these materials. In this respect, recent theoretical efforts, mostly on SII clathrate structures, have been dedicated to (i) the estimation of H<sub>2</sub>/D<sub>2</sub> cage occupancies<sup>258,283,284</sup>, implicitly determining upper H<sub>2</sub> storage limits (see section 4.3); (ii) the evaluation of translational-rotational (TR) eigenstates/eigenvalues in each hydrate cage<sup>285–287</sup>, providing insight to the interpretation of Raman and INS spectra; and (iii) the determination of free energy profiles associated with cage hopping<sup>280,281,288</sup> obtained by NMR measurements and related to the activation energy involved in the diffusion of H<sub>2</sub> molecules in the clathrate cages (see section 4.4).<sup>279</sup> However, the greatest technological challenge that hinders the successful implementation of clathrates in practical applications is the slow kinetics of clathrate growth and to circumvent the typically harsh temperature and pressure conditions necessary to stabilize them. In this light, current computational studies on hydrogen clathrates therefore focus on identifying and understanding alternative approaches to speed up clathrate growth and stabilize clathrate structures. Herein we specifically highlight the use of promoter molecules and surfactants and the synthesis of clathrates in nanoconfinement, with particular emphasis on how theory can help to design pathways for formation of clathrates under more feasible pressure and temperature conditions. As will become clear, new avenues in modelling are necessary to model clathrate formation and stabilization in more complex environments, therefore we end the theoretical section with a brief discussion on the current challenges in computational clathrate research.

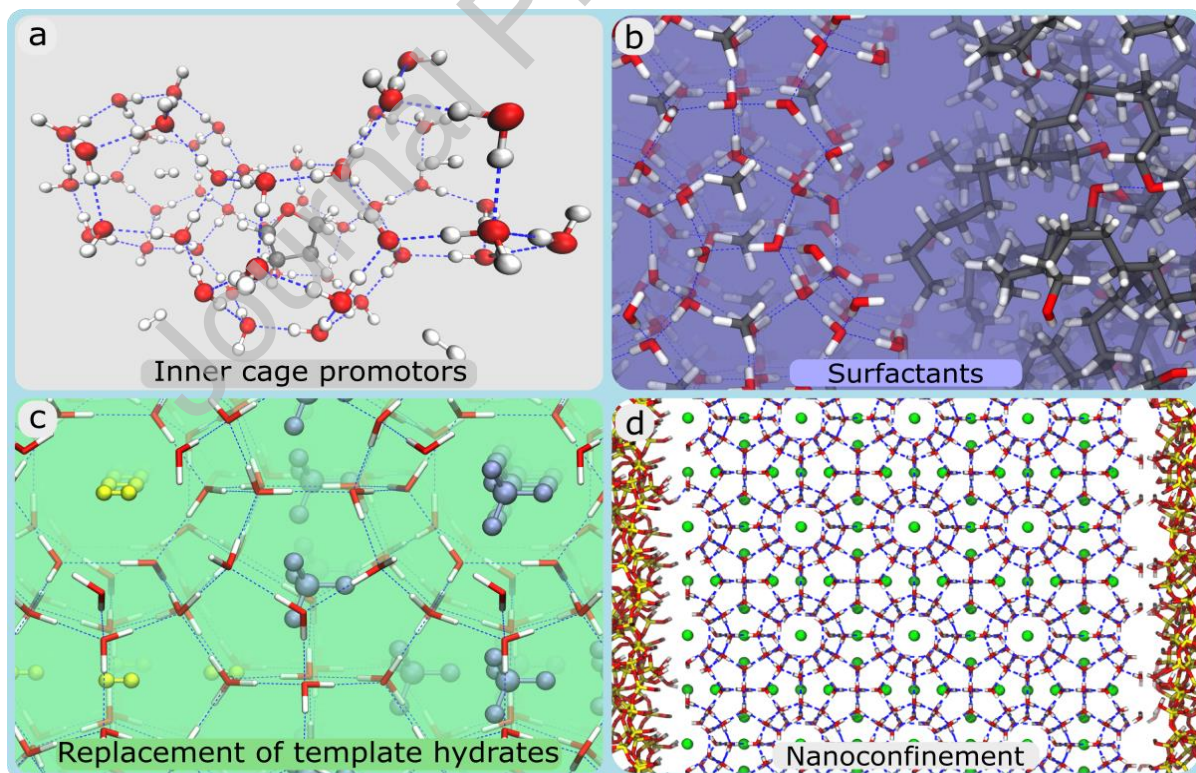


Figure 17. Representations of new technological approaches employed in relenting the operational conditions and accelerating the kinetics of formation of H<sub>2</sub> clathrates: introduction of (a) small molecules or (b) surfactants as promoting agents, (c) guest replacement in template clathrate scaffolds and (d) confinement in nanopores.

### 11.1. Clathrate growth and stabilization using promoter molecules and surfactants

Computational studies seeking to improve the kinetics of clathrate growth and the stability of H<sub>2</sub>-containing clathrate matrices have mostly focused on the role of promoter molecules, such as small alkanes and tetrahydrofuran (THF) (Figure 17a). For instance, Tsimpanogiannis *et al.*<sup>262</sup> estimated the H<sub>2</sub> storage capacity at different temperatures and pressures in pure and binary H<sub>2</sub> hydrates via Monte Carlo (MC) simulations, reaching the conclusion that the H<sub>2</sub> storage capacity increases if promoter molecules occupy the medium-sized cages instead of the large cages in SII clathrates. Liu *et al.*<sup>289</sup> combined static and dynamic *ab initio* calculations to propose that, when populated with THF, the larger SII clathrate cages can accommodate an additional H<sub>2</sub> molecule. This is an important observation, as it challenges the common assumption of the segregation of these gases in different cages. Using *ab initio* geometry optimizations, they shed light on the mechanism of formation of clathrate cages around THF and determined the interaction energies and most stable geometries of THF and water and THF, water and other gases (CO<sub>2</sub>, CH<sub>4</sub>, H<sub>2</sub>). THF clathrate cages were shown to be formed initially from the adsorption of THF onto a hexagonal water ring and other guest molecules were seen to be preferentially located next to pentagonal cages.<sup>290</sup> Using a combined static/dynamic *ab initio* approach, they furthermore investigated different alkanes as promoter molecules at various temperatures, showing that alkanes follow an interesting pattern in the stabilization of the structure H hydrogen clathrate matrix: linear shaped lighter molecules and heavier cyclic molecules.<sup>237</sup> However, to accurately evaluate the growth rate, cage occupancy, and growth mechanism of these clathrates, substantially longer dynamic simulations are necessary. To this end, Zhang *et al.*<sup>291</sup> used the generic force fields to model the water and methane molecules, complemented with specific force fields terms to model the interaction with the hydrogen molecules.<sup>292</sup> Their microsecond-long molecular dynamics (MD) simulations of a binary (CH<sub>4</sub>/H<sub>2</sub>) clathrate reveal that the growth process is dominated by the solubility and diffusivity of the promoter, in line with previous approximative simulations<sup>293</sup> considering a THF/H<sub>2</sub> clathrate. Although these works have given considerable insight to understand clathrate formation and stabilization with promoter molecules, other recently employed experimental strategies to enhance the formation of hydrogen clathrates have been less targeted by computational studies and deserve further investigations, as outlined below.

A typical example of such ill-understood strategies is the use of surfactants (e.g. sodium dodecylsulfate) to promote hydrogen clathrates<sup>209,270,294,295</sup> (cf. Figure 17b). While interesting theoretical research has been recently devoted to the understanding of the interactions of surfactant molecules and methane clathrates, these studies typically started from the perspective of using surfactants as inhibitors of clathrate nucleation in water/hydrocarbon mixtures, as undesired clathrate formation could block pipelines and subsea flowlines.<sup>296</sup> For instance, Bui *et al.*<sup>297</sup> employed combined standard and enhanced sampling MD simulations to a oil/water/clathrate system and verified that surfactants may both control the methane transport across the oil to the clathrate phase and structure neighboring water molecules into more ordered configurations, promoting hydrate growth. Bertolazzo *et al.*<sup>298</sup> and Naullage *et al.*<sup>299</sup> carried out MD simulations using coarse-graining (CG) approximations to enable the simulation of longer length/time scale simulations of water/hydrocarbon/surfactant systems. The former revealed that structure I clathrate surfaces are oleophilic and theoretically

quantified the effect of surfactant concentration on the nucleation rate of clathrates. Further investigations on this counterintuitive interaction patterns may help the development of other promoting molecules acting in the stabilization of surfaces of clathrate nuclei. Meanwhile, the coarse-grained based simulations investigated the factors controlling the thermodynamics and kinetics of water coalescence in bare and surfactant-covered clathrate surfaces surrounded by a water/alkane system, showing that dense monolayers composed solely of surfactants provide high barriers for water permeation and inhibit further clathrate growth. These works exemplify the potential of molecular simulation techniques to derive meaningful insights from clathrate/surfactant systems and could inspire future theoretical works to determine (i) the role of surfactants in the promotion of hydrogen clathrate coalescence and growth and (ii) the local atomic-level structure of these systems.

Computational methodologies are also attractive to explore alternative approaches still not extensively investigated experimentally due to the need for dedicated experimental setups or the cost for these experiments. One such promising approach is guest exchange (cf. Figure 17c), in which one would first grow clathrates at mild conditions using other guest molecules as templates to be later flushed through H<sub>2</sub> injection. Liu *et al.*<sup>221</sup> studied through static *ab initio* and classical MD calculations the replacement of N<sub>2</sub> with H<sub>2</sub> in SII clathrate hydrates. They revealed that (i) H<sub>2</sub> can potentially replace N<sub>2</sub> in the larger cages of the clathrate network, although this event is less likely to occur in the smaller cages, (ii) both gases can coexist in larger cages or in separate cages, and (iii) a maximum H<sub>2</sub> loading amount of ca. 4.4 wt.% could be achieved via this gas exchange method. Several other computational studies have described gas replacement mechanisms in clathrates, most of them aiming at describing the replacement of CH<sub>4</sub> by CO<sub>2</sub> either for accelerating the recovery of CH<sub>4</sub> or for the sequestration of CO<sub>2</sub> in clathrate matrices.<sup>300–305</sup> For instance, Liu *et al.*<sup>306</sup> applied *ab initio* MD calculations to investigate the thermodynamics and kinetic mechanisms involved in the replacement of CH<sub>4</sub> by a N<sub>2</sub>/CO<sub>2</sub> mixture in a structure I clathrate. They noticed that N<sub>2</sub> substitutions occur in the smaller cages and are kinetically dominated, while CO<sub>2</sub> exchanges occur in larger cages and are thermodynamically dominated. Matsui *et al.*<sup>307</sup> reinforced these results by carrying out microsecond-long MD simulations. They also showed that the experimentally-confirmed improvement of CH<sub>4</sub> recovery by injecting a CO<sub>2</sub>/N<sub>2</sub> mixture in comparison with injecting each gas individually<sup>308</sup> is obtained by the occurring of major disruptions of the clathrate structure. Wu *et al.*<sup>309</sup> demonstrated from MD calculations the role of CO<sub>2</sub> surface adsorption in the stabilization of a template clathrate matrix and the growth of secondary CH<sub>4</sub>-CO<sub>2</sub> heteroclathrates to be favoured after CH<sub>4</sub> molecules are displaced from the template matrix by CO<sub>2</sub> injection. These early results form a rich source of inspiration for additional theoretical studies concerning (i) the feasibility and kinetics/thermodynamics of mono- and multicomponent H<sub>2</sub> mixtures to replace guest molecules in template clathrate matrices and (ii) the role of H<sub>2</sub> replacement in the preservation, disruption or co-growth of the hydrogen bonded clathrate framework and in the creation of defects or self-healing of this structure.

## 11.2. Clathrate growth in nanoconfinement

A promising and completely different approach to facilitate clathrate growth and stabilize clathrate structures is by growing them under nanoconfinement (Figure 17d). Recent studies demonstrate that confining hydrate assemblies in nanoporous solids facilitates clathrate synthesis at mild pressures and temperatures and speeds up their nucleation and growth

kinetics, given the intimate interactions in the water/gas interfacial region under nanoconfinement.<sup>310–314</sup> A recent review explored experimental and theoretical aspects involved in the formation of hydrates in confinement, although these studies were focused on CH<sub>4</sub> clathrates.<sup>315</sup> In this contribution, the authors detailed the formation of clathrates in nanopores as a complex phenomenon involving multiple factors, with surface chemistry and pore sizes being among the most important ones. They also pointed out mesopores with moderate hydrophobicity as optimal candidates for promoting gas hydrate formation, as this allows finding a balance between (i) overcoming the capillary forces and (ii) preserving the preferential tetrahedral orientation of water molecules close to pore's surface. Computational efforts succeeded in providing more details on the microscopic mechanisms of clathrate formation and interaction with the surface of nanopores. DeFever and Sarupria<sup>316</sup> employed a coarse-graining approach to model guest and water molecules in pores formed by hydrophobic and hydrophilic self-assembly monolayers. In this work, a coarse graining approach was employed to show that the clathrate nucleation starts at the center of the pores and a more hydrophilic surface was noted to promote the kinetics of clathrate nucleation. Cox *et al.*<sup>317</sup> employed a similar modeling strategy using a kaolinite and a graphene surface to study the CH<sub>4</sub> clathrate nucleation, not observing noticeable differences in the nucleation pattern from one surface to the other while confirming the same nucleation pattern, initiated at the center of the pores. Li *et al.*<sup>318</sup> applied more detailed atomistic MD calculations to study the mechanisms of CH<sub>4</sub> clathrate formation on kaolinite surfaces. While the same nucleation mechanism was observed, the authors were able to further describe the topology of half cages formed by the clathrate nuclei at the vicinities of pore surfaces. This pattern of nucleation was also confirmed by similar calculations carried out by Yu and Yazaydin<sup>319</sup>, who also unambiguously showed the nucleation of CH<sub>4</sub> clathrates confined in silica pores to occur at pressures too low for the growth of the hydrate in the bulk. Such contributions are expected to provide a theoretical guiding towards future experimental studies allowing the growth of H<sub>2</sub> clathrates in nanoconfinement.

### 11.3. Current challenges and opportunities

Notwithstanding the diversity of computational studies related to the topic of hydrogen clathrates detailed in the last paragraphs, there are still considerable challenges ahead to computationally describe the formation and stabilization of clathrates at ambient conditions and in complex environments. The evaluation of the nucleation and growth of clathrates at mild conditions is particularly challenging due to the high free energy associated with these events. As a result, standard MD calculations would have to be performed for excessively long-time scales. As a result, several studies have attempted to simulate more efficiently such nucleation events, mostly by (i) increasing the driving force of nucleation by overcooling, overpressurizing or supersaturating the system<sup>291,320</sup>, (ii) reducing the complexity of the simulated species considering coarse graining water and solute models<sup>293,321</sup> or (iii) applying enhanced<sup>322,323</sup> sampling techniques. However, the introduction of bias or the oversimplification inherent to CG approximations severely affect the nucleation mechanism, generating amorphous or SII CH<sub>4</sub> clathrates instead of the SI structure observed experimentally.<sup>324</sup> More recently, transition path sampling techniques<sup>324,325</sup> have been suggested as an alternative methodology to overcome these limitations and correctly predict the nucleation of clathrates in mild conditions. However, path sampling techniques require the knowledge of the final clathrate configuration, which is troublesome if those final

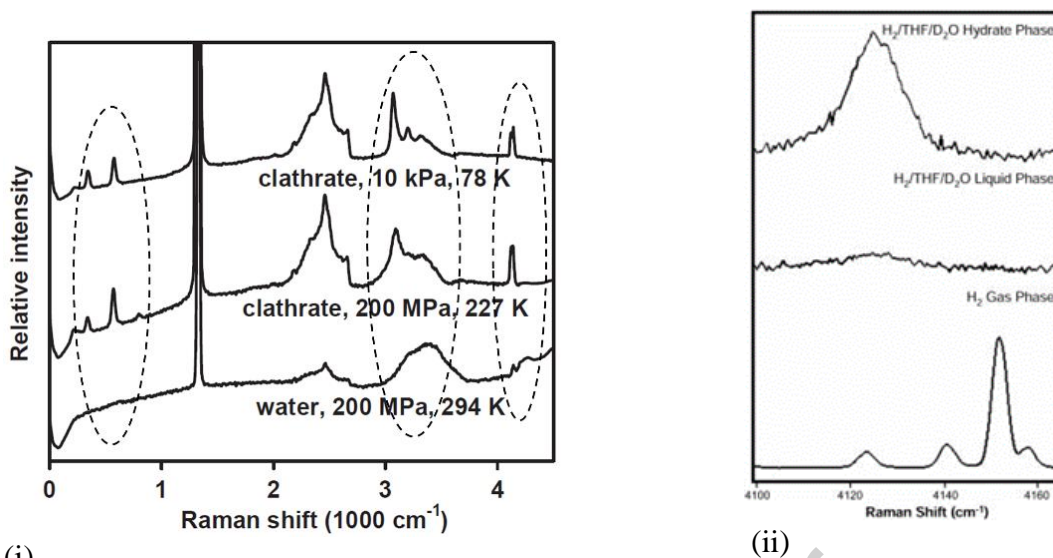
clathrate configurations are not directly known from experiments. Apart from these limitations, simulations of hydrogen clathrates pose additional challenges. Due to their light nature, nuclear quantum effects (NQE) substantially affect the behavior of hydrogen molecules, especially at the higher pressures and lower temperatures that facilitate clathrate growth.<sup>326</sup> These NQEs are essential as the quantization of the translational-rotational states inside clathrate cages at these experimental conditions cannot be fully ignored. Nevertheless, taking into account NQEs require advanced and highly computationally demanding techniques, such as path integral molecular dynamics.<sup>326</sup> Further advancing our computational insight in hydrogen clathrate formation and enabling highly accurate studies on hydrogen clathrates therefore crucially depends on the development of affordable yet robust computational techniques that allow to accelerate nucleation events and account for NQEs.

## 12. Characterisation techniques in clathrates

All the scientific studies in the field of hydrogen clathrates ultimately depend on the accuracy of the characterisation techniques used and their ability to detect and quantify the presence of hydrogen. Advance characterisation techniques such as in-situ Raman, NMR, HRXRD and Neutron diffraction have been utilised and several advancements have been made thereof. This section will briefly discuss these developments and highlight how these techniques have been vital to hydrogen clathrate research along with their limitations.

### 12.1. Raman Spectroscopy

The beginning of 2000s represented one of the most influential periods of time for the insertion of Raman spectroscopy into the study of water-based clathrates for hydrogen storage<sup>4,256</sup>. Notably, Mao *et al.*<sup>3,4,191</sup> defined the representative regions in the Raman spectra for which the hydrogen clathrates formation is clearly observed (Figure 18 (i)). The broad band between 3000-3600  $\text{cm}^{-1}$ , characteristic to OH from the liquid water, sharpened during the sII clathrate structure formation at 200 MPa and 227 K, as well as at 10 kPa and 78 K. At the same time, distinctive bands in the 300-850  $\text{cm}^{-1}$  region appeared and were correlated with the hydrogen roton peaks. Finally, the most representative bands for the hydrogen clathrates were found in the 4100 to 4200  $\text{cm}^{-1}$  region, assigned to the hydrogen vibrons present into the cages of sII clathrate structure. In contrast to roton peaks, which were observed at similar frequencies with the ones of pure hydrogen, the vibron bands were shifted to higher frequencies when compared to pure hydrogen, due to the increased vibrational coupling within the  $\text{H}_2$  molecules inside the cages. This discrimination suggests that, in the clathrate form, hydrogen is in free rotational state and at the same time, enclosed into the small cages of the sII structure. Their initial assignment of the bands in the hydrogen vibron region (4100 to 4200  $\text{cm}^{-1}$ ) suggested an equal distribution between the lower frequency group 5<sup>12</sup>6<sup>4</sup> (4115-4135  $\text{cm}^{-1}$ ) and higher frequency group 5<sup>12</sup> (4135-4155  $\text{cm}^{-1}$ ) cages.



(i) Figure 18. (i) Raman spectra of the selected regions for the hydrogen clathrates,  $300\text{--}850\text{ cm}^{-1}$ ,  $3000\text{--}3600\text{ cm}^{-1}$ ,  $4100\text{--}4200\text{ cm}^{-1}$  (reprinted with permission from Mao *et al.*<sup>4</sup>, Copyright 2002 The American Association for the Advancement of Science), (ii) Raman spectra of the hydrogen molecular rotors for  $\text{H}_2/\text{THF}/\text{D}_2\text{O}$  hydrate/liquid and pure  $\text{H}_2$  gas (reprinted with permission from Florusse *et al.*<sup>178</sup>, Copyright 2004 The American Association for the Advancement of Science).

In order to stabilize and facilitate the storage of hydrogen clusters at lower pressures, Florusse *et al.*<sup>178</sup> studied the effect of a second guest component, the case of tetrahydrofuran (THF), in a mixed system of  $\text{H}_2\text{O} + \text{H}_2 + \text{THF}$ . Their investigation suggested a completely different hydrogen cage occupancy than the one implied by Mao *et al.*<sup>4</sup> As the majority of the large cages of the sII structure were filled with THF molecules, the only available space for the hydrogen molecules to occupy in this arrangement was represented by the small cages. They concluded that for the  $\text{H}_2/\text{THF}$  hydrate, the H-H vibron band at  $4125\text{ cm}^{-1}$  is due to the hydrogen presence in the small cages  $5^{12}$  (Figure 18 (ii)). Lee *et al.*<sup>179</sup> studied the same system of THF +  $\text{H}_2$  through a series of experiments where pressure or THF concentration was varied. Here, Raman spectroscopy was used to gain information not only about the clathrates formation (qualitative) but also about the amount of hydrogen (quantitative) in the sII structure, when THF loading was varied. The Raman band intensities were used to approximate the composition of the hydrates, from their corresponding integral area. Based on the ratio between Raman intensity and the volumetrically measured  $\text{H}_2$  content obtained from the corroborated results of the multiple experiments at different THF concentrations, the authors assumed the extinction coefficients to be constant. Besides the cage occupancy of the  $\text{H}_2$  and THF guests in sII hydrate structure formed at 150 MPa and 250 K (Figure 6(i)), Strobel *et al.*<sup>185</sup> attempted to address the peculiar behaviour of the hydrogen frequency positions in the two cages of sII structure,  $5^{12}$  and  $5^{12}6^4$ . The widely regarded bias suggests that “the larger the cavity, the lower the frequency of the stretching vibration of the guest” and it is based on a complete study of Subramanian and Sloan<sup>327</sup>. The study focused on (i) a series of guest molecules in a sII hydrate, (ii) various guests in different hydrate cages and (iii) corroborated with qualitative “loose cage–tight cage” model of Pimentel and Charles<sup>328</sup>. In regards to this, Strobel *et al.*<sup>185</sup> assumed that the small cages stretching frequencies appear at lower values due to the presence of more hydrogen molecules in the large cages, thus creating a tighter environment when compared to the small cages.

Giannassi *et al.*<sup>192</sup> concentrated their efforts on a series of Raman experiments involving the use of heavy water (D<sub>2</sub>O), fully deuterated tetrahydrofuran (TDF) and H<sub>2</sub>, at low temperatures after the clathrates were formed at pressures of ~800 bars or ~2000 bars and the temperature was around -10 °C. The Raman cell allowed the clathrate samples to be cooled at very low temperature (~20 K), while helium gas was introduced at different pressures (500 mbar to 1 bar) and assured a good thermal conductivity as well as decreased the chance of laser-induced sample local heating effect. In their assessment for the H<sub>2</sub> + TDF clathrate, the well-defined peaks distinctive for the small cavities of the sII structure are found at 4118 cm<sup>-1</sup> and 4124 cm<sup>-1</sup> attributed to Q<sub>1</sub>(1) and Q<sub>1</sub>(0) modes, respectively, as concluded from previous studies<sup>3,4,185,256</sup> (Figure 19(i)). A similar behaviour was observed for D<sub>2</sub> + TDF clathrate system at considerable different frequencies shift (between 2960 cm<sup>-1</sup> and 2990 cm<sup>-1</sup>, Figure 19(ii)). However, the investigation of the large cavities of the same system led to a reversed assignment compared to the one found by Strobel *et al.*<sup>185</sup>. They observed that a maximum occupation of 4 molecules in the large cavities is negligible, as no bands corresponding to this were clearly observed, while the triple, double and single occupations are observed from low to high frequencies. The reasoning behind the assessment of the frequencies position related to the large cages occupations is based on the fact that a molecule in a large cage is less perturbed than more molecules present in the same confined space, thus behaving more similar to a free molecule. As the free molecules are found at higher frequencies, the signal of one molecule occupying the large cage should be closer to the signal of free molecules, followed by the double and triple large cages occupancy signal. At the same time, the stability of the simple (hydrogen) and binary clathrates was studied, comparing the results obtained right after the formation and after 3 months conservation in liquid nitrogen (all clathrates measured at 77 K). From the Q<sub>1</sub>(1) and Q<sub>1</sub>(0) pairs, attributed to ortho and para hydrogen, the authors concluded that over the time there is a switch between their concentrations. From an initial concentration of 75% - 25% ortho - para, to a 39% - 61% ortho - para, after 3 months.

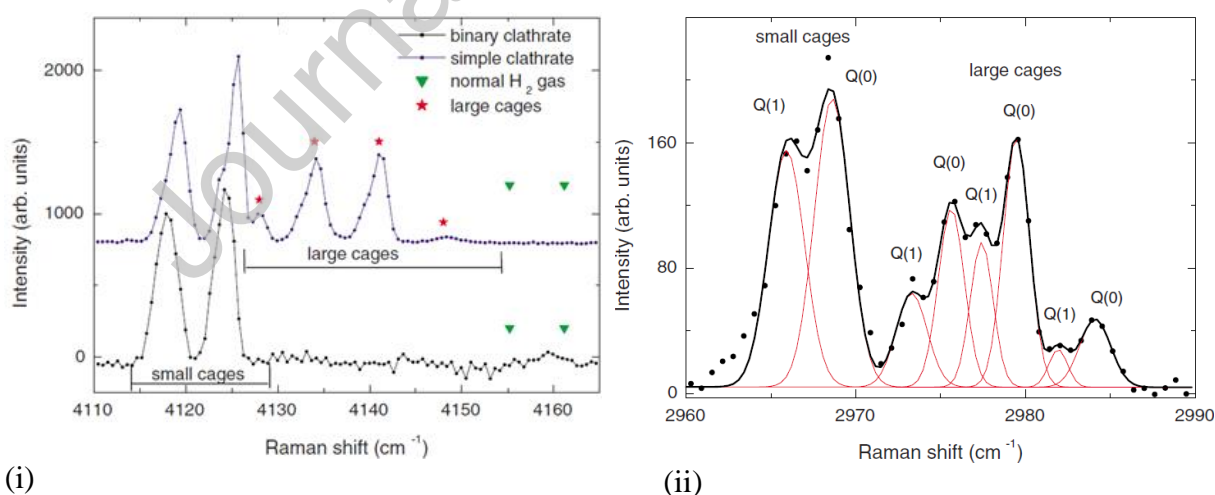


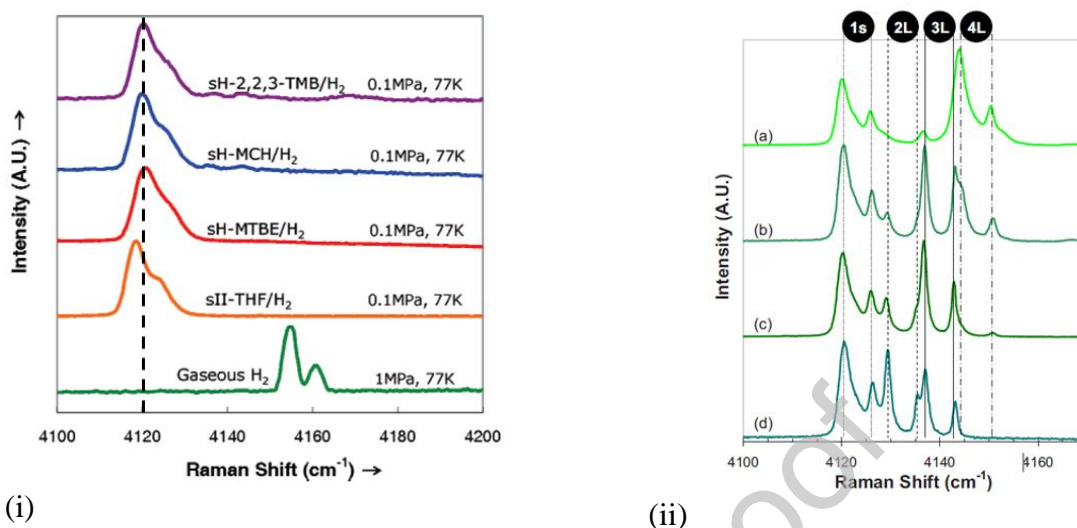
Figure 19. (i) Raman maxima for the well-defined small and large cages of simple (H<sub>2</sub>) and binary clathrates (H<sub>2</sub> + TDF) (ii) Vibrational spectrum and assigned deconvoluted peaks for simple D<sub>2</sub> clathrate (reprinted with permission from Giannasi *et al.*<sup>192</sup>, Copyright 2008 AIP Publishing).

Sugahara *et al.*<sup>329</sup> studied the cage occupancy of hydrogen in a series of ternary systems, involving carbon dioxide, ethane, cyclopropane and propane hydrates, measured at 276.1 K and up to 5 MPa. In the H<sub>2</sub> + CO<sub>2</sub> + water system they concluded that the H<sub>2</sub> is not present in the CO<sub>2</sub> hydrate cages, but rather absorbed on the surface of the hydrate. These

findings are not in agreement with the previous data reported by Kim *et al.*<sup>192</sup>, in which a clear broad band at  $4130\text{ cm}^{-1}$  was observed and correlated with the presence of  $\text{H}_2$  molecules trapped in the hydrate cage. This discrepancy is attributed to the different preparation methods for the hydrate samples. Similar to the previous system ( $\text{H}_2 + \text{CO}_2 + \text{water}$ ), Sugahara *et al.*<sup>329</sup> reported no  $\text{H}_2$  in the ethane or cyclopentane sI hydrate structure. However, in the system consisting of  $\text{H}_2 + \text{propane} + \text{water}$ , a broad band at  $4131\text{ cm}^{-1}$  is detected in the Raman spectra and assigned to the  $\text{H}_2$  encage in the small cage of the sII hydrate structure. They concluded that  $\text{CO}_2$ , ethane and cyclopentane sI hydrate structures are not able to encage  $\text{H}_2$ , while the propane sII hydrate structure is the only one able to store  $\text{H}_2$ , with respect to their experimental conditions. Initial experiments showed that the sapphire window is not suitable for this type of experiments, due to overlapping bands of  $\text{H}_2$  hydrate with the impurities from the sapphire ( $4100\text{-}4200\text{ cm}^{-1}$ ). To correct this, the Raman cell was equipped with a highly pure quartz window. Strobel *et al.*<sup>330</sup> reported the stabilization of hydrogen in a clathrate hydrate sH structure, facilitated by the presence of an additional large molecule (methyl tert-butyl ether MTBE, methylcyclohexane MCH, 2,2,3-trimethylbutane 2,2,3-TMB) at 150 MPa and 275 K. The Raman results of all the sH hydrate structures in the region  $4100\text{-}4200\text{ cm}^{-1}$  showed a small blue shift of the broad hydrogen vibron band, when compared to the sII-THF/ $\text{H}_2$  system (Figure 20 (i)). This shift was attributed to the discrete size differences between the sH and sII cages, which has direct implications on the hydrogen interactions with the host lattices. Moreover, after normalizing and overlapping the vibron region of the sII and sH hydrate, they noticed that the shoulder of the  $\text{H}_2$  in sH structure was less pronounced than the one of  $\text{H}_2$  in sII structure and the peaks of the  $\text{H}_2$  in sH was broader than the one characteristic to  $\text{H}_2$  in sII.

In a later study, Strobel *et al.*<sup>190</sup> performed a series of experiments to check if the Raman *ex-situ* analysis was in agreement with the Raman *in-situ* analysis for the study of simple sII hydrogen clathrates and binary sII THF +  $\text{H}_2$  clathrate hydrates. Their findings suggested a similar trend between the two techniques and for the further experiments the *ex-situ* technique was applied. At the same time, they confirmed the findings reported in previous work<sup>185</sup>, regarding the change of the ortho-para hydrogen ratio in time. Based on a heat/quench series of cycles, the Raman experiments measured at 76 K and 0.1 MPa, revealed that the large cages of the sII hydrate are occupied by hydrogen in order, from the highest frequency for the quadruply occupied cages to middle frequency for the triply occupied cages and finally the lowest frequency for the doubly occupied cages. This assessment was completely different than the one of Giannassi *et al.*<sup>192</sup>. The motivation was based on the Raman signal observations: (i) decrease of the signal for the quadruply occupied cavities, (ii) increase and then decrease of the signal for the triply occupied cavities and (iii) continuous increase of the signal for the doubly occupied cages, during the heat/quench cycles (Figure 20 (ii)). As a mechanism, they proposed a migration pathway for hydrogen through the hexagonal face sharing connectivity, as the highest amount of hydrogen in the hydrates was observed immediately after the formation, while the heat/quench measurements after each cycle were performed at ambient pressure. Moreover, during the diffusion of the  $\text{H}_2$  inside large cavities of the clathrate structure, the small cages occupancy remains unperturbed. Koh *et al.*<sup>210,233</sup> studied the effect of multiple guest occupancy and the tuning of the cage dimensions consequence in clathrate hydrates, using *ex-situ* Raman spectroscopy. The measurements were performed using an Ar-ion laser emitting 514.53 nm (green laser), with an intensity of 30 mW and a cooled CCD detector. Their experiments revealed, in some

of the cases, the presence of 2 H<sub>2</sub> molecules in the small cage at Raman shift values higher than the ones of multiple H<sub>2</sub> molecules in the L-cages. Moreover, they correlated well the assumption of 1% detection level of Raman with simulations and experimental observations for the H<sub>2</sub> doubly occupied small cages.



(i) (ii)  
Figure 20. (i) Vibrational region assigned to H<sub>2</sub> encaged into the sH hydrate cages and sII hydrate cages (reprinted with permission from Strobel *et al.*<sup>231</sup>, Copyright 2008 American Chemical Society), (ii) Raman spectra of (a) initial hydrogen hydrate and after each (b)-(d) heat/quench (reprinted with permission from Strobel *et al.*<sup>190</sup>, Copyright 2009 AIP Publishing).

Aside from the use as a promoting agent for H<sub>2</sub> storage in clathrate hydrates, Zhong *et al.*<sup>197</sup> proposed the use of THF as a highly selective membrane to separate H<sub>2</sub> from gas mixtures. They performed *in-situ* Raman resolved analyses on a THF hydrate layer and followed the diffusion of H<sub>2</sub>, CH<sub>4</sub> and CO<sub>2</sub>, concluding that only H<sub>2</sub> is able to penetrate a 5 mm thick THF hydrate membrane in 24h. The main part of the *in-situ* Raman setup able to measure at various positions with a depth between 0.0 to 0.5 mm is shown in Figure 21 (i). The competitive cage occupancy of Ar and H<sub>2</sub> in an Ar + H<sub>2</sub> + water as a ternary system (forming a sII hydrate structure at 276 K and pressures between 27 – 100 MPa) was studied by Amano *et al.*<sup>219</sup>. The vibron bands of H-H are very similar for the simple H<sub>2</sub> hydrate and H<sub>2</sub> + Ar mixed-gas hydrate. The experiments performed at equilibrium pressure lower than simple H<sub>2</sub> hydrate showed a tendency of Ar to be encaged in the hydrate structure cavities in a direct competition with H<sub>2</sub> for both cavities of the hydrate (S and L). Moreover, the peak corresponding to 4 H<sub>2</sub> molecules entrapped in the large cavity (4151 cm<sup>-1</sup>) appeared at lower pressure than expected (27 MPa), allowing a potential increased amount of H<sub>2</sub> to be stored at lower pressures. Finally, they observed that concomitant with the decrease of the equilibrium pressure, the maxima at 4143 cm<sup>-1</sup> assigned to 2 or 3 H<sub>2</sub> molecules in the L-cage, decays more than the 4151 cm<sup>-1</sup> maxima of the 4 H<sub>2</sub> molecules in L-cage for the Ar + H<sub>2</sub> hydrate, while the reverse trend was depicted for the simple H<sub>2</sub> hydrate. This suggests that the contribution of 4 H<sub>2</sub> in L-cage stabilizes at a similar level with the presence of Ar the structure, while 2 or 3 H<sub>2</sub> in L-cage provides a lower degree of stabilization. The other possibility involved the simultaneous presence of Ar and H<sub>2</sub> in the L-cages. Grim *et al.*<sup>195</sup> researched the influence of the quenching technique on the preservation of hydrogen hydrates for the *ex-situ* Raman analysis. The quenching technique involves the use of liquid N<sub>2</sub> to avoid the dissociation of the hydrates during the sample recovery in conditions of normal pressure, prior to Raman measurements. Their experiments focused on a series of steps

before the actual *ex-situ* Raman spectra were acquired (Figure 21 (ii)). After the hydrate formation (3 days), additional powdered ice was mixed with the seed hydrate and loaded again in a cool high-pressure cell for 4h, followed by a quenching step and Raman acquisition. Since Raman is a local technique, the addition of extra powdered ice (dilution ~90%) complicated the spectra acquisition. In order to correct this, the authors collected data from 5 to 15 points, while the experimental conditions were repeated at least 3 times. At the same time, Lu *et al.*<sup>331</sup> confirmed the inhomogeneous formation of the hydrates via Raman spectroscopy, using for each spectrum a 6 min. acquisition time with a ~15  $\mu\text{m}$  laser spot. In this case, the results acquired on a local part of the sample had a beneficial effect for the overall characterization of the clathrates. For the  $\text{N}_2 + \text{H}_2$  hydrate system (243 K and 15 MPa), they concluded that the peaks at 4150-4160  $\text{cm}^{-1}$  show the presence of 2  $\text{H}_2$  molecules in the small cavities and not 1  $\text{H}_2$  co-existing with 1  $\text{N}_2$ . For the spectra where only the bands for 2  $\text{H}_2$  molecules occupying the S-cage were observed, the L-cages were fully occupied by  $\text{N}_2$  molecules. The bands in 4129-4150  $\text{cm}^{-1}$  region represent multiple  $\text{H}_2$  in the L-cages without co-existing with  $\text{N}_2$  molecules, due to the almost perfectly match with the results obtained for pure  $\text{H}_2$  hydrate.

Park *et al.*<sup>217</sup> investigated the effect of the propylamine (i-PA, n-PA) concentration on tuning behaviour for hydrogen clathrate hydrates. Taking into account the observations of Grim *et al.*<sup>195</sup> regarding the fast formation of the  $\text{H}_2$  hydrate from preformed hydrate seeds during the quenching step, Park *et al.*<sup>217</sup> performed a series of *ex-situ* Raman analyses to differentiate this from the tuning effect. The independent results from the experiments carried out with and without liquid nitrogen confirmed the tuning effect, as the Raman spectra were very comparable for both separate ways to obtain the  $\text{H}_2$  hydrates. In a later study, Grim *et al.*<sup>224</sup> used a similar approach to incorporate  $\text{H}_2$  in a sI hydrate structure, using as base  $\text{CH}_4/\text{CO}_2$  hydrates and *ex-situ* Raman as the main characterization method. Additionally, they used a Linkam THMS 600 cooling stage to preserve the hydrates at 83 K during the *ex-situ* Raman. Based on their Raman results, the enclathration of  $\text{H}_2$  in the sI structure follows two potential pathways, namely diffusion and/or hydrate melting succeeded by reformation.

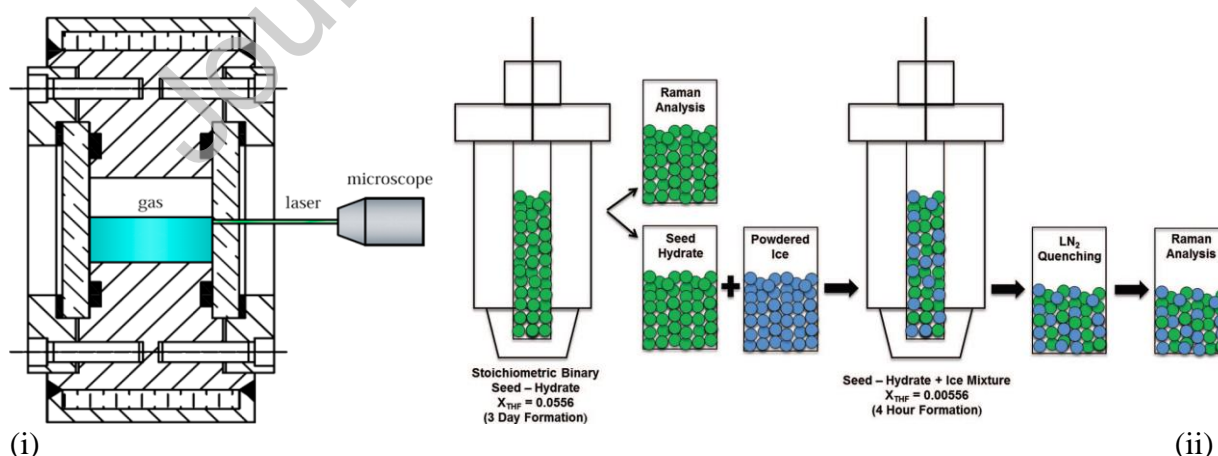


Figure 21. Schematic representation of the (i) main in-situ Raman equipment able to analyse different depths (reprinted with permission from Zhong *et al.*<sup>197</sup>, Copyright 2017 American Chemical Society) (ii) Hydrate seeding synthesis pathway (reprinted with permission from Grim *et al.*<sup>195</sup>, Copyright 2012 AIP Publishing).

Particularly, Del Rosso *et al.*<sup>255</sup> designed a remarkable *in-situ* Raman system able to withstand very high pressures (about 2 kbar). The high thermal conductivity beryllium-

copper alloy optical cell is designed to contain liquid water and H<sub>2</sub> as gas phase in the first step of the process, considering the simple H<sub>2</sub> hydrate. This allowed the acquisition of Raman spectra before and after the sample solidification and hydrogen clathrate formation. The optical access is insured by three vertical faces diamond windows, where the scattered radiation is collected at 90° vs. the incident radiation minimizing the acquisition of the incident radiation. The almost cubic shape geometry of the cell (internal volume ~ 0.4 cm<sup>3</sup>) is presented in Figure 22 (left), where the laser aim is coloured in yellow (left side). Their experiments suggest that Raman analysis was able to detect very small amounts of hydrogen hydrates, however quite larger than a critical nucleus. In this specific experimental setup, it was shown that the growth of the H<sub>2</sub> clathrates is slowed down by the diffusion of the H<sub>2</sub> molecules in water.

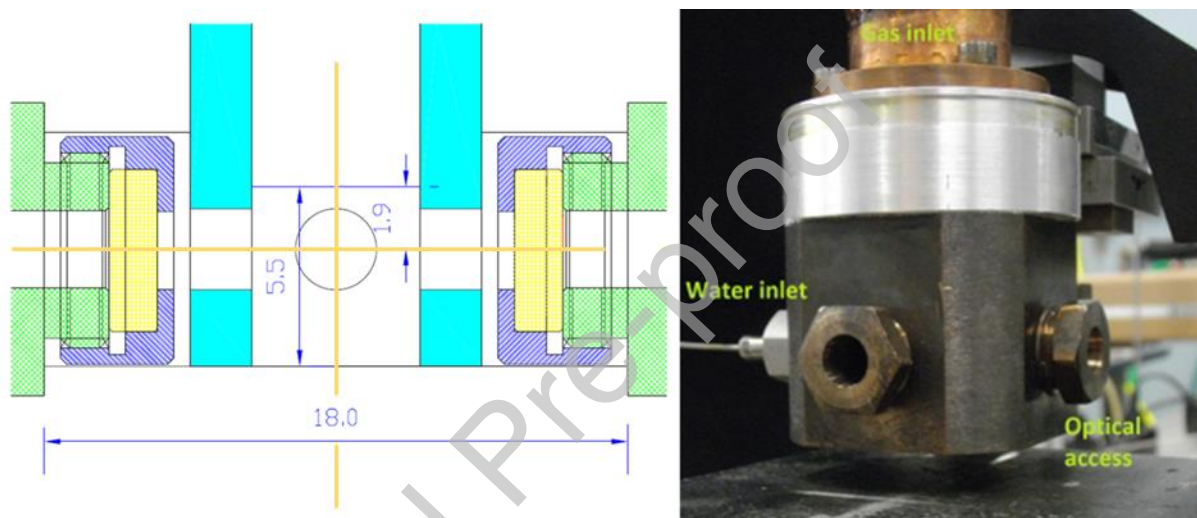


Figure 22. Schematic (left) and real (right) in-situ Raman cell able to withstand very high pressures (up to 3 kbar) (reprinted with permission from del Rosso *et al.*<sup>255</sup>, Copyright 2015 American Chemical Society).

Cai *et al.*<sup>264</sup> carried out *in-situ* Raman analyses on a THF-hydrogen binary hydrate focusing in and around the gas/liquid interface during the hydrate formation process. The results suggested that H<sub>2</sub> molecules tunnel among hydrate cavities in the hydrate layer and for the first time proved the tunnelling movement of H<sub>2</sub> molecules through the liquid system.

In the current section, all the Raman results (*in-situ/ex-situ*) were obtained on instruments equipped with green lasers (514 or 532 nm), while various intensities were used (<100 mW). As an easy to implement technique it allows rough quantifications of H<sub>2</sub> molecules in different hydrates cages as well as identifying orto-para H<sub>2</sub> species. Both *in-situ* and *ex-situ* analyses are fast and require a small amount of sample. The discrete differences between the cage sizes of each hydrate structure are noticeable as frequency shifts for the H<sub>2</sub> vibron molecules, thus allowing to distinguish between the hydrate structures in which the H<sub>2</sub> molecules are present. As a local technique and regarded in most of the applications as a drawback, for hydrogen hydrates characterisation provides unique information about the homogeneity of the sample, as well as specific structural insights, if used at the interface or different depths of the matrix.

Raman and infrared analyses are often regarded as complementary techniques for a complete study. In the case of hydrogen hydrates, infrared spectroscopy is not the most

straight forward technique, since  $H_2$  is a homonuclear molecule and as a result without a permanent electric dipole moment. As a direct consequence of this, in normal conditions, hydrogen does not absorb the infrared radiation. However, in solid hydrogen case, the infrared absorbance of  $H_2$  is due to an induced dipole moment, resulted from the interaction with the neighbouring molecules. Similar to this, in a confined space and high pressure systems as the case of hydrates cages, hydrogen can present collision-induced infrared activity<sup>332</sup>. Even if infrared spectroscopy can provide some useful information for the hydrogen hydrates structural characterization, Raman spectroscopy appears to be richer in information, thus preferred much more by the scientific research community.

## 12.2.NMR Spectroscopy

Nuclear magnetic resonance (NMR) spectroscopy provides a powerful and direct probe to investigate the local chemical environment of protons.  $^1H$  NMR quantitatively reveals all hydrogen atoms in a sample, independent of the local structure they are part of (i.e.  $^1H$  nuclei taking part in clathrate structures, confined molecules or other materials present), enabling to discriminate and identify all protons and their interactions.<sup>333</sup> This unique property renders  $^1H$  NMR spectroscopy particularly suited for characterizing clathrate hydrate structures *ex situ*, *in situ* and potentially even *operando*.

Because of the high-pressure required for their formation, NMR characterization of hydrogen containing clathrate hydrate samples is typically performed on *ex situ* prepared samples. Following their formation, the clathrates are quenched in liquid nitrogen, subsequently packed in a 4 mm zirconia rotor and transferred to a pre-cooled NMR probe (often at 183 K). Using this approach, Florusse *et al.*<sup>178</sup>, Lee *et al.*<sup>179</sup> and Strobel *et al.*<sup>180</sup> have been able to confirm the presence of  $H_2$  in the small cages of a binary sII clathrate hydrate structure formed with  $D_2O$  and perdeuterated THF (THF- $d_8$ ) as thermodynamic promotor.<sup>178,334,335</sup> They all reported a sharp  $^1H$  signal at 4.3 ppm which was attributed to the presence of one  $H_2$  molecule in the  $5^{12}$  cages of sII clathrate hydrate. Multiple hydrogen occupancy of the  $5^{12}$  cage has been hinted at by Florusse *et al.*<sup>178</sup>. Integration of the  $H_2$  resonance yielded an occupancy of 0.5  $H_2$  molecules per cage, whereas volumetric measurements on similar samples performed during hydrate dissociation revealed an average occupation of 1.0  $H_2$  molecules per cage.<sup>178,244,336</sup> This discrepancy was attributed to a loss of  $H_2$  during NMR measurements as the NMR rotor was exposed to atmospheric pressure.<sup>178</sup> The 4.3 ppm  $^1H$  NMR *fingerprint* of  $H_2$  molecules confined to  $5^{12}$  cages of SII and SI bulk clathrate hydrates was also observed in binary systems obtained with 1,4-dioxane and  $CO_2$  as promotors.<sup>337-339</sup> Lee *et al.*<sup>179</sup> reported a  $^1H$  NMR signal at 0.15 ppm appearing at low THF concentrations, which increased with decreasing THF concentration (Figure 23). This signal was assigned to  $H_2$  molecules occupying the large  $5^{12}6^4$  cages of the SII clathrate hydrate structure.<sup>334</sup> This experiment was repeated by Strobel *et al.*<sup>180</sup>, who failed to reproduce the (NMR) results obtained by Lee and co-workers, leaving their initial observations and  $^1H$  NMR assignments open for discussion.<sup>3,335</sup>

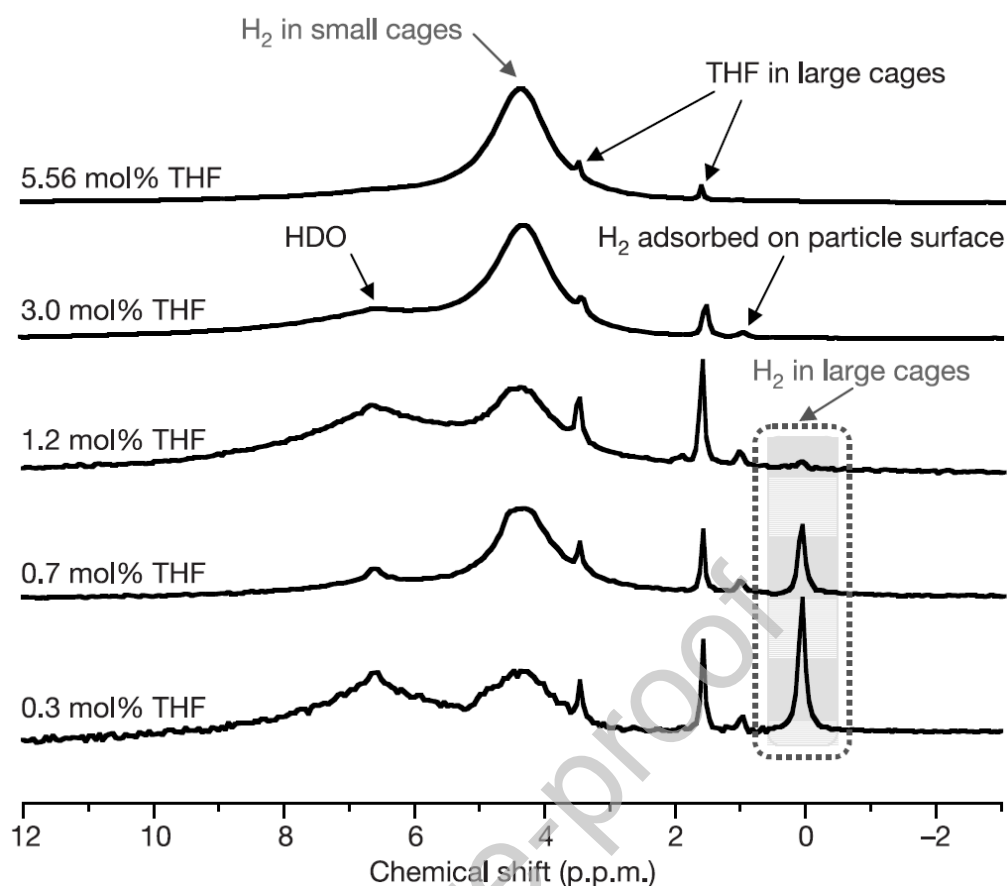


Figure 23. Evolution of the  $^1\text{H}$  NMR spectrum of the binary  $\text{H}_2/\text{THF}$  ( $\text{THF-d}_8$ ) clathrate hydrate with decreasing THF content (expressed as mol% THF in  $\text{D}_2\text{O}$ ). At lower concentrations ( $< 1.2$  mol% THF), a new signal emerges around 0.15 ppm which continues to grow with decreasing THF content. This  $^1\text{H}$  signal is attributed to  $\text{H}_2$  molecules residing in the large  $5^{12}6^4$  cages of the SII clathrate hydrate. The  $^1\text{H}$  signal originating from  $\text{H}_2$  molecules in the small  $5^{12}$  cages, typically observed around 4.3 ppm, is also highlighted (reprinted with permission from Lee *et al.*<sup>179</sup>, copyright Springer Nature 2005).

A more detailed characterization of the enclathration of hydrogen is obtained by following the hydrate formation process *in situ*. Okuchi *et al.*<sup>273</sup> proposed a sample environment based on a 10 mm sapphire tube (theoretically resisting pressures up to 20 MPa) to carry out static, *in situ* observations of the formation and dissociation of a binary  $\text{H}_2$  clathrate hydrate obtained from a perdeuterated  $\text{THF-D}_2\text{O}$  mixture.<sup>273</sup> Signal assignment proved challenging because of the limited spectral resolution, but Okuchi and his colleagues managed to isolate the 4.3 ppm  $^1\text{H}$  NMR signal characteristic of hydrogen in small clathrate cages by carefully decomposing the NMR spectrum.<sup>273</sup> Walter *et al.*<sup>340</sup> recently presented a new MAS NMR rotor design (the WHiMS rotor), capable of achieving internal pressures up to 40 MPa at lower temperatures.<sup>340</sup> This type of rotor has not yet been used for clathrate hydrate research, but its compatibility with hydrogen gas at elevated pressures opens up new perspectives for *in situ* NMR experimentation and characterization of  $\text{H}_2$  clathrate hydrates.

### 12.3.X-Ray and Neutron Diffraction

Diffraction techniques such as X-Ray Diffraction (XRD) and Neutron Diffraction (ND) are often performed to investigate the structural parameters of crystalline compounds. Also, the clathrate hydrates have been scrutinized using these techniques. Ever since their

discovery in the mid-1900s much work has been devoted to the elucidation of these inclusion compounds by researchers such as Clausen<sup>341</sup>, Mc Mullan<sup>342,343</sup>, Ripmeester<sup>344</sup> and Von Stackelberg<sup>345</sup>. G.A. Jeffrey<sup>343,346</sup> wrote several reviews on the subject, focusing on the clathrate host structures. As discussed earlier in this review, three major structures were identified (sI, sII and sH), all consisting of guest molecules engaged in polyhedra built from water molecules.

The use of X-Ray diffraction techniques for the structural analysis of hydrogen clathrates poses several problems. The first and major problem is the intrinsic instability of these materials in ambient conditions. Measuring these systems at their formation conditions (low temperatures and high pressures) is a challenging task that requires specialized equipment, often only found in synchrotron facilities<sup>347,348</sup>. It is also possible to measure the structures using lab-scale setups by quenching the sample cell in liquid nitrogen after the clathrate hydrate is formed, followed by a degassing step and analysis at ambient pressures and low temperatures. Most published reports use this latter (*ex situ*) approach for the determination of the structural parameters of hydrogen clathrates<sup>178,349,226,187,217,350,230</sup>.

The second problem originates from the limited interaction of x-rays with light elements such as hydrogen. This results in diffractograms that are dominated by oxygen-oxygen correlations, ultimately providing little to no information on the hydrogen atoms in the structure<sup>351</sup>. On top of that, hydrogen is prone to self-scattering and Compton scattering phenomena, inducing significant levels of noise in the final diffractograms.

Despite these challenging problems, X-Ray Diffraction has been successfully utilized to investigate structural changes in clathrates, either as a result of changing the promotor molecules, or evacuating and/or filling of clathrate hydrates<sup>350,352,220,222,224</sup>. These studies have offered great insights in the structures of these potential future hydrogen storage materials.

Synchrotron radiation sources generate X-Rays that are orders of magnitude more intense than the lab-scale diffractometers. As a consequence, the signal-to-noise ratios is enhanced substantially. Combined with Rietveld refinement, this method provides an excellent strategy for the accurate determination of the structural parameters of clathrate hydrates. Koh *et al.*<sup>210</sup> carefully examined the High Resolution Powder Diffraction (HRPD) data of hydrogen clathrates and showed that the lattice parameters, and thus cage sizes, are dependent on the nature of the guest molecule. This means that the cage sizes can be tuned. This studied confirmed the earlier work of Udachin *et al.*<sup>353</sup> This tuning effect could be very relevant to enhance the total hydrogen capacity of hydrogen clathrates by opening the possibility of H<sub>2</sub> double occupancy in the 5<sup>12</sup> cages of the sII framework. Additionally, the fine structure of these HRPD measurements as displayed in Figure 24 were used by Park *et al.*<sup>222</sup> to identify cage occupancies. Upon interchanging of nitrogen with hydrogen in a N<sub>2</sub>/THF hydrate system, a gradual decrease of unit cell size was observed while the sII structure was retained. Raman spectroscopy confirmed the gradual incorporation of hydrogen in both small and large cages with increased pressure, which was corroborated by a gradual shift and broadening of the reflections observed with HRPD. The X-Ray beams are of course also always improving and are becoming more and more brilliant, making the techniques virtually necessary when studying hydrogen clathrates.

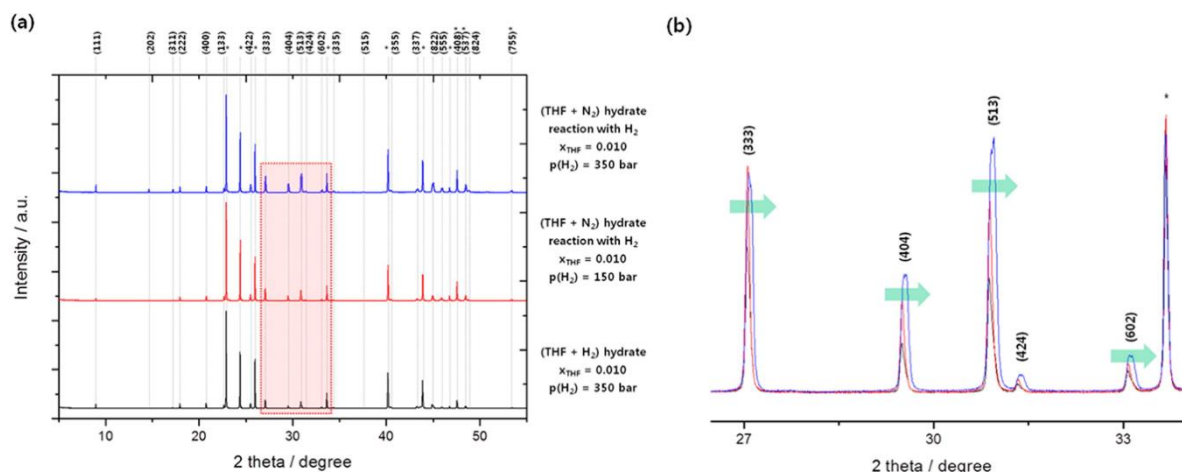


Figure 24. (a) HPRD patterns of the (THF + H<sub>2</sub>) hydrates and reaction product of (THF + N<sub>2</sub>) hydrates with H<sub>2</sub> recorded at ambient pressure and 80 K. (b) Enlarged region of 26.5° to 34.0°. Asterisks denote the reflections of the hexagonal ice-I<sub>h</sub> phase (reprinted with permission from Park *et al.*<sup>222</sup>, Copyright 2014 American Chemical Society).

Neutron diffraction techniques are more sensitive towards light elements, interacting with the target nucleus compared to the electronic shell as is the case with x-rays. As hydrogen only has one proton in its core that is able to interact with the incoming neutrons, deuterated systems are often studied instead. Deuterated samples show an increased intensity and a much less noise. Noise in neutron diffraction data comes from incoherent scattering and deuterium has a larger coherent scattering length and a smaller incoherent scattering cross section than hydrogen<sup>351</sup>. The technique has been used with great success to determine the structure of pure H<sub>2</sub> clathrates<sup>268,191</sup>, as well as the structure of binary clathrates<sup>245,211,183</sup>. The work of Hester *et al.*<sup>211</sup> provided a detailed mapping of a binary H<sub>2</sub>/THF clathrate where both structural information as well hydrogen occupancies could be determined. Donnelly *et al.*<sup>354</sup> utilized ND to study the phase diagram of hydrogen clathrate going from a C<sub>0</sub> to a sII structure through several P,T routes. The work provided evidence of the Ostwald Rule of Stages for hydrogen clathrates, meaning that the system transitions through a series of states of increasing stability. It should be noted that isotopic exchange between H and D results in the change of some physical properties of the system. Literature shows that this isotope effect induces a temperature shift in the phase transitions of D<sub>2</sub>O of approximately 10 K and 2-5 K for liquid and crystalline systems respectively<sup>351,355,356</sup>.

By utilizing the difference in incoherent scattering cross section between H and D, combined with Incoherent Neutron Scattering (INS), it is possible to study several properties of the included hydrogen in a deuterated host framework. In an in-depth work, Colognesi *et al.*<sup>357</sup> performed INS on several sII hydrogen clathrates. They were able to assign the bands in the resulting spectra to translational and rotational motions of encaged hydrogen molecules by using a quantum mechanical treatment of the system. Follow-up INS studies have further elucidated different morphologies of hydrogen clathrate systems, however this has proven to be quite complex<sup>358</sup>.

In Incoherent Quasi-Elastic Neutron Scattering (QENS), any dynamical process which takes place on a longer timescale than that of the measurement results in broadening of bands in the spectra. Incidentally, information on the diffusional motions of H<sub>2</sub> can be acquired by investigating broadening phenomena in the quasi-elastic region of the spectrum ( $\pm 3\text{meV}$ ), as

is illustrated in Figure 25. No  $H_2$  diffusion between cages could be observed on a picosecond timescale, as was concluded in the work of Pefoute *et al.*<sup>359</sup> for a binary  $H_2$ /THF clathrate.

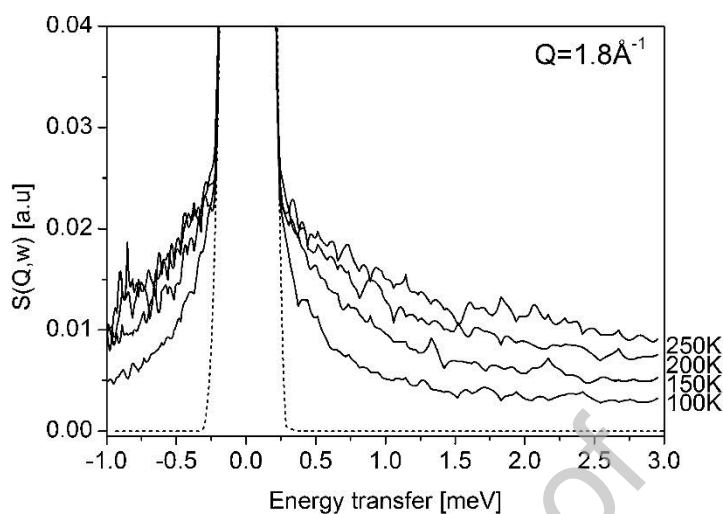


Figure 25. QENS spectra of the  $H_2$  molecules confined in the TDF clathrate hydrates recorded at various temperatures with the ToF spectrometer NEAT ( $\lambda_0 = 4.8 \text{ \AA}$ ). The dashed line corresponds to the spectrometer resolution function with  $\Delta E = 152 \text{ \mu eV}$  (determined from the vanadium QENS spectrum). All spectra are normalized (reprinted with permission from Pefoute *et al.*<sup>359</sup>, Copyright 2012 American Chemical Society).

### 13. Reactor Design: Industrial Level Scale-Up

From the industrial point of view, the main challenges associated with hydrate clathrates formation are: i) the extreme experimental conditions (low temperature coupled to high pressure), ii) their slow rate of formation, iii) the low storage capacity, iv) mass transfer limitations due to the interfacial nature of the conversion, and the v) heat transfer resistances associated with the interfacial phase-changing nature of the process and pressure vessels' thick walls. On the engineering side, as consequence of the required process conditions, the high refrigeration operational expenses and high capital expenses associated with pressure vessels are the key economic factors for feasibility. A convincing reactor technology should also be developed that proposes a solution to the challenges mentioned above.

In this section, we will review and comment over the scarce reactor design and scale-up attempts that were published for the production and storage of hydrogen and hydrogen hydrate clathrates (energy storage), but also  $CO_2$  hydrates (capture of  $CO_2$  from industrial flue gases).

#### 13.1. Kinetics-related and mass transfer limitations

Generally, the kinetics and transport limitations are hardly distinguishable and often confused. It is indeed difficult to discriminate between kinetic effects and mass transfer limitations in the context of this complex multiphase phenomenon: the hydrate guest molecules must be transported to the hydrate-forming interface where the reaction front solidifies. The solidification leads to a dynamic addition of resistance to mass transfer: the rate of hydrate formation is inversely proportional to the thickness of the growing hydrate and the surface area of the increasing hydrate particle<sup>360</sup>. To minimise mass transfer, the

formation of hydrate clathrates would have to be performed in a device allowing to continuously replenish the surface of the newly formed hydrate by chemical or mechanical means.

Most of the published research since the early 1990s focused on overcoming the slow kinetics/mass transfer limitations via the use of kinetic promoters (e.g. surfactants)<sup>360,361</sup>. However, the development of innovative gas-liquid contacting modes and materials have also raised some interests in order to maximize the gas-liquid interface (increasing the mass transfer driving force), as well as rapidly removing the heat of formation of hydrates (increasing the heat transfer). Some reactor concepts are presented below.

The slow rate of formation is a common challenge to all types of hydrates, as well as the low conversion of water to hydrates<sup>2</sup>. Linga *et al.*<sup>362</sup> showed that the rate of methane hydrates using packed columns filled with silica sand particles was increased, and that the particles could also assist in minimizing the fraction of unconverted water (they reported water conversion as high as 98%). The rate of methane hydrates formation was even faster than in stirred tanks, at least for the initial fast hydrate formation phase<sup>363</sup>. They also showed that in stirred vessels, the rate decreased rapidly due to the increasing viscosity as the extent of reaction increased. They also observed a 10-fold decrease reaction time in packed beds to reach the final conversion values. By using silica gel, i.e. porous particles, Seo *et al.*<sup>364</sup> achieved an additional 10 fold decrease in reaction time for CO<sub>2</sub> hydrates, reaching 85% conversion in 1 hour. It was also showed that 40-75  $\mu$ m particles with 100 nm pores were the most efficient for CO<sub>2</sub> consumption and water conversion<sup>365</sup>. Polyurethane foam showed hydrate growth rate and water conversion in between that of silica gel (lowest) and silica sand particles (highest)<sup>2</sup>.

Common to any hydrate clathrate formation is the need for high dispersion of gas bubbles leading to high concentration of gas dissolved in water, which can represent a strong constraint on the reactor design. While the additional of chemicals (either gas or chemical additives to lower pressure requirements, surfactants, etc.) do not strongly interfere with reactor design constraints, mechanical agitation almost dictates the reactor type. Mechanical enhancement is obtained via mixing, spraying of liquids (in which case the gas is the continuous phase), bubbling of a gas (the liquid is selected as the continuous phase), etc. Bubble columns is a conventional reactor configuration to deal with gas-liquid applications, but the formation of a hydrate at the gas-liquid interface hinders the mass transfer driving force and it is difficult to break by relying only on the shear stress generated by bubbling. It has also been observed that methane hydrate-covered methane bubbles tend to agglomerate<sup>366</sup>. Stirring is typically performed in batch stirred tanks, but sealing challenges due to the high pressure required must be overcome. The mechanical energy consumption is also problematic: As the reaction proceeds, the increase in the extent of the reaction is associated with an increase of the mixture's viscosity. It has been suggested to maintain the fraction of hydrate to 5% due to the high viscosity<sup>367</sup>. In addition to power consumption, the increase of the mixture viscosity leads to a decrease in turbulence during operation, leading to a decrease in the requires shear stress to remove the hydrate shell around the bubbles and so the maintaining of the active surface area for mass transfer.

A better approach might be to select the water as the dispersed phase so to maximize the interfacial area, and making sure to "peel" off the hydrate shell to avoid slowing the reaction. Chemical reactors with high heat and mass transfer, and enhanced attrition via particle-

particle and particle-walls collisions could be envisioned for this application. The adaptation of ablative reactor developed in the 1980s<sup>368</sup> and based on the cyclonic reactor concept, with typical application in biomass pyrolysis where the outer char shell must be removed to enhance the pyrolysis rate, could be an interesting research avenue. Ablative cyclone-type reactor working at high pressures (up to 100 bar) are not unconventional but would have to be adapted for the low temperatures required<sup>369</sup>. Still, centrifugal reactors are known for their high heat transfer rates. However, due to the long formation time of hydrate clathrates, for this approach to be successful, the particle residence time in a similar device would have to match the required reaction time. A semi-batch centrifugal reactor with permanent bed formed of hydrate crystals or via the use of the dry water concept<sup>370,371</sup> (c.f. section 5.2) could be an interesting approach.

### 13.2. Low storage capacities

The low storage capacity of methane hydrates cannot be improved via clever reactor design, except if it is due to high amounts of unreacted interstitial water, in fact a commonly mentioned problem<sup>360,371</sup>. In order to circumvent this issue without having to rely on impractical and costly solutions typically implemented in small-scale laboratory units, Wang *et al.*<sup>371</sup> developed the dry water concept for methane hydrates based on the work of Binks and Murakami<sup>10</sup>, a free-flowing water-in-air inverse foam formed by a network of fumed silica surrounding water droplets. This concept prevents droplet coalescence and the particle size can be controlled by sampling varying the mixing speed. This concept has a low dead weight disadvantage as the weight of silica is approximately 5 wt %. The main drawback is that upon increasing the number of heating/cooling cycles (i.e. storage and release), particle agglomeration is observed accompanied by a loss of storage capacity and slowed kinetics. At the end, mixing is thus required.

However, even though the dry water concept relies on small particles (classified as Geldart-C in the fluidization literature, and thus very difficult to fluidize), a reactor concept based on the use of centrifugal fluidization could be envisioned: Qian *et al.*<sup>372</sup> demonstrated that by imparting a centrifugal acceleration to small particles, fluidization is indeed possible (the boundaries of the different particle types shift to the “right” in Geldart chart, i.e. towards easier fluidization). This avenue has not been explored yet in the clathrate literature, even though it has been thoroughly investigated for gas-solid applications<sup>373–375</sup>, and slightly tested for gas-liquid applications<sup>376</sup>. Again, while it is quite easy to adapt such reactors for the high pressure required, no attempts has been made in the literature for low temperatures. We note however several patents for gas hydrates formation in conventional fluidized beds<sup>377–379</sup>.

### 13.3. Heat transfer limitations

A growing amount of effort has been devoted on increasing the mass transfer driving force, (i.e. the gas-liquid interface) during the formation of the hydrates. Unfortunately, the design considerations to limit heat and mass transfer are antagonistic. Indeed, increasing the gas-liquid contact is favoured in a dispersed liquid phase, but doing so limits the removal of the heat of formation of the hydrates from the hydrate forming sites (gas have lower thermal conductivities and heat capacities). To efficiently remove the heat of formation of the hydrates, water should be selected as the continuous phase<sup>380</sup>. However, in such case, and if guest molecules are bubbled, we are facing the potential issues due to bubble coalescence and so mass transfer limitations, as discussed above, unless of course some mechanical means are

planned for (e.g. with mesh-like inserts, or vibrations, etc.). For example, the spinning fluid reactor (SFR), based on the air sparged hydrocyclone concept<sup>381</sup>, takes advantage of the size reduction of gas bubbles by shear stress and an internal porous mesh to break coalesced bubbles, resulting in very high interfacial area (up to  $16,000 \text{ m}^2 \text{ m}^{-3}$ )<sup>382</sup>.

When considering the heat transfer limitation at industrially relevant scale, we also have to account for the fact that the required high pressures imply the use of thick wall stainless steel reactors, which represents an important conduction resistance for heat transfer. Vessel or tube walls heat transfer limitation is an underestimated issue in hydrate clathrates reactor design and scale-up. Mori<sup>380</sup> estimated that for industrial-scale stirred tanks (i.e. when the diameter exceeds 0.2-0.4 m), the main thermal resistances shifts from inside the reactor to the reactor walls, and suggested that this issue should be solved by inserting a cooling coil inside the reactor. However, in the case of tubular reactors, as scaling-up rarely ends up in a considerable increase in the tube diameters, heat transfer limitation through reactor walls is limited. Unfortunately, the use of small tubes logically limits the possibilities for mixing, so clathrate agglomeration could be an important issue.

The challenge is different for  $\text{H}_2$  release: The pressure must be decreased and heat efficiently provided at the hydrate forming sites, ideally without melting the hydrates for an optimal heat balance (reutilization of the ice, allowing 67% and 64% in energy gains for plain  $\text{H}_2$  hydrates and THF- $\text{H}_2$  hydrates, respectively, c.f. section 13.5).

#### 13.4. Reactor concepts developed

Besides the potential reactor development avenues briefly presented, some reactor concepts were published in the open literature and in patents database. Bench-scale or pilot plant scale hydrate forming reactors are scarce, and almost non-existing in the case of hydrogen hydrate clathrates<sup>383</sup>. Hartman *et al.*<sup>384</sup> published a patent in which they describe a microfluidic apparatus for producing hydrogen hydrates, from  $\text{H}_2$  and a THF solution. In their device, the hydrate particles grow along the length of the microreactor, in either a gas-liquid, or a liquid-liquid (including an inert oil phase) multiphase segmented flow in the channels of the microreactor, i.e. in the form of micro-scale batch reactors with high circulation separated by an inert phase. The authors of this device foresee the scale-up to relevant industrial production both by scaling-up and scaling-out (using an array of microreactors). They claim that the continuous operation eliminates the transport resistances that limits of the THF+ $\text{H}_2$  hydrate (diffusion of  $\text{H}_2$  into THF hydrate crystals) by increasing the interfacial area between the phases. Clogging of the channels by the clathrates is claimed to be avoided by keeping their size in the sub-micrometers range. Separation of the clathrates from the excess  $\text{H}_2$  is envisioned via the use of polymeric membranes into which  $\text{H}_2$  can permeate, while separation of the clathrate particles from the solution is achieved with flow acoustic separation (positioning of the particles at pressure nodes), or via capillary separation.

#### 13.5. Scale-up, engineering and economic aspects

$\text{H}_2$  storage at large scale is yet to be demonstrated. The main industrial challenge for hydrogen hydrate clathrates is the considerable pressure required, i.e. around 200 MPa at 273 K for sII clathrate hydrates, even though promoters can considerably reduce this pressure. For example, the addition of THF reduces the pressure to 7 MPa at 273 K but can also reduce the storage capacity (the large cages are filled with the promoter)<sup>360</sup>, unless  $\text{H}_2$  can also enter in

the large cages of sII hydrates while keeping the kinetics to industrially relevant values. Lee *et al.*<sup>179</sup> proposed a path to be followed to achieve those two goals: by dispersing the reacting phase in silica gel. However, the authors mentioned the obvious disadvantage of this approach, namely that the clathrate formation is limited to the pores of the silica gel (which then acts as a dead volume). This approach can only be relevant if the support material has a very low density<sup>385</sup>.

For large scale storage, the material's gravimetric or volumetric capacity is of less importance than the costs for the construction and maintenance of the storage plant, as well as the utility costs and the safety<sup>386</sup>. Besides the high pressure and low temperature conditions required, mass transfer limitation and high energy costs for continuous stirring was pointed to by Veluswamy *et al.*<sup>174</sup>. They highlighted the work of Veluswamy and Linga<sup>271</sup>, as well as Treuba *et al.*<sup>263,387</sup> where H<sub>2</sub> storage was limited to 0.01 wt.% when using large sample sizes (around 100 g), versus smaller sample sizes where higher storage capacities were measured. They also suggested that future research should focus on the effects of scale-up (namely increasing heat and mass transfer rates) on the kinetics.

The IHI Corporation published conceptual designs for hydrate storage plants (based on batch agitated tank reactors) at 35 MPa/140 K and 30 MPa/223 K, for H<sub>2</sub> and THF-H<sub>2</sub>, respectively<sup>388</sup>. The storage temperature was selected 50 K below the hydrate synthesis temperature to minimize the potential sintering of the hydrate particles. Shibata *et al.*<sup>389</sup> suggested to limit the pile high to 10 m based on pressure sintering of snow data. Both large scale and smaller scale urban area storage, with capacities of 3000 and 500 Nm<sup>3</sup> hr<sup>-1</sup> were considered in their study. The author concluded that due to the huge cooling energy requirements, a strong industrial constraint is that the storage plants must be located to adjacent LNG facilities, where the energy of vaporization of LNG is available. Indeed, their study show that the use of conventional refrigerator would lead to prohibitive electricity requirements. Based on their conceptual designs, a 3000 Nm<sup>3</sup> hr<sup>-1</sup> would require thirty 0.45 m<sup>3</sup> batch hydrate forming reactors, and 15.12 and 21.17 GJ/h of electricity for H<sub>2</sub> hydrates and THF-H<sub>2</sub> hydrate, respectively, using conventional refrigerators and without ice reuse (i.e. up to 40% of the energy content of the H<sub>2</sub> of the plant for plain H<sub>2</sub> hydrates). Reusing the ice and assuming a heat integration scheme with a neighbouring LNG plant reduces the electricity requirements to 5.04 and 7.56 GJ/h for the H<sub>2</sub> hydrates and THF-H<sub>2</sub> hydrates, respectively. The total plant costs were estimated at 61 and 96 M€ for simple H<sub>2</sub> and THF-H<sub>2</sub> hydrates, respectively (using the average 2010 JPY to EUR exchange rate).

Sumitomo Mitsui Construction complemented the IHI Corporation study in 2012, considering this time reactor concepts based on the mining industry. Shibata *et al.*<sup>389</sup> described a large scale underground tank type and cavity type storage system for simple H<sub>2</sub> hydrates consistent with the Japanese context where ground-based storage plants is difficult due to their densely populated country. The described conceptual design is based on a 35 000 m<sup>3</sup> silo, i.e. for H<sub>2</sub> consumption of 3000 Nm<sup>3</sup>/h for 75 days. As in the previous study, heat removal is planned via heat integration of adjacent LNG facilities. The total costs for the cavern type storage systems amount to an average of 151 M€ (using the average 2012 JPY to EUR exchange rate), for which two thirds is attributable to the refrigeration work around in the underground storage tunnel. Tank-type silo, i.e. the storage technology used in numerous underground tanks for storing LNG at 110 K, is also described. The cost is less than that of the cavern type, but without the freezing works. Also, to make a definite decision between the

cavern and tank-type more difficult, the authors mentioned that for the tank-type storage, it is impossible to change its capacity to accommodate potential change in the demand for H<sub>2</sub>. Finally, Shibata *et al.*<sup>389</sup> concluded over the superiority of hydrate-based H<sub>2</sub> storage over compressed gas and metal hydrides, based on both the economics and the inherent higher safety.

The IHI Corporation compared the annual costs for different H<sub>2</sub> storage technologies (liquified H<sub>2</sub>, compressed gas and low and high pressures, i.e. 9.5 and 350 bars, respectively, metal hydrides as well as ground-based hydrate clathrates plants) for large scale storage (90 days storage of 3000 Nm<sup>3</sup>/y, followed by 90 days of H<sub>2</sub> release, and the remaining 90 days or so without operation). Their engineering study concludes that H<sub>2</sub> storage in clathrates represents the lowest annual costs, if the cooling energy can be supplied by a LNG transportation line (without additional costs). The total annual costs (construction, electricity, fuel, and loss of water) for H<sub>2</sub> hydrate clathrates amounts to 11 M€ (1.55 M JPY, using the yearly averaged exchange rate for 2014), i.e. 64% of the annual costs of high pressure compressed gas, the next best technology<sup>386</sup>. Even at high pressure, the density of H<sub>2</sub> remains low, leading to large storage volumes and thus high investment costs<sup>142</sup>. Interestingly, H<sub>2</sub> storage in hydrate clathrates is superior to LH<sub>2</sub>, even if the cooling requirements of the hydrates does not come from a neighbouring LNG plant but either electrically-powered refrigerators, while that of LH<sub>2</sub> do. In their designs, Ozaki *et al.*<sup>386</sup> planned for a sequential operation of the hydrate synthesis-storage, and the H<sub>2</sub> release plant. By doing so, water is recycled thus decreasing the cooling utility requirements. Their reactor concept is also inspired by mining operations (stockpiling ice particles sprinkled from the top of the tank using a rotary stocker, pressurising for hydrate clathrate synthesis, and pneumatic conveying from the bottom of the tank for hydrate clathrates transportation to the H<sub>2</sub> release unit). The cost estimation provided by the IHI Corporation and Sumitomo Mitsui Construction only represent “desktop” estimates as there are no existing construction or operation practice of commercial hydrate clathrates<sup>386</sup>.

On-board hydrogen storage, coupled with fuel cell, remains one of the most sought-after areas commercially. It has been estimated more than 10,000 commercial fuel cell light duty vehicles have been sold worldwide, till early 2019<sup>390</sup>. The cost estimates formulated by DOE for the on-board hydrogen storage target a price a \$8/KWh for a commercially viable solution (driving range greater than 300 miles). Current status review has predicted that price tag of \$24/KWh will be borne by the industry if the production volumes are kept low. These numbers could be reduced to \$15/KWh at best, if the production volumes are high (upto 5,00,000 units per year). These estimates are based on the high-pressure gas storage in carbon fibre composite tanks, with carbon fibre contributing to the maximum percentage of the total cost. These tanks utilise the concept of storage of hydrogen at low temperature, without aiming for complete liquefaction. For example, in lieu of 700 bar tank and 288 K, 500 bar at 200 K is utilised. This leads to higher density of hydrogen without the need for complete liquefaction. A comparison has also been drawn with the metal hydride-based storage system with 350 bar hybrid tank, as proposed by Argonne National Laboratory<sup>391</sup>. This system utilises the on-board fuel cell stack coolant to heat the metal hydride bed to release hydrogen and offboard station coolant to cool the bed during refuelling. The projected costs are \$13/KWh for 5,00,000 systems per year. This is an improvement with respect to the compressed gas storage, however, the additional materials and auxiliary present a significant

challenge to be integrated into a commercial vehicle. It is important to note that in this cost analysis, the metal hydride (\$2.7/KWh) constitutes just 20% of the total cost. This highlights the importance of the additional accessories to be installed when using metal hydride based on-board storage solution. Moreover, it has been assumed that the material shows 5.6 wt.% hydrogen storage capacity, which is still a challenge for the large-scale performance under the temperature and pressure conditions present. As of now no literature exists of the cost estimates of the clathrates for on-board hydrogen storage, but above two options lead us to an important conclusion regarding the feasibility of the clathrates for the on-board storage. Two important conditions such as low temperatures (~200 K) in the first technology and the requirement of 5.6 wt.% hydrogen storage capacity, can be met by clathrate to provide a reversible hydrogen storage medium, provided the factors such as heat and mass transfer can be controlled. A summary of cost comparisons has been provided in Table 5 as well as in Figure 26.

Table 5 Comparison of financial costs incurred for the implementation of the hydrogen storage technology for on-board and stationary application.

| Application                                    | Type of Storage   | T (K) | P (bar) | Annual Cost (\$/ton) <sup>5</sup> | Comments  | Ref |
|--|---|-------|---------|-----------------------------------|---|-----|
| Stationary <sup>1</sup>                        | Compressed Gas  | 298   | 9.5     | 58                                | Low Pressure System   | 386 |
|  |   | 298   | 350     | 38                                | High Pressure System  |     |
|  | Liquified Gas   | 20    | 1.1     | 43                                | LNG Supported Cooling System                                |     |
|  | Metal Hydride   | 298   | 5       | 108                               | Assumes 3.3 wt.% hydrogen storage capacity of metal hydride |     |
|  | Clathrates <sup>2,3</sup>                               | 140   | 1.1     | 24                                | Assuming 3.03 wt.% hydrogen storage capacity of clathrates  |     |
|  | Clathrates <sup>4</sup>                                 | 140   | 1.1     | 41                                |   |     |
| On-board (coupled with Fuel Cell) <sup>6</sup> | Compressed Gas  | <100  | 350     | 12 (\$ per KWh) <sup>6</sup>      | Cryo-compressed hydrogen                                    | 391 |
|  |   | 298   | 350     | 14 (\$ per KWh)                   | Standard Compressed Hydrogen                                |     |
|  | Metal Hydrides (including all the auxiliary components) | 298   | 350     | 13 (\$ per KWh)                   | Assumes 5.6 wt.% hydrogen storage capacity of metal hydride |     |

<sup>1</sup>For an estimated storage of 3000 Nm<sup>3</sup>/h for a period of 90 days (total of 582 tons of hydrogen).

<sup>2</sup>Taking into account the "self-preservation effect", the storage conditions (1.1 bar and 140 K) for the clathrates are different from the production conditions (350 bar and 140 K).

<sup>3</sup>Assuming that the source of cooling is available from freely available LNG from the nearby industrial sources.

<sup>4</sup>Without the availability of the LNG nearby.

<sup>5</sup>The values have been rounded off to the nearest integer.

<sup>6</sup>The costs of the on-board hydrogen storage solutions are based on per unit energy produced by the fuel cell.

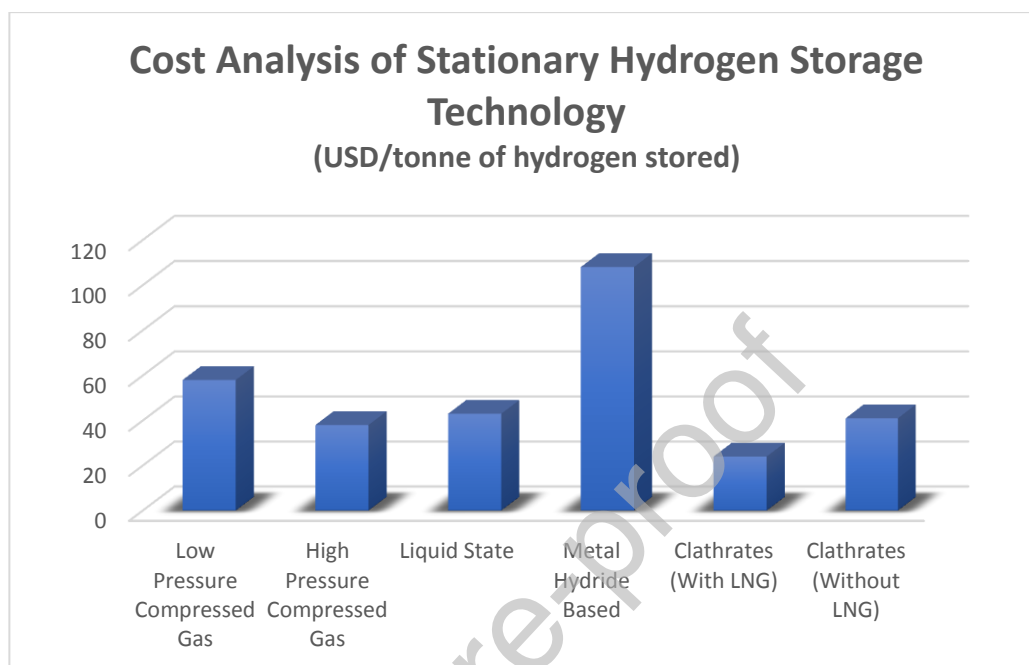


Figure 26. A comparison of cost estimates for various hydrogen storage technologies for stationary applications<sup>386</sup>.

## 14. Summary and Conclusions

The search for the “holy grail” of hydrogen storage material remains an elusive dream for the scientific community. On one hand, physisorption based materials such as high surface area activated carbons show promising performance at cryogenic temperatures, on the other hand chemisorption-based materials such as complex hydrides offer exceptional properties at high temperatures, often exhibiting irreversible nature. An alternative proposed by storing hydrogen in clathrates holds promise in the future. Although the results remain conflicting with regard to the quantification of the hydrogen in clathrates, qualitative analysis has provided a confirmed evidence of the multiple strategies that have been successful in this regard. A summary of the these strategies used to tackle the three corners of the problem; hydrogen storage capacity, thermodynamics and kinetics of the reaction have been summarised in Figure 27. A sharp decline in the pressure of absorption from 200 MPa (Mao *et al.*<sup>4</sup> in 2002 for pure hydrogen hydrates) to 9 MPa (Ahn *et al.*<sup>212</sup> in 2020 for methane and ethane supported hydrogen hydrates), massive improvement in the kinetics of the reaction from a week (Strobel *et al.*<sup>180</sup> in 2006) to few seconds (Profio *et al.*<sup>198</sup> in 2018) are some of the successful outcomes of the utilisation of these strategies. Additional unique properties of clathrates such as their zero-environment interference, abundant supply in nature, completely reversible exchange with hydrogen, high safety and reliability makes them stand apart from the variety of other materials. The ultimate aim of combining these characteristics to produce

an ideal hydrogen storing clathrate remains not very far if the efforts and resources are continued to be invested in the right direction.

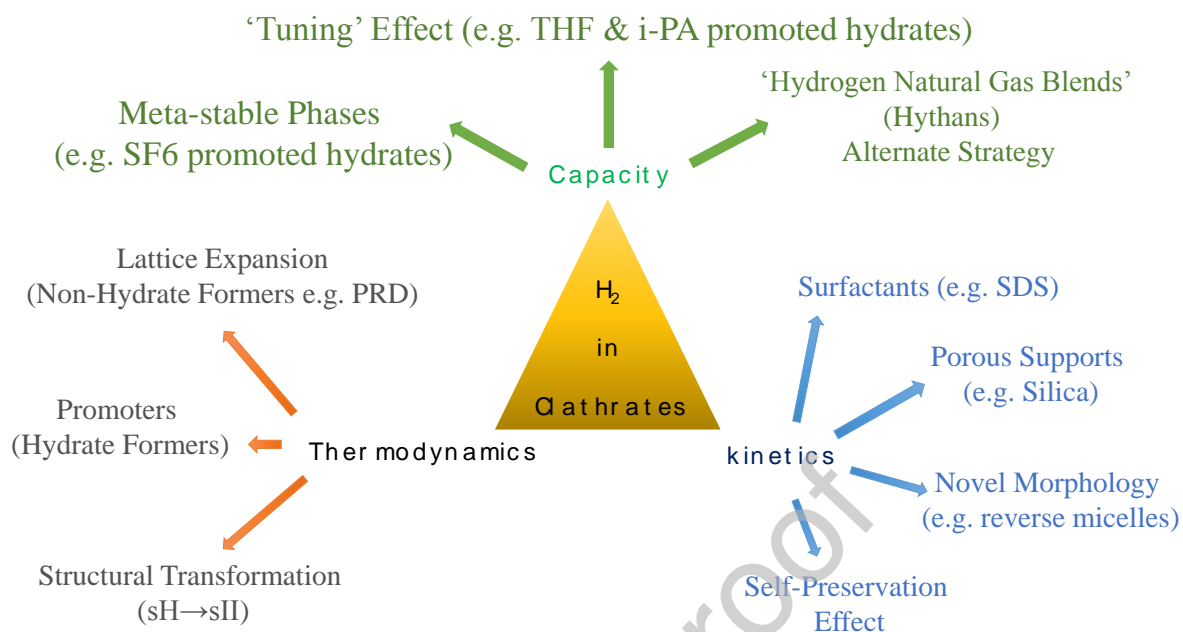


Figure 27. Three-pronged strategy for improving the hydrogen storage characteristics of clathrates.

**List of Abbreviations**

|                     |                                   |
|---------------------|-----------------------------------|
| SDS                 | Sodium dodecyl sulfate            |
| THF                 | Tetrahydrofuran                   |
| i-PA                | iso-propylamine                   |
| n-PA                | n-propylamine                     |
| LH <sub>2</sub>     | Liquid hydrogen                   |
| LNG                 | Liquified Natural Gas             |
| t-BuNH <sub>2</sub> | Tert-Butylamine                   |
| t-BA                | Tertiary Butyl Alcohol            |
| PRD                 | Pyrrolidine                       |
| TBAB                | Tetra-n-butylammonium bromide     |
| HCFC                | Hydrochlorofluorocarbon           |
| TBACL               | Tetrabutylammonium chloride       |
| DTAC                | Dodecyltrimethylammonium chloride |
| THT                 | Tetrahydrothiophene               |
| CP                  | Cyclopentadienide                 |
| DXL                 | D-Xylaric acid                    |
| HRXRD               | High Resolution X-Ray Diffraction |

**Conflicts of interest**

The authors report no conflict of interest.

**Authors Contributions**

Anshul Gupta and Joeri F.M. Denayer were responsible for the conceptualisation, review and editing of the article. Anshul Gupta was responsible for the visualisation and supervision. All the authors contributed to the writing of the original draft of the article.

**Acknowledgements**

The authors would like to acknowledge VLAIO for the financial support. Anshul Gupta acknowledges Prof. Anandh Subramaniam (IIT Kanpur, India) for help with the Crystal Maker illustrations and Dr. Mohammad Faisal (KIST, Korea) for helpful discussions.

## References

- 1 M. Hirscher, *Handbook of Hydrogen Storage*, Wiley-VCH Verlag GmbH & Co. KGaA, Weinheim, Germany, 2010.
- 2 L. E. Klebanoff, K. C. Ott, L. J. Simpson, K. O'Malley and N. T. Stetson, *Metall. Mater. Trans. E*, 2014, **1**, 81–117.
- 3 V. V Struzhkin, B. Militzer, W. L. Mao, H. K. Mao and R. J. Hemley, *Chem. Rev.*, 2007, 107, 4133–4151.
- 4 W. L. Mao, H. Mao, A. F. Goncharov, V. V Struzhkin, Q. Guo, J. Hu, J. Shu, R. J. Hemley, M. Somayazulu and Y. Zhao, *Science (80-. )*, 2002, **297**, 2247 LP – 2249.
- 5 I. N. Tsimpanogiannis and I. G. Economou, *J. Supercrit. Fluids*, 2018, **134**, 51–60.
- 6 C. Yu, L. Chen and B. Sun, *Chinese J. Chem. Eng.*, 2019, **27**, 2189–2206.
- 7 R. C. Lochan and M. Head-Gordon, *Phys. Chem. Chem. Phys.*, 2006, **8**, 1357–1370.
- 8 E. Klontzas, E. Tylianakis and G. E. Froudakis, *J. Phys. Chem. Lett.*, 2011, **2**, 1824–1830.
- 9 B. Schmitz, U. Müller, N. Trukhan, M. Schubert, G. Férey and M. Hirscher, *ChemPhysChem*, 2008, **9**, 2181–2184.
- 10 M. Schlichtenmayer and M. Hirscher, *J. Mater. Chem.*, 2012, **22**, 10134–10143.
- 11 M. Thommes, K. Kaneko, A. V Neimark, J. P. Olivier, F. Rodriguez-Reinoso, J. Rouquerol and K. S. W. Sing, *Pure Appl. Chem.*, 2015, **87**, 1051–1069.
- 12 D. P. Broom, *Hydrogen Storage Materials*, Springer London, London, 2011.
- 13 E. Boateng and A. Chen, *Mater. Today Adv.*, 2020, **6**, 100022.
- 14 D. P. Broom, C. J. Webb, K. E. Hurst, P. A. Parilla, T. Gennett, C. M. Brown, R. Zacharia, E. Tylianakis, E. Klontzas, G. E. Froudakis, T. A. Steriotis, P. N. Trikalitis, D. L. Anton, B. Hardy, D. Tamburello, C. Corngale, B. A. van Hassel, D. Cossement, R. Chahine and M. Hirscher, *Appl. Phys. A Mater. Sci. Process.*, 2016, **122**, 1–21.
- 15 E. C. E. Rönnebro and E. H. Majzoub, *MRS Bull.*, 2013, **38**, 452–458.
- 16 S. Satyapal, J. Petrovic, C. Read, G. Thomas and G. Ordaz, *Catal. Today*, 2007, **120**, 246–256.

- 17 T. S. Blankenship II, N. Balahmar and R. Mokaya, *Nat. Commun.*, 2017, **8**, 1545.
- 18 A. Ahmed, Y. Liu, J. Purewal, L. D. Tran, A. G. Wong-Foy, M. Veenstra, A. J. Matzger and D. J. Siegel, *Energy Environ. Sci.*, 2017, **10**, 2459–2471.
- 19 G. Xia, H. Leng, N. Xu, Z. Li, Z. Wu, J. Du and X. Yu, *Int. J. Hydrogen Energy*, 2011, **36**, 7128–7135.
- 20 Y. Jia, C. Sun, L. Cheng, M. Abdul Wahab, J. Cui, J. Zou, M. Zhu and X. Yao, *Phys. Chem. Chem. Phys.*, 2013, **15**, 5814–5820.
- 21 X. Zhang, Z. Ren, Y. Lu, J. Yao, M. Gao, Y. Liu and H. Pan, *Appl. Mater. Interfaces*, 2018, **10**, 15767–15777.
- 22 X. Zhang, Y. Liu, Z. Ren, X. Zhang, J. Hu, Z. Huang, Y. Lu, M. Gao and H. Pan, *Energy Environ. Sci.*, 2021, **14**, 2302–2313.
- 23 W. Li, C. Li, H. Ma and J. Chen, *J. Am. Chem. Soc.*, 2007, **129**, 6710–6711.
- 24 Á. Berenguer-Murcia, J. P. Marco-Lozar and D. Cazorla-Amorós, *Chem. Rec.*, 2018, **18**, 900–912.
- 25 Y. Xia, Z. Yang and Y. Zhu, *J. Mater. Chem. A*, 2013, **1**, 9365.
- 26 V. Tozzini and V. Pellegrini, *Phys. Chem. Chem. Phys.*, 2013, **15**, 80–9.
- 27 M. Mohan and V. Kumar, *Energy Storage*, 2019, 1–26.
- 28 M. Bastos-Neto, C. Patzschke, M. Lange, J. Möllmer, A. Möller, S. Fichtner, C. Schrage, D. Lässig, J. Lincke, R. Staudt, H. Krautscheid and R. Gläser, *Energy Environ. Sci.*, 2012, **5**, 8294–8303.
- 29 M. Sevilla and R. Mokaya, *Energy Environ. Sci.*, 2014, **7**, 1250–1280.
- 30 S.-E. Zhu, F. Li and G.-W. Wang, *Chem. Soc. Rev.*, 2013, **42**, 7535–70.
- 31 A. Salehabadi, M. Faisal and U. Akil, *Int. J. Energy Res.*, 2020, 1–15.
- 32 R. Chahine and T. K. Bose, *Int. J. Hydrogen Energy*, 1994, **19**, 161–164.
- 33 J. Burrell, M. Kraus, M. Beckner, R. Cepel, G. Suppes, C. Wexler and P. Pfeifer, *Nanotechnology*, 2009, **20**, 204026.
- 34 B. Kuchta, L. Firlej, A. Mohammadhosseini, P. Boulet, M. Beckner, J. Romanos and

- P. Pfeifer, *J. Am. Chem. Soc.*, 2012, **134**, 15130–7.
- 35 A. Züttel, P. Sudan, P. Mauron and P. Wenger, *Appl. Phys. A*, 2004, **78**, 941–946.
- 36 M. Hirscher and B. Panella, *Eur. J. Control - EUR J Control*, 2005, **30**, 519–529.
- 37 L. Wang and R. T. Yang, *Catal. Rev.*, 2010, **52**, 411–461.
- 38 S. Y. Lee and S. J. Park, *Int. J. Hydrogen Energy*, 2011, **36**, 8381–8387.
- 39 D. S. Pyle, E. M. A. Gray and C. J. Webb, *Int. J. Hydrogen Energy*, 2016, **41**, 19098–19113.
- 40 S. K. Konda and A. Chen, *Biochem. Pharmacol.*, 2016, **19**, 100–108.
- 41 V. B. Parambath, R. Nagar, K. Sethupathi and S. Ramaprabhu, *J. Phys. Chem. C*, 2011, **115**, 15679–15685.
- 42 Q. Li and A. D. Lueking, *J. Phys. Chem. C*, 2011, **115**, 4273–4282.
- 43 J. Romanos, M. Beckner, D. Stalla, A. Tekeei, G. Suppes, S. Jalisatgi, M. Lee, F. Hawthorne, J. D. Robertson, L. Firlej, B. Kuchta, C. Wexler, P. Yu and P. Pfeifer, *Carbon N. Y.*, 2013, **54**, 208–214.
- 44 N. Nishimiya, Y. Date, Y. Kojima and T. Toyama, *J. Alloys Compd.*, 2013, **580**, S305–S308.
- 45 D. Qu, *Chemistry*, 2008, **14**, 1040–6.
- 46 S. J. Yang, J. H. Cho, G. H. Oh, K. S. Nahm and C. R. Park, *Carbon N. Y.*, 2009, **47**, 1585–1591.
- 47 J. Romanos, M. Beckner, M. Prosniewski, T. Rash, M. Lee, J. D. Robertson, L. Firlej, B. Kuchta and P. Pfeifer, *Sci. Rep.*, 2019, 1–8.
- 48 T. S. Blankenship and R. Mokaya, *Energy Environ. Sci.*, 2017, **10**, 2552–2562.
- 49 P. Moretto, C. Zlotea, F. Dolci, a. Amieiro, J.-L. Bobet, a. Borgschulte, D. Chandra, H. Enoki, P. De Rango, D. Fruchart, J. Jepsen, M. Latroche, I. L. Jansa, D. Moser, S. Sartori, S. M. Wang and J. a. Zan, *Int. J. Hydrogen Energy*, 2013, **38**, 6704–6717.
- 50 D. Broom, *Int. J. Hydrogen Energy*, 2007, **32**, 4871–4888.
- 51 D. P. Broom and C. J. Webb, *Int. J. Hydrogen Energy*, 2017, **42**, 29320–29343.

- 52 Z. Yang, Y. Xia and R. Mokaya, *J. Am. Chem. Soc.*, 2007, **129**, 1673–1679.
- 53 H. G. Schimmel, G. J. Kearley, M. G. Nijkamp, C. T. Visser, K. P. de Jong and F. M. Mulder, *Chemistry*, 2003, **9**, 4764–70.
- 54 A. Reyhani, S. Z. Mortazavi, S. Mirershadi, A. Z. Moshfegh, P. Parvin and A. N. Golikand, *J. Phys. Chem. C*, 2011, **115**, 6994–7001.
- 55 Y. Han and S. Park, *Appl. Surf. Sci.*, 2017, **415**, 85–89.
- 56 N. Matsumoto, H. Kinoshita, Y. Shimanaka and N. Ohmae, *Chem. Phys. Lett.*, 2020, **751**, 137530.
- 57 B. Assfour, S. Leoni, G. Seifert and I. A. Baburin, *Adv. Mater.*, 2011, **23**, 1237–1241.
- 58 H. W. Langmi, J. Ren, B. North, M. Mathe and D. Bessarabov, *Electrochim. Acta*, 2014, **128**, 368–392.
- 59 V. R. Bakuru, M. E. DMello and S. B. Kalidindi, *ChemPhysChem*, 2019, **20**, 1177–1215.
- 60 M. Tong, W. Zhu, J. Li, Z. Long, S. Zhao, G. Chen and Y. Lan, *Chem. Commun.*, 2020, **56**, 6376–6379.
- 61 S. S. Han, H. Furukawa, O. M. Yaghi and W. A. Goddard, *J. Am. Chem. Soc.*, 2008, **130**, 11580–11581.
- 62 J. Dong, X. Wang, H. Xu, Q. Zhao and J. Li, *Int. J. Hydrogen Energy*, 2007, **32**, 4998–5004.
- 63 D. Ramimoghadam, E. M. Gray and C. J. Webb, *Int. J. Hydrogen Energy*, 2016, **41**, 16944–16965.
- 64 N. L. Rosi, J. Eckert, M. Eddaoudi, D. T. Vodak, J. Kim, M. O’Keeffe and O. M. Yaghi, *Science*, 2003, **300**, 1127–9.
- 65 A. Ahmed, S. Seth, J. Purewal, A. G. Wong-Foy, M. Veenstra, A. J. Matzger and D. J. Siegel, *Nat. Commun.*, 2019, **10**, 1568.
- 66 M. Eddaoudi, J. Kim, N. Rosi, D. Vodak, J. Wachter, M. O’Keeffe and O. M. Yaghi, *Science (80-. )*, 2002, **295**, 469 LP – 472.
- 67 D. A. Gómez-Gualdrón, T. C. Wang, P. García-Holley, R. M. Sawelewa, E. Argueta,

- R. Q. Snurr, J. T. Hupp, T. Yildirim and O. K. Farha, *ACS Appl. Mater. Interfaces*, 2017, **9**, 33419–33428.
- 68 J. D. Tarver, H. Z. H. Jiang, M. T. Kapelewski, K. E. Hurst, P. A. Parilla, A. Ayala, T. Gennett, S. A. Fitzgerald, C. M. Brown and R. Long, *Chem. Mater.*, 2018, **30**, 8179–8189.
- 69 T. Islamoglu, M. Weston, J. T. Hupp and O. K. Farha, *ACS Energy Lett.*, 2018, **3**, 748–754.
- 70 C. Rösler and R. A. Fischer, *CrystEngComm*, 2015, **17**, 199–217.
- 71 P. Ryan, L. J. Broadbelt and R. Q. Snurr, *Chem. Commun.*, 2008, 4132–4134.
- 72 Z. Li, G. Zhu, G. Lu, S. Qiu and X. Yao, *J. Am. Chem. Soc.*, 2010, **132**, 1490–1491.
- 73 Z. Ma, Q. Zhang, S. Panda, W. Zhu, F. Sun, D. Khan, J. Dong, W. Ding and J. Zou, *Sustain. Energy Fuels*, 2020, **4**, 4694–4703.
- 74 J. L. C. Rowsell and O. M. Yaghi, *Angew. Chemie Int. Ed.*, 2005, **44**, 4670–4679.
- 75 K. Pareek, R. Rohan, Z. Chen, D. Zhao and H. Cheng, *Int. J. Hydrogen Energy*, 2017, **42**, 6801–6809.
- 76 D. Czarna-Juszkiewicz, J. Cader and M. Wdowin, *J. Clean. Prod.*, 2020, **270**, 122355.
- 77 H. W. Langmi, A. Walton, M. M. Al-Mamouri, S. R. Johnson, D. Book, J. D. Speight, P. P. Edwards, I. Gameson, P. A. Anderson and I. R. Harris, *J. Alloys Compd.*, 2003, **356–357**, 710–715.
- 78 J. G. Vitillo, G. Ricchiardi, G. Spoto and A. Zecchina, *Phys. Chem. Chem. Phys.*, 2005, **7**, 3948–3954.
- 79 P. M. Budd, A. Butler, J. Selbie, K. Mahmood, N. B. McKeown, B. Ghanem, K. Msayib, D. Book and A. Walton, *Phys. Chem. Chem. Phys.*, 2007, **9**, 1802–1808.
- 80 C. D. Wood, B. Tan, A. Trewin, H. Niu, D. Bradshaw, M. J. Rosseinsky, Y. Z. Khimiyak, N. L. Campbell, R. Kirk, E. Stöckel and A. I. Cooper, *Chem. Mater.*, 2007, **19**, 2034–2048.
- 81 Y. J. Choi, J. W. Lee, J. H. Choi and J. K. Kang, *Appl. Phys. Lett.*, 2008, **92**, 173102.
- 82 M. Wieliczko and N. Stetson, *MRS Energy Sustain.*, 2020, **7**, E41.

- 83 V. A. Yartys, M. V Lototsky, E. Akiba, R. Albert, V. E. Antonov, J. R. Ares, M. Baricco, N. Bourgeois, C. E. Buckley, M. Dornheim, M. Felderhoff, D. M. Grant, B. C. Hauback, T. D. Humphries, I. Jacob, T. R. Jensen, P. E. De Jongh, J. Joubert, M. A. Kuzovnikov, M. Latroche, M. Paskevicius, L. Pasquini, G. Walker, H. Wang, C. J. Webb and M. Zhu, *Int. J. Hydrogen Energy*, 2019, **44**, 7809–7859.
- 84 J. Zhang, Z. Li, Y. Wu, X. Guo, J. Ye and B. Yuan, *RSC Adv.*, 2019, **9**, 408–428.
- 85 J. J. Reilly and R. H. Wiswall, *Inorg. Chem.*, 1968, **7**, 2254–2256.
- 86 A. A. Asselli and J. Huot, *Met.*, 2014, **4**.
- 87 V. M. Skripnyuk and E. Rabkin, *Int. J. Hydrogen Energy*, 2012, **37**, 10724–10732.
- 88 H. C. Zhong, H. Wang, J. W. Liu, D. L. Sun and M. Zhu, *Scr. Mater.*, 2011, **65**, 285–287.
- 89 T. Z. Si, J. B. Zhang, D. M. Liu and Q. A. Zhang, *J. Alloys Compd.*, 2013, **581**, 246–249.
- 90 J. J. Vajo, F. Mertens, C. C. Ahn, R. C. Bowman and B. Fultz, *J. Phys. Chem. B*, 2004, **108**, 13977–13983.
- 91 D. Wu, L. Ouyang, C. Wu, H. Wang, J. Liu, L. Sun and M. Zhu, *J. Alloys Compd.*, 2015, **642**, 180–184.
- 92 L. Z. Ouyang, F. X. Qin and M. Zhu, *Scr. Mater.*, 2006, **55**, 1075–1078.
- 93 R. A. Varin, S. Li, C. Chiu, L. Guo, O. Morozova, T. Khomenko and Z. Wronski, *J. Alloys Compd.*, 2005, **404–406**, 494–498.
- 94 J.-L. Bobet, E. Akiba, Y. Nakamura and B. Darriet, *Int. J. Hydrogen Energy*, 2000, **25**, 987–996.
- 95 A. Denis, E. Sellier, C. Aymonier and J.-L. Bobet, *J. Alloys Compd.*, 2009, **476**, 152–159.
- 96 G. Liang, J. Huot, S. Boily, A. Van Neste and R. Schulz, *J. Alloys Compd.*, 1999, **292**, 247–252.
- 97 J.-L. Bobet, B. Chevalier, M. Y. Song, B. Darriet and J. Etourneau, *Mater. Manuf. Process.*, 2002, **17**, 351–361.

- 98 J. Zou, X. Zeng, Y. Ying, X. Chen, H. Guo, S. Zhou and W. Ding, *Int. J. Hydrogen Energy*, 2013, **38**, 2337–2346.
- 99 K. Edalati, R. Uehiro, Y. Ikeda, H. Li and H. Emami, *Acta Mater.*, 2018, **149**, 88–96.
- 100 A. Gupta, S. Shervani, M. Faisal, K. Balani and A. Subramaniam, *J. Alloys Compd.*, 2015, **645**, S397–S399.
- 101 M. Faisal, A. Gupta, S. Shervani, K. Balani and A. Subramaniam, in *20th World Hydrogen Energy Conference, WHEC 2014*, 2014, vol. 2.
- 102 M. Faisal, K. Balani and A. Subramaniam, *Int. J. Hydrogen Energy*, 2021, **46**, 5507–5519.
- 103 A. Gupta, M. Faisal, S. Shervani, K. Balani and A. Subramaniam, *Int. J. Hydrogen Energy*, 2020, **45**, 11632–11640.
- 104 K.-J. Jeon, H. R. Moon, A. M. Ruminski, B. Jiang, C. Kisielowski, R. Bardhan and J. J. Urban, *Nat. Mater.*, 2011, **10**, 286–90.
- 105 C. Zhou and J. A. Szpunar, *ACS Appl. Mater. Interfaces*, 2016, **8**, 25933–25940.
- 106 X. Yao, C. Wu, A. Du, G. Q. Lu, H. Cheng, S. C. Smith, J. Zou and Y. He, *J. Phys. Chem. B*, 2006, **110**, 11697–703.
- 107 L. F. Wan, Y. Liu, E. S. Cho, J. D. Forster, S. Jeong, H. Wang, J. Urban, J. Guo and D. Prendergast, *Nano Lett.*, 2017, **17**, 5540–5545.
- 108 E. S. Cho, A. M. Ruminski, S. Aloni, Y. Liu, J. Guo and J. J. Urban, *Nat. Commun.*, 2016, 1–8.
- 109 Y. Wang, Q. Zhang, Y. Wang, L. Jiao and H. Yuan, *J. Alloys Compd.*, 2015, **645**, S509–S512.
- 110 H. Gu, Y. Zhu and L. Li, *Int. J. Hydrogen Energy*, 2009, **34**, 2654–2660.
- 111 Y. Wang, Y. Wang, L. Li, C. An, C. Chen, L. Jiao and H. Yuan, *Nanoscale*, 2014, **6**, 6684–6691.
- 112 Y. Wang, C. An, Y. Wang, Y. Huang, C. Chen, L. Jiao and H. Yuan, *J. Mater. Chem. A*, 2014, **2**, 16285–16291.
- 113 T. Spassov and U. Köster, *J. Alloys Compd.*, 1999, **287**, 243–250.

- 114 Y. Wu, W. Han, S. X. Zhou, M. V Lototsky, J. K. Solberg and V. A. Yartys, *J. Alloys Compd.*, 2008, **466**, 176–181.
- 115 H. J. Lin, L. Z. Ouyang, H. Wang, J. W. Liu and M. Zhu, *Int. J. Hydrogen Energy*, 2012, **37**, 1145–1150.
- 116 Y. S. Au, M. K. Obbink, S. Srinivasan, P. C. M. M. Magusin, K. P. de Jong and P. E. de Jongh, *Adv. Funct. Mater.*, 2014, **24**, 3604–3611.
- 117 T. K. Nielsen, K. Manickam, M. Hirscher, F. Besenbacher and T. R. Jensen, *ACS Nano*, 2009, **3**, 3521–3528.
- 118 Z. Zhao-Karger, J. Hu, A. Roth, D. Wang, C. Kübel, W. Lohstroh and M. Fichtner, *Chem. Commun.*, 2010, **46**, 8353–8355.
- 119 M. Konarova, A. Tanksale, J. Norberto Beltramini and G. Qing Lu, *Nano Energy*, 2013, **2**, 98–104.
- 120 D. Peng, Z. Ding, Y. Fu, Y. Wang, J. Bi and S. Han, *RSC Adv.*, 2018, **8**, 28787–28796.
- 121 M. S. El-eskandarany, M. Banyan and F. Al-ajmi, *RSC Adv.*, 2019, **9**, 27987–27995.
- 122 C. Zlotea, Y. Oumellal, S.-J. Hwang, C. M. Ghimbeu, P. E. de Jongh and M. Latroche, *J. Phys. Chem. C*, 2015, **119**, 18091–18098.
- 123 G. Xia, Y. Tan, X. Chen, D. Sun, Z. Guo, H. Liu, L. Ouyang, M. Zhu and X. Yu, *Adv. Mater.*, 2015, **27**, 5981–5988.
- 124 L. Ouyang, K. Chen, J. Jiang, X.-S. Yang and M. Zhu, *J. Alloys Compd.*, 2020, **829**, 154597.
- 125 Y. Wang and Y. Wang, *Prog. Nat. Sci. Mater. Int.*, 2017, **27**, 41–49.
- 126 A. Baran and M. Polański, *Mater. (Basel, Switzerland)*, 2020, **13**, 3993.
- 127 K. J. Gross, P. Spatz, A. Züttel and L. Schlapbach, *J. Alloys Compd.*, 1996, **240**, 206–213.
- 128 G. S. Walker, M. Abbas, D. M. Grant and C. Udeh, *Chem. Commun. (Camb.)*, 2011, **47**, 8001–3.
- 129 N. Terashita, K. Kobayashi, T. Sasai and E. Akiba, *J. Alloys Compd.*, 2001, **327**, 275–280.

- 130 J. J. Vajo, F. Mertens, C. C. Ahn, R. C. Bowman and B. Fultz, *J. Phys. Chem. B*, 2004, **108**, 13977–13983.
- 131 S. Zhou, X. Zhang, T. Li, N. Wang, H. Chen, T. Zhang, H. Yu, H. Niu and D. Liu, *Int. J. Hydrogen Energy*, 2014, **39**, 13628–13633.
- 132 S. Zhou, Q. Zhang, H. Chen, X. Zang, X. Zhou, R. Wang, X. Jiang, B. Yang and R. Jiang, *Int. J. Hydrogen Energy*, 2015, **40**, 11484–11490.
- 133 A. Lys, J. O. Fadonougbo, M. Faisal, J.-Y. Suh, Y.-S. Lee, J.-H. Shim, J. Park and Y. W. Cho, *Hydrog.*, 2020, 1.
- 134 K. L. Lim, H. Kazemian, Z. Yaakob and W. R. W. Daud, *Chem. Eng. Technol.*, 2010, **33**, 213–226.
- 135 R. A. Varin, T. Czujko, Z. S. Wronski, P. Prachi, M. M. Wagh and G. Aneesh, *Adv. Energy Power*, 2009, **4**, 11–22.
- 136 K. Tatsumi, I. Tanaka, H. Inui, K. Tanaka, M. Yamaguchi and H. Adachi, *Phys. Rev. B*, 2001, **64**, 184105.
- 137 M. Faisal, J.-Y. Suh and Y.-S. Lee, *Int. J. Hydrogen Energy*, 2021, **46**, 4241–4251.
- 138 J. Y. Jung, S.-I. Lee, M. Faisal, H. Kim, Y.-S. Lee, J.-Y. Suh, J.-H. Shim, J.-Y. Huh and Y. W. Cho, *Int. J. Hydrogen Energy*, ,  
DOI:<https://doi.org/10.1016/j.ijhydene.2021.03.096>.
- 139 H. Kim, M. Faisal, S.-I. Lee, J. Y. Jung, H.-J. Kim, J. Hong, Y.-S. Lee, J.-H. Shim, Y. W. Cho, D. H. Kim and J.-Y. Suh, *J. Alloys Compd.*, 2021, **864**, 158876.
- 140 G. K. Sujan, Z. Pan, H. Li, D. Liang and N. Alam, *Crit. Rev. Solid State Mater. Sci.*, 2020, **45**, 410–427.
- 141 A. Züttel, *Naturwissenschaften*, 2004, **91**, 157–72.
- 142 J. Andersson and S. Grönkvist, *Int. J. Hydrogen Energy*, 2019, **44**, 11901–11919.
- 143 T. He, H. Cao and P. Chen, *Adv. Mater.*, 2019, **31**, 1–19.
- 144 M. B. Ley, L. H. Jepsen, Y.-S. Lee, Y. W. Cho, J. M. Bellosta von Colbe, M. Dornheim, M. Rokni, J. O. Jensen, M. Sloth, Y. Filinchuk, J. E. Jørgensen, F. Besenbacher and T. R. Jensen, *Mater. Today*, 2014, **17**, 122–128.

- 145 L. H. Jepsen, M. Paskevicius and T. R. Jensen, in *Nanotechnology for Energy Sustainability*, 2017, pp. 415–432.
- 146 E. Callini, Z. Ö. K. Atakli, B. C. Hauback, S. Orimo, C. Jensen, M. Dornheim, D. Grant, Y. W. Cho, P. Chen, B. Hjörvarsson, P. de Jongh, C. Weidenthaler, M. Baricco, M. Paskevicius, T. R. Jensen, M. E. Bowden, T. S. Autrey and A. Züttel, *Appl. Phys. A*, 2016, **122**, 353.
- 147 Y. Liu, Y. Yang, M. Gao and H. Pan, *Chem. Rec.*, 2016, **16**, 189–204.
- 148 B. Bogdanović and M. Schwickardi, *J. Alloys Compd.*, 1997, **253–254**, 1–9.
- 149 C. Milanese, S. Garroni, F. Gennari, A. Marini, T. Klassen, M. Dornheim and C. Pistidda, *Metals (Basel)*, 2018, 8.
- 150 C. P. Baldé, B. P. C. Hereijgers, J. H. Bitter and K. P. de Jong, *Angew. Chemie Int. Ed.*, 2006, **45**, 3501–3503.
- 151 L. Li, F. Qiu, Y. Wang, G. Liu, Y. Xu, C. An, Y. Wang, L. Jiao and H. Yuan, *J. Mater. Chem.*, 2012, **22**, 13782–13787.
- 152 X. Fan, X. Xiao, L. Chen, L. Zhang, J. Shao, S. Li, H. Ge and Q. Wang, *J. Mater. Chem. A*, 2013, **1**, 9752–9759.
- 153 S. Zheng, F. Fang, G. Zhou, G. Chen, L. Ouyang, M. Zhu and D. Sun, *Chem. Mater.*, 2008, **20**, 3954–3958.
- 154 Q. Gao, G. Xia and X. Yu, *Nanoscale*, 2017, **9**, 14612–14619.
- 155 A. Schneemann, J. L. White, S. Kang, S. Jeong, L. F. Wan, E. S. Cho, T. W. Heo, D. Prendergast, J. J. Urban, B. C. Wood, M. D. Allendorf and V. Stavila, *Chem. Rev.*, 2018, **118**, 10775–10839.
- 156 C. P. Baldé, B. P. C. Hereijgers, J. H. Bitter and K. P. de Jong, *J. Am. Chem. Soc.*, 2008, **130**, 6761–6765.
- 157 Y. Liu, X. Zhang, W. Ke, Y. Yang, M. Gao and H. Pan, *J. Mater. Chem. A*, 2016, **4**, 1087–1095.
- 158 S. I. Orimo, Y. Nakamori, J. R. Eliseo, A. Züttel and C. M. Jensen, *Chem. Rev.*, 2007, 107, 4111–4132.

- 159 J. Jepsen, J. M. Bellosta Von Colbe, T. Klassen and M. Dornheim, *Int. J. Hydrogen Energy*, 2012, **37**, 4204–4214.
- 160 K. T. Møller, D. Sheppard, D. B. Ravnsbæk, C. E. Buckley, E. Akiba, H.-W. Li and T. R. Jensen, *Energies*, 2017, 10.
- 161 H. Feng, L. Tang, G. Zeng, Y. Zhou, Y. Deng, X. Ren, B. Song, C. Liang, M. Wei and J. Yu, *Adv. Colloid Interface Sci.*, 2019, **267**, 26–46.
- 162 M. Zarezadeh, J. Abdi and M. Rezakazemi, *Int. J. Hydrogen Energy*, 2020, **45**, 17583–17604.
- 163 A. Subramaniam, A. Gupta, S. Shervani and K. Balani, in *Smart Nanocontainers: Micro and Nano Technologies*, 2019, pp. 499–514.
- 164 Y. Lei, G. Wang, S. Song, W. Fan, M. Pang, J. Tang and H. Zhang, *Dalt. Trans.*, 2010, **39**, 3273–3278.
- 165 S. Dalai, S. Vijayalakshmi, P. Shrivastava, S. P. Sivam and P. Sharma, *Microelectron. Eng.*, 2014, **126**, 65–70.
- 166 S. Shervani, P. Mukherjee, A. Gupta, G. Mishra, K. Illath, T. G. Ajithkumar, S. Sivakumar, P. Sen, K. Balani and A. Subramaniam, *Int. J. Hydrogen Energy*, 2017, **42**, 24256–24262.
- 167 A. Gupta, S. Shervani, F. Amaladasse, S. Sivakumar, K. Balani and A. Subramaniam, *Int. J. Hydrogen Energy*, 2019, **44**, 22032–22038.
- 168 A. Gupta, S. Shervani, P. Rani, S. Sivakumar, K. Balani and A. Subramaniam, *Int. J. Hydrogen Energy*, 2020, **45**, 24076–24082.
- 169 F. Amaladasse, A. Gupta, S. Shervani, S. Sivakumar, K. Balani and A. Subramaniam, *Part. Sci. Technol.*, 2020, 1–7.
- 170 A. Davoodabadi, A. Mahmoudi and H. Ghasemi, *iScience*, 2021, **24**, 101907.
- 171 A. K. Sum, C. A. Koh and E. D. Sloan, *Ind. Eng. Chem. Res.*, 2009, **48**, 7457–7465.
- 172 Y. H. Hu and E. Ruckenstein, *Angew. Chemie - Int. Ed.*, 2006, **45**, 2011–2013.
- 173 A. Hassanpouryouzband, E. Joonaki, M. Vasheghani Farahani, S. Takeya, C. Ruppel, J. Yang, N. J. English, J. M. Schicks, K. Edlmann, H. Mehrabian, Z. M. Aman and B.

- Tohidi, *Chem. Soc. Rev.*, 2020, **49**, 5225–5309.
- 174 H. P. Veluswamy, R. Kumar and P. Linga, *Appl. Energy*, 2014, **122**, 112–132.
- 175 J. Lyu, V. Kudiiarov and A. Lider, *Nanomaterials*, 2020, 10.
- 176 R. V Belosludov, R. K. Zhdanov, O. S. Subbotin, H. Mizuseki, Y. Kawazoe and V. R. Belosludov, *J. Renew. Sustain. Energy*, 2014, **6**, 53132.
- 177 D. Palmer, 2014.
- 178 L. J. Florusse, C. J. Peters, J. Schoonman, K. C. Hester, C. A. Koh, S. F. Dec, K. N. Marsh and E. D. Sloan, *Science (80-. )*, 2004, **306**, 469–471.
- 179 H. Lee, J. Lee, D. Y. Kim, J. Park, Y.-T. Seo, H. Zeng, I. L. Moudrakovski, C. I. Ratcliffe and J. A. Ripmeester, *Nature*, 2005, **434**, 743–746.
- 180 T. A. Strobel, C. J. Taylor, K. C. Hester, S. F. Dec, C. A. Koh, K. T. Miller and E. D. Sloan, *J. Phys. Chem. B*, 2006, **110**, 17121–17125.
- 181 R. Anderson, A. Chapoy and B. Tohidi, *Langmuir*, 2007, **23**, 3440–3444.
- 182 S. Hashimoto, T. Sugahara, H. Sato and K. Ohgaki, *J. Chem. Eng. Data*, 2007, **52**, 517–520.
- 183 F. M. Mulder, M. Wagemaker, L. Van Eijck and G. J. Kearley, *ChemPhysChem*, 2008, **9**, 1331–1337.
- 184 K. Ogata, S. Hashimoto, T. Sugahara, M. Moritoki, H. Sato and K. Ohgaki, *Chem. Eng. Sci.*, 2008, **63**, 5714–5718.
- 185 T. A. Strobel, C. A. Koh and E. D. Sloan, *Fluid Phase Equilib.*, 2007, **261**, 382–389.
- 186 A. Nishikawa, T. Tanabe, K. Kitamura, Y. Matsumoto, K. Ohgaki and T. Sugahara, *Chem. Eng. Sci.*, 2013, **101**, 1–4.
- 187 T. Sugahara, J. C. Haag, A. A. Warntjes, P. S. R. Prasad, E. D. Sloan, C. A. Koh and A. K. Sum, *J. Phys. Chem. C*, 2010, **114**, 15218–15222.
- 188 J. Liu, J. Hou, J. Xu, H. Liu, G. Chen and J. Zhang, *Int. J. Hydrogen Energy*, 2017, **42**, 17136–17143.
- 189 N. I. Papadimitriou, I. N. Tsimpanogiannis, I. G. Economou and A. K. Stubos, *Mol.*

- Phys.*, 2017, **115**, 1274–1285.
- 190 T. A. Strobel, E. D. Sloan and C. A. Koh, *J. Chem. Phys.*, 2009, **130**, 14506.
- 191 K. A. Lokshin, Y. Zhao, D. He, W. L. Mao, H. K. Mao, R. J. Hemley, M. V. Lobanov and M. Greenblatt, *Phys. Rev. Lett.*, 2004, **93**, 1–4.
- 192 A. Giannasi, M. Celli, L. Ulivi and M. Zoppi, *J. Chem. Phys.*, 2008, **129**, 84705.
- 193 C. A. TULK, J. A. RIPMEESTER and D. D. KLUG, *Ann. N. Y. Acad. Sci.*, 2000, **912**, 859–872.
- 194 N. Plattner and M. Meuwly, *J. Chem. Phys.*, 2014, **140**, 24311.
- 195 R. G. Grim, P. B. Kerkar, E. D. Sloan, C. A. Koh and A. K. Sum, *J. Chem. Phys.*, 2012, **136**, 234504.
- 196 T. Sugahara, J. C. Haag, P. S. R. Prasad, A. A. Warntjes, E. D. Sloan, A. K. Sum and C. A. Koh, *J. Am. Chem. Soc.*, 2009, **131**, 14616–14617.
- 197 J. R. Zhong, L. T. Chen, T. C. Liu, X. Y. Zeng, Y. F. Sun, C. Y. Sun, B. Liu, G. J. Chen and J. A. Ripmeester, *J. Phys. Chem. C*, 2017, **121**, 27822–27829.
- 198 P. Di Profio, V. Canale, R. Germani, S. Arca and A. Fontana, *J. Colloid Interface Sci.*, 2018, **516**, 224–231.
- 199 J. Cai, R. Yan, C. G. Xu, Z. Y. Chen and X. Sen Li, *Energy Procedia*, 2019, **158**, 5149–5155.
- 200 H. P. Veluswamy, W. I. Chin and P. Linga, *Int. J. Hydrogen Energy*, 2014, **39**, 16234–16243.
- 201 E. D. Sloan Jr, C. A. Koh and C. Koh, *Clathrate hydrates of natural gases*, CRC press, 2007.
- 202 Y. Matsumoto, R. G. Grim, N. M. Khan, T. Sugahara, K. Ohgaki, E. D. Sloan, C. A. Koh and A. K. Sum, *J. Phys. Chem. C*, 2014, **118**, 3783–3788.
- 203 S. S. Skiba, E. G. Larionov, A. Y. Manakov, B. A. Kolesov and V. I. Kosyakov, *J. Phys. Chem. B*, 2007, 111, 11214–11220.
- 204 S. S. Skiba, E. G. Larionov, A. Y. Manakov, B. A. Kolesov, A. I. Ancharov and E. Y. Aladko, *J. Incl. Phenom. Macrocycl. Chem.*, 2009, **63**, 383–386.

- 205 S. Maghsoodloo Babakhani, B. Bouillot, S. Ho-Van, J. Douzet and J. M. Herri, *Fluid Phase Equilib.*, 2018, **472**, 22–38.
- 206 V. R. Belosludov, Y. Yu Bozhko, K. V. Gets, O. S. Subbotin and Y. Kawazoe, *J. Phys. Conf. Ser.*, , DOI:10.1088/1742-6596/1128/1/012031.
- 207 Z. Zhang, P. G. Kusalik and G. J. Guo, *J. Phys. Chem. C*, 2018, **122**, 7771–7778.
- 208 H. P. Veluswamy, J. C. Yew and P. Linga, *J. Chem. Eng. Data*, 2015, **60**, 228–237.
- 209 H. P. Veluswamy, J. Y. Chen and P. Linga, *Chem. Eng. Sci.*, 2015, **126**, 488–499.
- 210 D. Y. Koh, H. Kang, J. Jeon, Y. H. Ahn, Y. Park, H. Kim and H. Lee, *J. Phys. Chem. C*, 2014, **118**, 3324–3330.
- 211 K. C. Hester, T. A. Strobel, E. D. Sloan, C. A. Koh, A. Hug and A. J. Schultz, *J. Phys. Chem. B*, 2006, **110**, 14024–14027.
- 212 Y. Ahn, S. Moon, D. Koh, S. Hong, H. Lee, J. W. Lee and Y. Park, *Energy Storage Mater.*, 2020, **24**, 655–661.
- 213 D. Li, S. Wang, Q. Du and R. Huang, *J. Renew. Sustain. Energy*, 2018, **10**, 034902.
- 214 N. I. Papadimitriou, I. N. Tsimpanogiannis, I. G. Economou and A. K. Stubos, *Mol. Phys.*, 2016, **114**, 2664–2671.
- 215 S. Lee, Y. Lee, S. Park, Y. Kim, J. D. Lee and Y. Seo, *J. Phys. Chem. B*, 2012, **116**, 9075–9081.
- 216 W. Shin, S. Park, J.-W. Lee, Y. Seo, D.-Y. Koh, J. Seol and H. Lee, *J. Phys. Chem. C*, 2012, **116**, 16352–16357.
- 217 S. Park, H. Kang, K. Shin, Y. Seo and H. Lee, *Phys. Chem. Chem. Phys.*, 2015, **17**, 1949–1956.
- 218 S. Hashimoto, K. Yamamoto, T. Tsuda and Y. Inoue, *J. Chem. Eng. JAPAN*, 2012, **45**, 444–451.
- 219 S. Amano, T. Tsuda, S. Hashimoto, T. Sugahara and K. Ohgaki, *Fluid Phase Equilib.*, 2010, **298**, 113–116.
- 220 H. Lu, J. Wang, C. Liu, C. I. Ratcliffe, U. Becker, R. Kumar and J. Ripmeester, *J. Am. Chem. Soc.*, 2012, **134**, 9160–9162.

- 221 J. Liu, J. Hou, J. Xu, H. Liu, S. Li, G. Chen and J. Zhang, *Chem. Phys. Lett.*, 2016, **660**, 266–271.
- 222 S. Park, D. Y. Koh, H. Kang, J. W. Lee and H. Lee, *J. Phys. Chem. C*, 2014, **118**, 20203–20208.
- 223 B. R. Lee, J. H. Sa, S. Y. Hong, J. D. Lee, K. H. Lee, Y. Seo and A. K. Sum, *J. Phys. Chem. C*, 2019, **123**, 3811–3816.
- 224 R. G. Grim, P. B. Kerkar, M. Shebowich, M. Arias, E. D. Sloan, C. A. Koh and A. K. Sum, *J. Phys. Chem. C*, 2012, **116**, 18557–18563.
- 225 N. I. Papadimitriou, I. N. Tsimpanogiannis and A. K. Stubos, *Colloids Surfaces A Physicochem. Eng. Asp.*, 2010, **357**, 67–73.
- 226 P. S. R. Prasad, T. Sugahara, A. K. Sum, E. D. Sloan and C. A. Koh, *J. Phys. Chem. A*, 2009, **113**, 6540–6543.
- 227 T. Tanabe, T. Sugahara, K. Kitamura, T. Yamazaki, T. Fujimoto and K. Ohgaki, *J. Chem. Eng. Data*, 2015, **60**, 222–227.
- 228 D. Y. Kim, J. W. Lee, Y. T. Seo, J. A. Ripmeester and H. Lee, *Angew. Chemie - Int. Ed.*, 2005, 44, 7749–7752.
- 229 P. S. R. Prasad, T. Sugahara, E. D. Sloan, A. K. Sum and C. A. Koh, *J. Phys. Chem. A*, 2009, **113**, 11311–11315.
- 230 T. A. Strobel, C. A. Koh and E. D. Sloan, *J. Phys. Chem. B*, 2008, **112**, 1885–1887.
- 231 A. R. C. Duarte, A. Shariati, L. J. Rovetto and C. J. Peters, *J. Phys. Chem. B*, 2008, **112**, 1888–1889.
- 232 A. R. C. Duarte, A. Shariati and C. J. Peters, *J. Chem. Eng. Data*, 2009, **54**, 1628–1632.
- 233 D. Y. Koh, H. Kang and H. Lee, *Chem. Commun.*, 2013, **49**, 6782–6784.
- 234 M. R. Walsh, C. A. Koh, E. D. Sloan, A. K. Sum and D. T. Wu, *Science (80-. )*, 2009, **326**, 1095 LP – 1098.
- 235 M. N. Khan, L. J. Rovetto, C. J. Peters, E. D. Sloan, A. K. Sum and C. A. Koh, *J. Chem. Eng. Data*, 2015, **60**, 418–423.

- 236 A. A. Atamas, S. W. De Leeuw and H. M. Cuppen, *RSC Adv.*, 2015, **5**, 26376–26382.
- 237 J. Liu, Y. Yan, G. Chen, J. Hou, Y. Yan, H. Liu, S. Li and J. Zhang, *Chem. Phys.*, 2019, **516**, 15–21.
- 238 K. Tezuka, T. Taguchi, S. Alavi, A. K. Sum and R. Ohmura, *Energies*, 2012, **5**, 459–465.
- 239 P. K. Chattaraj, S. Bandaru and S. Mondal, *J. Phys. Chem. A*, 2011, **115**, 187–193.
- 240 J. L. Daschbach, T. M. Chang, L. René Corrales, L. X. Dang and P. McGrail, *J. Phys. Chem. B*, 2006, **110**, 17291–17295.
- 241 T. A. Strobel, Y. Kim, G. S. Andrews, J. R. Ferrell, C. A. Koh, A. M. Herring and E. D. Sloan, *J. Am. Chem. Soc.*, 2008, **130**, 14975–14977.
- 242 K. W. Han, Y. J. Lee, J. S. Jang, T. I. Jeon, J. Park, T. Kawamura, Y. Yamamoto, T. Sugahara, T. Vogt, J. W. Lee, Y. Lee and J. H. Yoon, *Chem. Phys. Lett.*, 2012, **546**, 120–124.
- 243 Y. Woo, B. S. Kim, J. W. Lee, J. Park, M. Cha, S. Takeya, J. Im, Y. Lee, T. I. Jeon, H. Bae, H. Lee, S. S. Han, B. C. Yeo, D. Kim and J. H. Yoon, *Chem. Mater.*, 2018, **30**, 3028–3039.
- 244 A. T. Trueba, L. J. Rovetto, L. J. Florusse, M. C. Kroon and C. J. Peters, *Fluid Phase Equilib.*, 2011, **307**, 6–10.
- 245 T. A. Strobel, K. C. Hester, E. D. Sloan and C. A. Koh, *J. Am. Chem. Soc.*, 2007, **129**, 9544–9545.
- 246 V. F. Rozsa and T. A. Strobel, *J. Phys. Chem. Lett.*, 2014, **5**, 1880–1884.
- 247 W. Krätschmer, L. D. Lamb, K. Fostiropoulos and D. R. Huffman, *Nature*, 1990, **347**, 354–358.
- 248 D. Neiner, N. L. Okamoto, P. Yu, S. Leonard, C. L. Condrón, M. F. Toney, Q. M. Ramasse, N. D. Browning and S. M. Kauzlarich, *Inorg. Chem.*, 2010, **49**, 815–822.
- 249 D. Neiner, N. L. Okamoto, C. L. Condrón, Q. M. Ramasse, P. Yu, N. D. Browning and S. M. Kauzlarich, *J. Am. Chem. Soc.*, 2007, **129**, 13857–13862.
- 250 K. S. Chana, M. A. Millera and X. Peng, *Mater. Res. Lett.*, 2018, **6**, 72–78.

- 251 Y. Luo, X. Li, G. Guo, G. Yue, Z. Xu, Q. Sun, A. Liu and X. Guo, *J. Chem. Eng. Data*, 2018, **63**, 3975–3979.
- 252 Q. Zhang, G.-J. Chen, Q. Huang, C.-Y. Sun, X.-Q. Guo and Q.-L. Ma, *J. Chem. Eng. Data*, 2005, **50**, 234–236.
- 253 C. Yu, S. Fan, X. Lang, Y. Wang, G. Li and S. Wang, *Int. J. Hydrogen Energy*, 2020, **45**, 14915–14921.
- 254 J. Deschamps and D. Dalmazzone, *J. Chem. Eng. Data*, 2010, **55**, 3395–3399.
- 255 L. Del Rosso, M. Celli and L. Ulivi, *J. Phys. Chem. Lett.*, 2015, **6**, 4309–4313.
- 256 W. L. Mao and H. K. Mao, *Proc. Natl. Acad. Sci. U. S. A.*, 2004, **101**, 708–710.
- 257 S. N. Ishmaev, A. A. Chernyshov, V. A. Sukhoparov, S. Telepnev and G. V. Kobelev, *Sov. Phys. JETP*, 1983, **57**, 228–233.
- 258 P. E. Brumby, D. Yuhara, T. Hasegawa, D. T. Wu, A. K. Sum and K. Yasuoka, *J. Chem. Phys.*, , DOI:10.1063/1.5084785.
- 259 Q. Lu, X. He, W. Hu, X. Chen and J. Liu, *J. Phys. Chem. C*, 2019, **123**, 12052–12061.
- 260 S. P. Kaur and C. N. Ramachandran, *Int. J. Hydrogen Energy*, 2018, **43**, 19559–19566.
- 261 C. J. Burnham, Z. Futera and N. J. English, *Phys. Chem. Chem. Phys.*, 2017, **19**, 717–728.
- 262 I. N. Tsimpanogiannis, I. G. Economou and A. K. Stubos, *J. Chem. Eng. Data*, 2020, **65**, 1289–1299.
- 263 A. T. Trueba, I. R. Radović, J. F. Zevenbergen, C. J. Peters and M. C. Kroon, *Int. J. Hydrogen Energy*, 2013, **38**, 7326–7334.
- 264 J. Cai, Y. Q. Tao, N. von Solms, C. G. Xu, Z. Y. Chen and X. Sen Li, *Appl. Energy*, 2019, **243**, 1–9.
- 265 X. H. Wang, H. B. Qin, A. Dandekar, Y. F. Wang, Y. F. Sun, Q. L. Ma, B. Liu, L. Y. Yang, C. Y. Sun and G. J. Chen, *Fluid Phase Equilib.*, 2015, **403**, 160–166.
- 266 Z. Li, Z. Xia, Z. Chen, X. Li, C. Xu and R. Yan, *Appl. Energy*, 2019, **238**, 195–201.
- 267 D. Saha and S. Deng, *Langmuir*, 2010, **26**, 8414–8418.

- 268 K. A. Lokshin and Y. Zhao, *Appl. Phys. Lett.*, 2006, **88**, 1–4.
- 269 B. Song, A. H. Nguyen and V. Molinero, *J. Phys. Chem. C*, 2014, 118, 23022–23031.
- 270 H. P. Veluswamy, W. J. Ang, D. Zhao and P. Linga, *Chem. Eng. Sci.*, 2015, **132**, 186–199.
- 271 H. P. Veluswamy and P. Linga, *Int. J. Hydrogen Energy*, 2013, **38**, 4587–4596.
- 272 R. V. Belosludov, Y. Y. Bozhko, R. K. Zhdanov, O. S. Subbotin, Y. Kawazoe and V. R. Belosludov, *Fluid Phase Equilib.*, 2016, **413**, 220–228.
- 273 T. Okuchi, I. L. Moudrakovski and J. A. Ripmeester, *Appl. Phys. Lett.*, 2007, **91**, 2005–2008.
- 274 Y. Nagai, H. Yoshioka, M. Ota, Y. Sato, H. Inomata, R. L. Smith and C. J. Peters, *AIChE J.*, 2008, 54, 3007–3016.
- 275 H. Yoshioka, M. Ota, Y. Sato, M. Watanabe, H. Inomata, R. L. Smith and C. J. Peters, *AIChE J.*, 2011, 57, 265–272.
- 276 H. Komatsu, M. Ota, Y. Sato, M. Watanabe and R. L. Smith, *Chem. Eng. Sci.*, 2014, **108**, 270–282.
- 277 T. J. Frankcombe and G. J. Kroes, *J. Phys. Chem. C*, 2007, **111**, 13044–13052.
- 278 S. Alavi and J. A. Ripmeester, *Angew. Chemie - Int. Ed.*, 2007, **46**, 6102–6105.
- 279 S. Alavi and J. A. Ripmeester, *Mol. Simul.*, 2017, **43**, 808–820.
- 280 C. J. Burnham and N. J. English, *J. Phys. Chem. C*, 2016, **120**, 16561–16567.
- 281 J. R. Cendagorta, A. Powers, T. J. H. Hele, O. Marsalek, Z. Bačić and M. E. Tuckerman, *Phys. Chem. Chem. Phys.*, 2016, **18**, 32169–32177.
- 282 T. Hasegawa, P. E. Brumby, K. Yasuoka and A. K. Sum, *J. Chem. Phys.*, 2020, **153**, 054706.
- 283 N. I. Papadimitriou, I. N. Tsimpanogiannis, A. T. Papaioannou and A. K. Stubos, *J. Phys. Chem. C*, 2008, **112**, 10294–10302.
- 284 R. Ma, H. Zhong, J. Liu, J. Zhong, Y. Yan, J. Zhang and J. Xu, *Processes*, 2019, **7**, 1–12.

- 285 U. Ranieri, M. M. Koza, W. F. Kuhs, R. Gaal, S. Klotz, A. Falenty, D. Wallacher, J. Ollivier, P. Gillet and L. E. Bove, *J. Phys. Chem. C*, 2019, **123**, 1888–1903.
- 286 M. Xu, P. M. Felker and Z. Bačić, *Int. Rev. Phys. Chem.*, 2020, **39**, 425–463.
- 287 D. M. Benoit, D. Lauvergnat and Y. Scribano, *Faraday Discuss.*, 2018, **212**, 533–546.
- 288 T. T. Trinh, M. H. Waage, T. S. Van Erp and S. Kjelstrup, *Phys. Chem. Chem. Phys.*, 2015, **17**, 13808–13812.
- 289 J. Liu, J. Hou, J. Xu, H. Liu, G. Chen and J. Zhang, *Int. J. Hydrogen Energy*, 2017, **42**, 17136–17143.
- 290 J. Liu, S. Shi, Z. Zhang, H. Liu, J. Xu, G. Chen, J. Hou and J. Zhang, *J. Chem. Thermodyn.*, 2018, **120**, 39–44.
- 291 Z. Zhang, P. G. Kusalik and G.-J. Guo, *J. Phys. Chem. C*, 2018, **122**, 7771–7778.
- 292 S. Alavi, J. A. Ripmeester and D. D. Klug, *J. Chem. Phys.*, 2005, **123**, 24507.
- 293 B. Song, A. H. Nguyen and V. Molinero, *J. Phys. Chem. C*, 2014, **118**, 23022–23031.
- 294 P. Di, V. Canale, R. Germani, S. Arca and A. Fontana, *J. Colloid Interface Sci.*, 2018, **516**, 224–231.
- 295 H. Pahlavanzadeh, M. Khanlarkhani, S. Rezaei and A. H. Mohammadi, *Fuel*, 2019, **253**, 1392–1405.
- 296 A. Striolo, A. Phan and M. R. Walsh, *Curr. Opin. Chem. Eng.*, 2019, **25**, 57–66.
- 297 T. Bui, F. Sicard, D. Monteiro, Q. Lan, M. Ceglio, C. Burrell and A. Striolo, *J. Phys. Chem. Lett.*, 2018, **9**, 3491–3496.
- 298 A. A. Bertolazzo, P. M. Naullage, B. Peters and V. Molinero, *J. Phys. Chem. Lett.*, 2018, **9**, 3224–3231.
- 299 P. M. Naullage, A. A. Bertolazzo and V. Molinero, *ACS Cent. Sci.*, 2019, **5**, 428–439.
- 300 Z. Ma and P. G. Ranjith, *Fuel*, 2019, **255**, 115644.
- 301 Y. Qi, M. Ota and H. Zhang, *Energy Convers. Manag.*, 2011, **52**, 2682–2687.
- 302 J. Liu, Y. Yan, H. Liu, J. Xu, J. Zhang and G. Chen, *Chem. Phys. Lett.*, 2016, **648**, 75–80.

- 303 D. Bai, X. Zhang, G. Chen and W. Wang, *Energy Environ. Sci.*, 2012, **5**, 7033–7041.
- 304 Y. T. Tung, L. J. Chen, Y. P. Chen and S. T. Lin, *J. Phys. Chem. B*, 2011, **115**, 15295–15302.
- 305 Y. Iwai, H. Nakamura and M. Hirata, *Mol. Simul.*, 2012, **38**, 481–490.
- 306 J. Liu, Y. Yan, J. Xu, S. Li, G. Chen and J. Zhang, *Comput. Mater. Sci.*, 2016, **123**, 106–110.
- 307 H. Matsui, J. Jia, T. Tsuji, Y. Liang and Y. Masuda, *Fuel*, 2020, **263**, 116640.
- 308 X. Zhou, D. Liang, S. Liang, L. Yi and F. Lin, *Energy & Fuels*, 2015, **29**, 1099–1106.
- 309 G. Wu, L. Tian, D. Chen, M. Niu and H. Ji, *J. Phys. Chem. C*, 2019, **123**, 13401–13409.
- 310 M. E. Casco, J. L. Jordá, F. Rey, F. Fauth, M. Martínez-Escandell, F. Rodríguez-Reinoso, E. V. Ramos-Fernández and J. Silvestre-Albero, *Chem. - A Eur. J.*, 2016, **22**, 10028–10035.
- 311 C. Cuadrado-Collados, J. Farrando-Pérez, M. Martínez-Escandell, L. A. Ramírez-Montoya, J. A. Menéndez, A. Arenillas, M. A. Montes-Morán and J. Silvestre-Albero, *Chem. Eng. J.*, 2020, **402**, 126276.
- 312 G. Zhang, X. Shi, R. Zhang, K. Chao and F. Wang, *Front. Chem.*, 2020, **8**, 6–11.
- 313 C. Cuadrado-Collados, G. Mouchaham, L. Daemen, Y. Cheng, A. Ramirez-Cuesta, H. Aggarwal, A. Missyul, M. Eddaoudi, Y. Belmabkhout and J. Silvestre-Albero, *J. Am. Chem. Soc.*, 2020, **142**, 13391–13397.
- 314 M. E. Casco, J. Silvestre-Albero, A. J. Ramírez-Cuesta, F. Rey, J. L. Jordá, A. Bansode, A. Urakawa, I. Peral, M. Martínez-Escandell, K. Kaneko and F. Rodríguez-Reinoso, *Nat. Commun.*, 2015, **6**, 6432.
- 315 N. N. Nguyen, M. Galib and A. V. Nguyen, *Energy and Fuels*, 2020, **34**, 6751–6760.
- 316 R. S. DeFever and S. Sarupria, *J. Chem. Thermodyn.*, 2018, **117**, 205–213.
- 317 S. J. Cox, D. J. F. Taylor, T. G. A. Youngs, A. K. Soper, T. S. Totton, R. G. Chapman, M. Arjmandi, M. G. Hodges, N. T. Skipper and A. Michaelides, *J. Am. Chem. Soc.*, 2018, **140**, 3277–3284.

- 318 Y. Li, M. Chen, H. Song, P. Yuan, D. Liu, B. Zhang and H. Bu, *Appl. Clay Sci.*, 2020, **186**, 105439.
- 319 K. Bin Yu and A. O. Yazaydin, *J. Phys. Chem. C*, 2020, **124**, 11015–11022.
- 320 L. Li, J. Zhong, Y. Yan, J. Zhang, J. Xu, J. S. Francisco and X. C. Zeng, *Proc. Natl. Acad. Sci. U. S. A.*, 2020, **117**, 24701–24708.
- 321 L. C. Jacobson and V. Molinero, *J. Am. Chem. Soc.*, 2011, **133**, 6458–6463.
- 322 M. Lauricella, S. Meloni, N. J. English, B. Peters and G. Ciccotti, *J. Phys. Chem. C*, 2014, **118**, 22847–22857.
- 323 M. Lauricella, S. Meloni, S. Liang, N. J. English, P. G. Kusalik and G. Ciccotti, *J. Chem. Phys.*, 2015, **142**, 244503.
- 324 Arjun, T. A. Berendsen and P. G. Bolhuis, *Proc. Natl. Acad. Sci.*, 2019, **116**, 19305–19310.
- 325 A. Arjun and P. G. Bolhuis, *J. Phys. Chem. B*, 2020, **124**, 8099–8109.
- 326 T. E. Markland and M. Ceriotti, *Nat Rev Chem*, 2018, **2**, 1–14.
- 327 S. Subramanian and E. D. Sloan, *J. Phys. Chem. B*, 2002, **106**, 4348–4355.
- 328 G. C. Pimental and S. W. Charles, *Pure Appl. Chem.*, **7**, 111–124.
- 329 K. Ohgaki, T. Sugahara, H. Mori, J. Sakamoto, S. Hashimoto and K. Ogata, *Open Thermodyn. J.*, 2008, **2**, 1–6.
- 330 T. A. Strobel, C. A. Koh and E. D. Sloan, *J. Phys. Chem. B*, 2008, **112**, 1885–1887.
- 331 H. Lu, J. Wang, C. Liu, C. I. Ratcliffe, U. Becker, R. Kumar and J. Ripmeester, *J. Am. Chem. Soc.*, 2012, **134**, 9160–9162.
- 332 J. Van Kranendonk and G. Karl, *Rev. Mod. Phys.*, 1968, **40**, 531–555.
- 333 M. Houleberghs, A. Hoffmann, D. Dom, C. E. A. Kirschhock, F. Taulelle, J. A. Martens and E. Breynaert, *Anal. Chem.*, 2017, **89**, 6940–6943.
- 334 H. Lee, J.-W. Lee, D. Y. Kim, J. Park, Y.-T. Seo, H. Zeng, I. L. Moudrakovski, C. I. Ratcliffe and J. a Ripmeester, *Nature*, 2005, **434**, 743–746.
- 335 T. A. Strobel, C. J. Taylor, K. C. Hester, S. F. Dec, C. A. Koh, K. T. Miller and E. D.

- Sloan, *J. Phys. Chem. B*, 2006, **110**, 17121–17125.
- 336 L. Senadheera and M. Conradi, *J. Phys. Chem. B*, 2008, **112**, 13695–13700.
- 337 J.-H. Yoon, J. Han, J. Park, S. Choi, S.-H. Yeon and H. Lee, *J. Phys. Chem. Solids*, 2008, **69**, 1432–1435.
- 338 D.-Y. Kim and H. Lee, *J. Am. Chem. Soc.*, 2005, **127**, 9996–9997.
- 339 R. Kumar, P. Englezos, I. Moudrakovski and J. A. Ripmeester, *AIChE J.*, 2009, **55**, 1584–1594.
- 340 E. D. Walter, L. Qi, A. Chamas, H. S. Mehta, J. A. Sears, S. L. Scott and D. W. Hoyt, *J. Phys. Chem. C*, 2018, **122**, 8209–8215.
- 341 W. F. Claussen, *J. Chem. Phys.*, 1951, **19**, 259–260.
- 342 T. C. W. Mak and R. K. McMullan, *J. Chem. Phys.*, 1965, **42**, 2432–2737.
- 343 G. A. Jeffrey and R. K. McMullan, 2007, vol. 8, pp. 43–108.
- 344 D. W. Davidson, Y. P. Handa, C. I. Ratcliffe, J. A. Ripmeester, J. S. Tse, J. R. Dahn, F. Lee and L. D. Calvert, *Mol. Cryst. Liq. Cryst.*, 1986, **141**, 141–149.
- 345 M. v. Stackelberg, *Naturwissenschaften*, 1949, **36**, 327–333.
- 346 G. A. Jeffrey, *J. Incl. Phenom.*, 1984, **1**, 211–222.
- 347 L. C. Van Den Bergh, J. A. Schouten and N. J. Trappeniers, *Phys. A Stat. Mech. its Appl.*, 1987, **141**, 524–538.
- 348 K. A. Lokshin and Y. Zhao, *Rev. Sci. Instrum.*, 2005, **76**, 12–15.
- 349 K. A. Udachin, J. Ltpkowski and M. Tkacz, *Supramol. Chem.*, 1994, **3**, 181–183.
- 350 L. Del Rosso, M. Celli and L. Ulivi, *Nat. Commun.*, 2016, **7**, 1–7.
- 351 K. Amann-Winkel, M. C. Bellissent-Funel, L. E. Bove, T. Loerting, A. Nilsson, A. Paciaroni, D. Schlesinger and L. Skinner, *Chem. Rev.*, 2016, **116**, 7570–7589.
- 352 Y. Matsumoto, R. G. Grim, N. M. Khan, T. Sugahara, K. Ohgaki, E. D. Sloan, C. A. Koh and A. K. Sum, *J. Phys. Chem. C*, 2014, **118**, 3581–3589.
- 353 K. A. Udachin, C. I. Ratcliffe and J. A. Ripmeester, *J. Supramol. Chem.*, 2002, **2**, 405–408.

- 354 M. E. Donnelly, P. Teeratchanan, C. L. Bull, A. Hermann and J. S. Loveday, *Phys. Chem. Chem. Phys.*, 2018, **20**, 26853–26858.
- 355 K. Röttger, A. Endriss, J. Ihringer, S. Doyle and W. F. Kuhs, *Acta Crystallogr. Sect. B*, 1994, **50**, 644–648.
- 356 J. C. Dore, M. Garawi and M. C. Bellissent-Funel, *Mol. Phys.*, 2004, **102**, 2015–2035.
- 357 D. Colognesi, M. Celli, L. Ulivi, M. Xu and Z. Bačić, *J. Phys. Chem. A*, 2013, **117**, 7314–7326.
- 358 M. Celli, A. Powers, D. Colognesi, M. Xu, Z. Bačić and L. Ulivi, *J. Chem. Phys.*, 2013, **139**, 1–9.
- 359 E. Pefoute, E. Kemner, J. C. Soetens, M. Russina and A. Desmedt, *J. Phys. Chem. C*, 2012, **116**, 16823–16829.
- 360 X. Lang, S. Fan and Y. Wang, *J. Nat. Gas Chem.*, 2010, **19**, 203–209.
- 361 P. Linga and M. A. Clarke, *Energy & Fuels*, 2017, **31**, 1–13.
- 362 P. Linga, C. Haligva, S. C. Nam, J. A. Ripmeester and P. Englezos, *Energy & Fuels*, 2009, **23**, 5496–5507.
- 363 P. Linga, N. Daraboina, J. A. Ripmeester and P. Englezos, *Chem. Eng. Sci.*, 2012, **68**, 617–623.
- 364 Y.-T. Seo, I. L. Moudrakovski, J. A. Ripmeester, J. Lee and H. Lee, *Environ. Sci. Technol.*, 2005, **39**, 2315–2319.
- 365 A. Adeyemo, R. Kumar, P. Linga, J. Ripmeester and P. Englezos, *Int. J. Greenh. Gas Control*, 2010, **4**, 478–485.
- 366 Y.-T. Luo, J.-H. Zhu, S.-S. Fan and G.-J. Chen, *Chem. Eng. Sci.*, 2007, **62**, 1000–1009.
- 367 A. Vysniauskas and P. R. Bishnoi, *Chem. Eng. Sci.*, 1983, **38**, 1061–1072.
- 368 J. Diebold and J. Scahill, *14th Biomass Thermochem. Convers. Contract. Rev. Meet.*, 1982, **1**, 1–40.
- 369 V. K. Venkatakrisnan, J. C. Degenstein, A. D. Smeltz, W. N. Delgass, R. Agrawal and F. H. Ribeiro, *Green Chem.*, 2014, **16**, 792–802.

- 370 B. P. Binks and R. Murakami, *Nat. Mater.*, 2006, **5**, 865–869.
- 371 W. Wang, C. L. Bray, D. J. Adams and A. I. Cooper, *J. Am. Chem. Soc.*, 2008, **130**, 11608–11609.
- 372 G.-H. Qian, I. Bágyi, I. W. Burdick, R. Pfeffer, H. Shaw and J. G. Stevens, *AIChE J.*, 2001, **47**, 1022–1034.
- 373 A. Gonzalez-Quiroga, P. A. Reyniers, S. R. Kulkarni, M. M. Torregrosa, P. Perreault, G. J. Heynderickx, K. M. Van Geem and G. B. Marin, *Chem. Eng. J.*, 2017, **329**, 198–210.
- 374 J. De Wilde and A. de Broqueville, *AIChE J.*, 2007, **53**, 793–810.
- 375 S. R. Kulkarni, L. A. Vandewalle, A. Gonzalez-Quiroga, P. Perreault, G. J. Heynderickx, K. M. Van Geem and G. B. Marin, *Energy & Fuels*, 2018, **32**, 10169–10183.
- 376 A. O. Kuzmin, M. K. Pravdina, A. I. Yavorsky, N. I. Yavorsky and V. N. Parmon, *Chem. Eng. J.*, 2005, **107**, 55–62.
- 377 US Patent Office, US6180843B1, 1997.
- 378 US 20040143145, 2004.
- 379 European Patent Office, EP1159238B1, 2001.
- 380 Y. H. Mori, *Chem. Eng. Res. Des.*, 2017, **117**, 715–724.
- 381 US Patent Office, 4,279,743, *US Pat.*, 1981, 14.
- 382 R. Aranowski, P. Wojewódka, A. Zielińska-Jurek, R. Bokotko and C. Jungnickel, *Chem. Eng. Process. Process Intensif.*, 2017, **116**, 40–47.
- 383 Y. H. Mori, *Energies*, 2015, **8**, 1317–1335.
- 384 US Patent Office, US20150008367A1, 2015.
- 385 H. P. Veluswamy, W. I. Chin and P. Linga, *Int. J. Hydrogen Energy*, 2014, **39**, 16234–16243.
- 386 M. Ozaki, S. Tomura, R. Ohmura and Y. H. Mori, *Int. J. Hydrogen Energy*, 2014, **39**, 3327–3341.

- 387 A. T. Trueba, I. R. Radović, J. F. Zevenbergen, M. C. Kroon and C. J. Peters, *Int. J. Hydrogen Energy*, 2012, **37**, 5790–5797.
- 388 T. Nakayama, S. Tomura, M. Ozaki, R. Ohmura and Y. H. Mori, *Energy & Fuels*, 2010, **24**, 2576–2588.
- 389 T. Shibata, H. Yamachi, R. Ohmura and Y. H. Mori, *Int. J. Hydrogen Energy*, 2012, **37**, 7612–7623.
- 390 E. L. Miller, S. T. Thompson, K. Randolph, Z. Hulvey, N. Rustagi and S. Satyapal, *US Department of Energy hydrogen and fuel cell technologies perspectives*, 2020, vol. 45.
- 391 B. D. James and C. Houchins, *Hydrogen Storage System Cost Analysis: Summary of FY 2017 Activities*, 2017.